UNIVERSITY OF SOUTHAMPTON

FACULTY OF Physical Sciences and Engineering

Department of Electronics and Computer Science

THERMAL PROGNOSTIC CONDITION MONITORING FOR MV CABLE SYSTEMS

by

Stelios Christou

Thesis for the degree of Doctor of Philosophy

June 2016

UNIVERSITY OF SOUTHAMPTON

ABSTRACT

FACULTY OF PHYSICAL SCIENCES AND ENGINEERING

Thesis for the degree of Doctor of Philosophy

THERMAL PROGNOSTIC CONDITION MONITORING FOR MV CABLE SYSTEMS

by Stelios Christou

Large-scale investment in transmission and distribution power networks is planned over the next decades to meet the future demand and changes in power generation. Nevertheless, it is still of a great importance that the existing assets continue to operate reliably and their health is maintained. Moreover, the failures of distribution cables are extremely disruptive, costly to repair and have a serious impact on customer confidence. As a result, developing a reliable on-line prognostic tool is of a great importance.

This research investigates a method of developing a prognostic capability for evaluation of the health and long term performance of aging distribution cable circuits. Developing such prognostic models will significantly improve the prognosis accuracy, allowing the targeting of maintenance and reduction of in-service failures. Real-time measurements taken close to underground cables can update the models giving a more accurate prognostic tool. The aging of the cable begins the moment it is installed and put in service due to a combination of mechanical, thermal, electrical and environmental factors.

A thermal prognostic model is suggested. It enables prediction of the likely temperature impact on underground cable joints at the burial level and terminations according to weather conditions and known loading. Anomalies of temperature measurements along the cable compared to predicted temperatures will indicate the possible degradation activity in the cable. An experimental surface trough has been set up where operation of power cables was simulated with control system which is able to model any cable loading. The surface temperature of the cable is continuously monitored as well as the weather conditions such as solar radiation, wind speed, humidity, rainfall and air temperature.

The research involved cooperation with University of Cyprus and the Electricity Authority of Cyprus which has given an opportunity to implement, install and study the

performance of the condition monitoring thermal prognostic model in a distribution network with different environmental and loading conditions than found in the UK.

Table of Contents

iii

DECLARATION OF AUTHORSHIP

I,..[please print name]

declare that this thesis and the work presented in it are my own and has been generated by me as the result of my own original research.

[title of thesis] ....

....

I confirm that:

1. This work was done wholly or mainly while in candidature for a research degree at this University;
2. Where any part of this thesis has previously been submitted for a degree or any other qualification at this University or any other institution, this has been clearly stated;
3. Where I have consulted the published work of others, this is always clearly attributed;
4. Where I have quoted from the work of others, the source is always given. With the exception of such quotations, this thesis is entirely my own work;
5. I have acknowledged all main sources of help;
6. Where the thesis is based on work done by myself jointly with others, I have made clear exactly what was done by others and what I have contributed myself;
7. [Delete as appropriate] None of this work has been published before submission [or] Parts of this work have been published as: [please list references below]:

Signed: ....

Date:..

Acknowledgements

First of all I would like to express the sincerest gratitude to Professor Paul Lewin for giving me the opportunity to proceed with PhD study, for his continuous and invaluable support, patience, advice and guidance in all the aspects throughout my research. I could not have asked for a better mentor. I would also like to thank my supervisors Dr James Pilgrim and Professor Steve Swingler for their support, guidance and motivation over the years of my PhD.

Furthermore I would like to gratefully acknowledge the financial support of this research provided by the Research Councils UK, through the HubNet consortium as well as the collaboration with the Electricity Authority of Cyprus and University of Cyprus that allowed to perform experiments in MV substation in Cyprus and immensely contributed to this research.

I would as well like to express my gratitude to all the members of the Tony Davies High Voltage Laboratory. Special thank you to Neil Palmer, Mike Smith, Brian Rodgers, Richard Howell and Barry Bailey for their assistance and provided technical support.

Moreover, my sincere thanks goes to Dr Demetres Evagorou for his endless support and counsel as well as to Dr Richard Chippendale, Dr Mathew Praeger and Dr Jack Hunter for their patience, understanding and all the hours spent with me answering all my questions and patiently advising and guiding me through the whole period of my PhD. Obviously I should not forget my colleagues with who I spend endless hours in the office and thus particular thank you to Dr Rui Huang, Dr Pedro Amaro, Dr Ziyi Huang, Raed Ayoob, Aine Izzati, Sijun Wu and the rest of research team. From day one and up until now you all never stopped to motivate me and made these last four years a truly amazing experience.

Last but not least, I would like to thank my family and specially Irena Atminis for their encouragement, patience and support during my academic years. You never stopped believing in me and all your support was truly priceless during the thesis writing as well as to reach the point of my life where I am today.

Symbols and Abbreviations

A	conductor cross section	m^2
E	Young's modulus of the conductor material	Nm^{-2}
F	expansion force	N
α	thermal expansion coefficient	$℃^{-1}$
Δθ	temperature increases with respect to the ambient temperature of the cable	℃
std	standard deviation	
y_a	real value of thermocouple temperature	℃
y_p	predicted value of thermocouple temperature	℃
n	total number of samples	
x_i	input features for SVR training	
y_i	target value to be estimated from SVR training	
$φ(x)$	function used to map training samples x_i to higher dimensional feature space	
C	penalty factor that controls the trade-off between model complexity and frequency of errors	
$α_i$	Lagrange multipliers	
$α_i^*$	Lagrange multipliers	
γ	variable in RBF kernel function	
ε	determines the maximum deviation from the target output value y_i	
$ξ_i$	slack variables	
$ξ_i^*$	slack variables	
X	original data before scaling	
X_{scale}	scale data	
X_{max}	maximum value of original data before scaling	
X_{min}	minimum value of original data before scaling	

T$_{mean(S11,S2)}$	mean temperature difference between thermocouples S11 and S2 before the introduction of hot-spots	℃
TC$_{(s)}$	Thermocouple(s)	
ΔT	Temperature increase	℃
ΔR	real uncertainty of the system	℃
ΔP	predicted uncertainty of the system	℃

To my dearest family …

"Γηράσκω δ' αεί πολλά διδασκόμενος" Σόλων

"I grow old ever learning many things" Solon

Chapter 1 Introduction

An ultimate aim of every Distribution Network Operator is to maintain a reliable power supply to its customers. With a constantly increasing power demand existing transmission and distribution underground power networks are exposed to a number of factors which speed up cable aging leading to breakdown of power cables that are very inconvenient and expensive to repair. Thus developing a reliable online condition monitoring prognostic indicator tool is of great demand and importance in order to predict and prevent upcoming failures, make maintenance easier, reduce operational costs as well as to increase the confidence of the customers.

The health of the electricity networks has a great financial and social impact to the society. In 1998 a 6 weeks power outage happened in Auckland due to overheating of four power cables. It had an estimated long-term economic impact equivalent 0.1 to 0.3 per cent of New Zealand's gross domestic product and over half of businesses within the central business district were forced to move out at least temporarily [1].

The research presented in this thesis involved collaboration between the University of Southampton, the University of Cyprus and the Electricity Authority of Cyprus in order to install condition monitoring units in underground cable joints inside an MV substation. This enabled the analysis of real-time data from cable circuits in Cyprus which contributed towards the development of an online thermal condition monitoring prognostic indicator tool.

1.1   Research Motivation

Cables start to age the moment they are put in operation. The lifetime of an aging cable is affected by a combination of mechanical, thermal and electrical stresses as well as weather conditions [2]. Most of the failures within a distribution network have been reported by the cable joints and terminations and for that reason they are considered to be the weakest accessories in the distribution networks [3][4][5].

Over the past decade there has been a significant breakthrough in development of online diagnostic and condition monitoring tools which enabled network operators to a certain extent prioritize the required repairs or replacements in power networks. Partial discharge

(PD) monitoring tools can detect the defect prior to the failure of insulation [6]. Hydro Quebec Research Institute and KEMA have developed an online monitoring systems which are able to detect and localize PD in cable and cable joints and to indicate the upcoming failures by spotting the abnormal PD activity [7][8]. Another way of condition monitoring is the monitoring of the temperature on the joint of underground cable. Hydro Quebec developed an online monitoring software which records temperatures of the cable joints and can indicate the health of the monitored joints [9]. Thermal imaging cameras have been used as a diagnostic technique for assessing the health of cable terminations [10]. The Electric Power Research Institute (EPRI) suggested the above technique to periodically inspect the current health state of the cable accessories such as joints and terminations [11]. Unfortunately, existing condition monitoring and diagnostic techniques are not always capable of detecting and preventing failures prior to their occurrence [10] [12]. Thus it is vital to identify the early stages of a possible degradation activity within the cable systems by developing improved prognostic capabilities.

Developing such a prognostic capability will significantly improve the prognostic accuracy, allowing the targeting of maintenance and reduction of in-service failures. The existing condition monitoring systems are costly to implement and maintain. Furthermore the abovementioned condition monitoring systems are often able to identify only the final stages of an upcoming failures thus proving unreliable for network operators to schedule necessary maintenance.

Hence a development of a condition monitoring prognostic indicator tool which is cost effective and is able to predict upcoming catastrophic failures sometime before its occurrence is of a great demand.

1.2   Feasibility of a Thermal Prognostic Model

Development of models can significantly improve the accuracy of prognostics, it can reduce the cost of maintenance and prevent in service failures. Real-time measurements taken close to underground cables can update the models input variables giving a more accurate prognostic model by reducing the real-time error of the prognostic output value.

In this work a thermal prognostic model is introduced and implemented for cables in air filled and soil filled trenches as well as in underground cable joints in a MV substation in Cyprus. The developed thermal prognostic model is based on a Support Vector

Regression (SVR) algorithm that is able to predict the likely temperature along the cable 30 minutes into the future and is able to detect temperature anomalies which can indicate upcoming failures.

Weather parameters such as solar radiation and air ambient temperature as well as load profile demands and cable temperature are used to develop the SVR models. A number of various sensitivity tests were performed in order to create a new methodology through which more efficient thermal prognostic models could be developed and adopted globally.

1.3   Contribution of this Thesis

The feasibility of predicting abnormal temperature anomalies along the surface of the cable accessories has been investigated. A simulation model in COMSOL as well as the experiments performed in air filled and soil filled trenches have verified that a set of potential faults will generate heat and the rise of temperature can be detected on the surface of the investigated accessories. A SVR machine learning algorithm has been used to develop thermal prognostic models which are able to identify abnormal cable surface temperature increases. Weather parameters such as solar radiation, air ambient temperature as well as cable loading conditions were taken into to account during the development of the thermal prognostic models.

From the outcomes of the experiments in air filled and soil trenches as well as through the series of different sensitivity tests and the pre-processing data analysis, a methodology has been established which was then used during the installation and implementation of an online prognostic condition monitoring system for an MV substation in Cyprus. Field data collected from Cyprus was analysed and used to develop the thermal prognostic condition monitoring system.

A thermal online condition monitoring prognostic indicator tool has been developed and implemented in the MV substation in Cyprus. The above prognostic capability is able to identify and predict the healthy state of the cable accessories such as joints and terminations. It was able to identify an upcoming failure in the real field underground cable joint approximately 2 months prior to failure. The developed thermal anomaly decision algorithm (TADA) combined with the developed prognostic tool is able to give an insight on the current scale and size of degradation activity happening within the cable

joint and can provide the network operator with the needed confidence to take necessary actions and precautions. The suggested thermal online condition monitoring prognostic indicator tool will be able to fill the gap of demanded prognostic capability for common cable accessory faults. This research proves that the concept of predictive maintenance as well as the transition from diagnostics to prognostics is achievable.

1.4   Thesis Structure

This chapter has described the research motivation, the reasons why a reliable thermal prognostic model is of a great demand and the contributions of this thesis. An online condition monitoring thermal prognostic indicator system based on SVR is proposed.

Chapter 2 presents a more detailed investigation of the underground cables used in the MV distribution networks. It outlines the construction of cables and the aging mechanism, factors and effects affecting lifetime of a cable. This Chapter also describes possible underground joint and termination failures and aging mechanisms as well as existing diagnostic and condition monitoring methods for the underground cable joints and terminations.

Chapter 3 investigates the possibility to identify abnormal changes of temperature on the surface of a cable using a simple thermal cable model created in COMSOL. A comparison between Artificial Neural Network (ANN), Multiple Linear Regression (MLR), Gradient Bosting (Mboost) and Support Vector Regression (SVR) machine learning algorithms is performed and the reasons why the SVR is chosen and ultimately implemented are explained. The theoretical background of the SVR is presented and the description of the development of a thermal prognostic model using the SVR algorithm is described.

Chapter 4 outlines a series of sensitivity tests performed in the air-filled trench. The results of the sensitivity tests are taken into account for the development and implementation of the thermal prognostic models in the soil filled trench and in the Cyprus field experiment as it is described later in Chapters 5 and 6. Furthermore the air-filled thermal prognostic model is developed and is able to detect the abnormal temperatures along the air-filled trench produced by an external heat source. The sensitivity of the thermocouples (TCs) is investigated in order to identify if they are appropriate temperature sensing devices to detect the existence of the increased temperature produced by the hot-spots on specific part of an underground cable system

such a joints and terminations. An experiment on a 33kV termination is performed in order to identify if the thermal prognostic model is sensitive enough to detect abnormal change of temperature on the termination surface after the introduction of hot-spots.

Chapter 5 describes the performance of the SVR thermal prognostic model in the soil filled trench under the influence of the hot-spots during constant and cyclic loads. A benchmarking between the 4 above mentioned algorithms for both constant and cyclic load experiments is performed. Moreover it outlines an in-depth analysis of possible system error and the verification of selected model parameters is presented.

Chapter 6 describes the development of a thermal condition monitoring system that has been designed and implemented for an MV substation in Cyprus. The field experimental data from Cyprus is used for the development of the thermal prognostic model. Finally the development of a thermal anomaly decision algorithm which is used to classify the upcoming failure alerts is presented.

Chapter 7 summarises the development of the thermal prognostic models established in this research, highlights the benefits of these developments and discusses the potential of further development of the techniques proposed in this thesis.

Chapter 2 Underground Cable Systems and the Mechanism of Cable Aging

Underground cables are used to transmit or distribute power within power networks. Underground cables are less liable to the impacts of severe weather, smaller land area is required for installation compared with overhead lines and finally they emit lower electromagnetic fields than overhead lines [13].

From the beginning of the 20th century, low and medium voltage underground cables were used to distribute electric power in congested urban areas. The development of technology, new ways of manufacturing and design of underground cables enabled them to be used for electric power transmission for short or medium distances.

2.1 Underground Cable Construction

An underground cable is mainly composed from: a) a conductor, b) insulation around the conductor and c) an external protecting covering. An example of a three-core cable is shown in Figure 1.
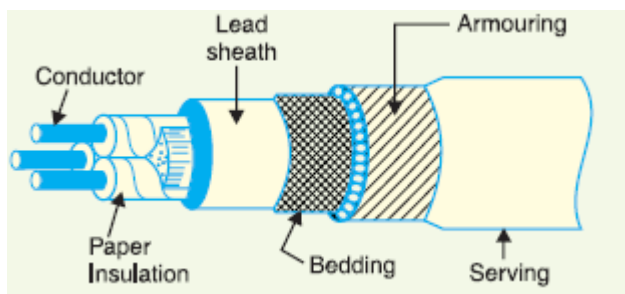
Fig. 1 Three-Core cable construction [14].

The number of conductors in an underground cable depends upon the purpose for which the cable is intended to be used. The conductors are built from stranded copper or aluminum to add flexibility to the cable. The conductors are surrounded with a layer of suitable insulation, thickness of which depends from the voltages the cable is carrying. Insulation is usually made from oil-impregnated paper, vulcanized, butyl rubber, PVC etc. The insulation is protected by a metallic sheath of lead or aluminum to minimize the damage from moisture, gases, damaging liquids from the soil and atmosphere. The metallic sheath is covered with a coating of bedding which is made of fibrous materials

like jute or hessian tape to protect the metallic sheath from corrosion and mechanical damage from armouring. The armouring is usually made from steel wire or steel tape which acts as a source of mechanical protection of the cable. Some types of cables do not include armouring. The serving is used to protect the armouring from environmental conditions and it is a coating of fibrous material similar to the one used in the bedding.

2.2   Mechanism of Cable Aging

The aging of cable insulation materials begins the moment a cable is installed and energized. The degradation of the cable insulation depends on a number of factors which can be extrinsic or intrinsic. Extrinsic factors are those due to voids, physical imperfections, contaminants, or poorly dispersed components due to manufacturing imperfections and poor workmanship faults. Intrinsic factors are those due to a combination of mechanical, thermal, electrical and environmental factors to which cable is exposed in the long run [3]. The typical ageing factors, mechanisms and effects of cable insulation are presented in Table 1 and typical power cable defects are shown in Figure 2.

Fig. 2 Typical power cable defects [3].

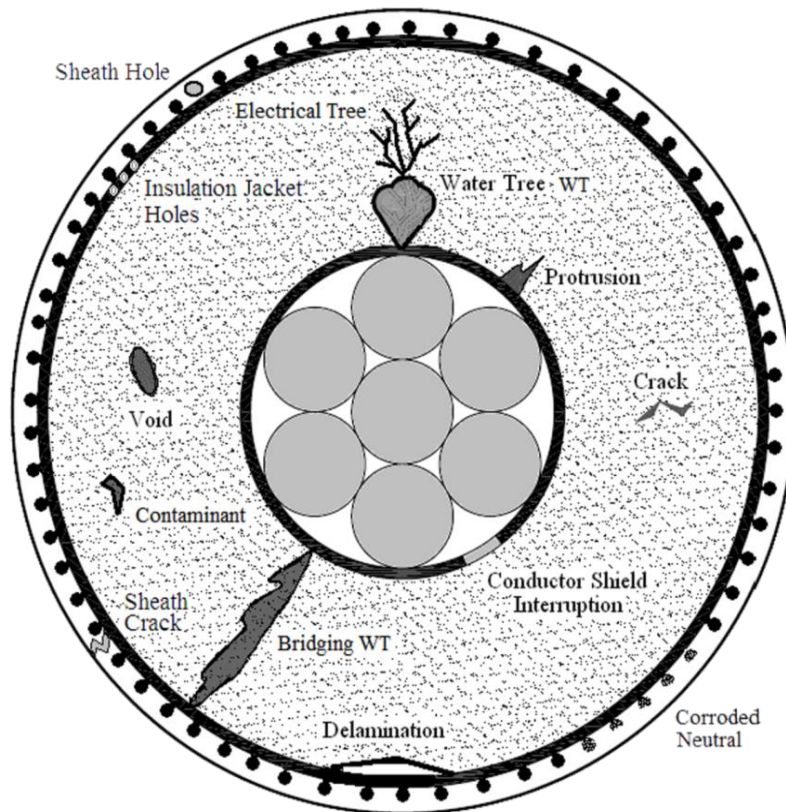| Aging factor	Aging mechanisms	Effects
Thermal		
• High temperature • Temperature cycling	• Chemical reaction • Incompatibility of materials • Thermal expansion • Diffusion • Anneal locked-in mechanical stresses • Melting / flow of insulation	• Hardening, softening, loss of mechanical strength, embrittlement • Increase tan delta • Shrinkage, loss of adhesion, separation, delamination at interfaces • Swelling • Loss of liquids, gases • Conductor penetration • Rotation of cable • Formation of soft spots, wrinkles • Increase migration of components
Low temperature	• Cracking • Thermal contraction	• Shrinkage, loss of adhesion, separation, delamination at interfaces • Loss / ingress of liquids, gases • Movement of joints, terminations
Electrical		
Voltage, ac, dc, impulse	• Partial discharge (PD) • Electrical treeing (ET) • Water treeing (WT) • Dielectric losses and capacitance • Charge injection • Intrinsic breakdown	• Erosion of insulation →ET • PD • Increased losses and ET • Increased temperature, thermal aging, thermal runaway • Immediate failure
Current	• Overheating	• Increased temperature, thermal aging, thermal runaway
Mechanical		
Tensile, compressive, shear stresses, fatigue, cyclic bending, vibration	• Yielding of materials • Cracking • Rupture	• Mechanical rupture • Loss of adhesion, separation, delamination at interfaces • Loss / ingress of liquids, gases
Environmental		
Water / humidity Liquids / gases Contamination	• Dielectric losses and capacitance • Electrical tracking • Water treeing • Corrosion	• Increased temperature, thermal aging, thermal runaway • Increased losses and ET • Flashover
Radiation	• Increase chemical reaction rate	• Hardening, softening, loss of mechanical strength, embrittlement

Table 1 Typical ageing factors, mechanisms and effects of cable insulation [2]

Cables fail when the insulation loses its dielectric strength. When a material is subjected to electric field heat can be generated due to conduction current and dielectric loss. Thermal instability is reached when the rate of heating exceeds the rate of cooling and the cable may undergo thermal breakdown.

Solid insulation may contain cavities and voids which might be very small in size. These voids might be either dielectric bounded or at the interface between dielectric and semiconducting screens which might have developed during the manufacturing or installation process. These voids are usually filled with a medium (gas or liquid) of lower

8

breakdown strength. This as a result can lead to electrical discharge inside the void which can only partially bridge the insulation. The above electrical discharges are called Patrial Discharges (PD) and do not immediately result in an insulation fault. However, the localised but intense electrical, thermal and chemical effects of the discharge are likely to degrade the insulation material over the time and might lead to a fault.

2.3   Thermomechanical Aging in Underground Cables

Power cables which handle daily load cycles are cyclically heated and cooled which results in the build-up of compressive and tensile stresses in the sheath of the cable due to the changing temperatures and the different thermal expansion factor of the insulation material compared to the conductor [15].

Studies of cable movement in a duct were undertaken for two fundamental purposes: a) to determine the portion of the theoretical expansion that appeared at the duct mouth under controlled conditions b) to ascertain the nature and extent of lateral movement (snaking), together with the relative performance of cable core and sheath while the cable is under compression during the heating cycle [16].

2.3.1   Movement of Underground Cables

Lateral movement (snaking) can be explained by considering an inactive cable laid in a duct line without any other cables around it. At the lowest ambient temperature the cable is contracted to its minimum length and is positioned along the bottom of the duct. As it is being put in service and with increase of earth temperature, cable temperature therefore gradually increases and the cable expands longitudinally. The primary length expansion of the cable is absorbed by lateral displacement, so called snaking of the cable inside the duct, because the mechanical resistance of the cable to the snaking is lower than longitudinal movement. However the insignificant expansion in cable length can be noticed in the manholes despite the fact the cable has enough space to readjust itself within a duct [15].

The longitudinal expansion of the cable occurs as a consequence of the larger thermal expansion of the lead sheath rather than copper/aluminium conductors of the cable. The above without any doubt creates a longitudinal mechanical force in the sheath of the cable which partially is transmitted through the insulation to the conductors which consequently

results in the expansion of the length of the whole cable. To a certain extent the expansion of the cable length is absorbed by lateral displacement within the duct. Nevertheless some of the stress in the sheath still has to be spread along the sheath of the cable and it can only be relieved by increasing the cable length into the manholes [15].

In addition to the lateral and longitudinal cable movements there are other configurations. Helical, part linear part helical, part helical part sinusoidal configurations can also be considered as cable movement configurations. According to [17][18] these configurations cannot be predicted as they depend on the previous elastic energy stored in the cable. Factors affecting cable movement are: temperature of the conductor, load cable demand, stiffness of the cable, weight of the cable and the diameter of the duct.

2.3.2   Fatigue Analysis of Underground cables due to Thermomechanical Bending

The lifetime of an operating power cable laid in underground ducts is highly dependent on the ability of the sheath to protect the insulation of the cable from air and moisture [19]. The effects of thermomechanical bending are caused by constant heating and cooling cycles due to the various daily load demands [18]. Thermal expansions and contractions of the cable generate the movement and bending of it causing damage and failure of the sheath. The movement of the cable causes fatigue cracks mainly in the manholes towards where the cable moves accumulated by longitudinal expansion force which is then reduced by the lateral movement of the joint [19].

Assuming the fact that the lead sheath can freely move with respect to the conductors of the underground cable then as a result the effect of longitudinal expansion of the sheath will be partially moved to the relevant sections of the sheath in the manhole. The stresses reach a maximum once the movement of the sheath is suppressed either by a bend, a reinforced joint or by a point where equivalent opposing forces of adjoining sections appear. In most cases because of the above suppression the lead sheath goes beyond its elastic limit at one of the above points which as a result creates a crack or ripple in sheath all around the cable. The moment this ripple develops all the future expansion of the sheath will be congested at that ripple and the failures will not appear at any other points of the sheath. This sort of failure is very commonly observed by the ends of joints specifically in systems without bends [20].

In the bent section of XPLE cable, introduction of tension stress may cause the formation of microvoids. When these microvoids are formed within wet conditions, water trees could be developed [21]. On the other hand in the case of dry conditions, partial discharge could be initiated in mechanically formed microvoids, as a result developing the electrical trees and reducing the breakdown strength of the insulation [22].

The main negative factor for PILC cables is moisture. According to [23] moisture can enter the cable, via holes and cracks in the lead sheath due to thermomechanical movement at locations with concentrated mechanical stresses such as joints and terminations. The introduction of the moisture inside the paper-insulated cable will result in the development of thermal runaway due to increased dielectric losses. Sheath life of the cable might be reduced due to a cyclic movement of cable even within normal operating temperatures allowed by cable specifications [16].

For the above reasons determining the sheath life of an underground cable is of a great demand. Nevertheless it is extremely difficult to determine the actual service life even under known operating conditions as it depends on a number of various factors. The sheath life depends on: a) size and type of cable, b) size and type of duct, c) size of manhole and configuration of the cable in the manhole especially as to bends and offset of the joint from the line of the ducts, d) temperature cycles of the conductor, e) temperature of the sheath, f) length and slope of the cable between manholes and g) the amount of vibration (e.g. street traffic) [19] [24].

2.4   Environmental Factors Influencing Underground Cable Aging

Global warming is predicted to result in generally hotter drier summers and milder, wetter winters in the UK [25]. Higher ambient temperatures cause an increase to the temperature of the ground, which as a result will cause the dry-out of the soil that potentially will increase the soil thermal resistivity. The dried out soil, especially one rich in clay will cause movement of the ground that may result in damage at the cable joints [26]. In the case which this occurs during the high cable loading demands there is a significant danger of the cable overheating which will cause mechanical, insulation damage and consequently the failure of the system [26].

The outage which happened in Auckland in 1998 is considered to be one of the major proofs that high soil thermal resistivity can cause the failure of the power system [27]. As

well as by a significant rise in the ground temperature which increased the soil thermal resistivity that led to the overheating of the cables causing conductors and sheath to expand and contract resulting in the system breakdown [28]. A similar failure occurred in 1962 in London where two 132 kV cables suffered successive failures. Investigation showed that high thermal resistivity developed around the cable region during the summer period and caused abnormal soil dry-out due to the water migration [29].

When a crack occurs on the lead sheath the insulation can be easily damage by the moisture from the surrounding underground environment. This will cause the loss of its dielectric strength due to the possible and potential formation of water treeing and will finally lead to the failure of the cable [30]. It is verified that the phenomenon of water treeing is related to the presence of humidity in the insulation. Water by the cover of the cable is enough to cause treeing; it does not necessarily have to enter through the conductor in order to grow; water trees need only relatively high moisture content within the insulation [31].

Lightning strikes can cause damage to underground cables in the cases when cables are positioned near striking points or when lightning current flows though the soil to the cable causing insulation failure [32].

2.5 Cable Accessories

In order to design and put into operation a fully functional cable circuit network, cables need to be both jointed and terminated. Thus cable joints and terminations are considered to be the most important cable accessories. Cable joints are used to interconnect and extend the length of underground cables while terminations are the accessories used to terminate the underground cables and to provide the connection to other assets in the power network.

Both cable joints and terminations are installed manually on site, very often under unfavourable environmental conditions without taking into account controlled tape tension, clean extruders surfaces and temperature or humidity [33]. The quality of installation almost purely depends on human factors and mistakes made during the installation can significantly reduce the lifetime of the accessories. For that reason cable joints and terminations are considered to be the weakest points of underground cables systems.

2.5.1   Cable Terminations

Cable terminations control the electric stresses of the cable insulation shield terminals as well as external insulation between the cable conductor(s) and ground. Terminations also provide a seal to the end of the cable against the entrance of the external environment and maintain the operating design of the cable system. Terminations are used for extruded dielectric cables, laminated dielectric cables and pressurized cable systems [34].

Terminations are divided into outdoor or indoor. Outdoor terminations are designed to endure weather phenomena such as precipitation, pollution and ultraviolet radiation. Indoor terminations are installed into a grounded protective metallic enclosures which can contain air, gas or liquid compounds [33].

2.5.2   Cable Joints

Over the past few decades the need to distribute the energy across every part of a country had resulted in the increased number of underground power cables. As the length of the cable is limited, additional accessories are needed to extend the cable length. These accessories are called cable joints.

Cable joints have to provide stress control and be able to restore the connection between the insulation phases and earth like the cables they are connected to. Furthermore joint design must provide mechanical protection against external damage and to stop moisture from the surrounding environment entering the joint [33].

The joints are used to connect cables which are both insulated with extruded dielectric materials (extruded joints), for cables which have a dielectric that consists of fluid-impregnated paper or paper/synthetic laminated tape or varnished cloth (laminated joints), or to connect an extruded dielectric cable to a laminated dielectric cable (transition joints) [33].

2.6   Failures and Aging Mechanisms in cable accessories

The power network distributors aim to supply electricity as safely and reliably as possible. Nevertheless failures in the power distribution networks are still very common [28][35][36][37]. The most common location of cable failures are at the cable joints or terminations [3][4][5]. The biggest percentage of the failures in North America according

with NEETRAC, as shown in Figure 3, is due to the cable accessories (joints and terminations) failures [4].

The different types of cable joint defects which can occur in the different types of joint constructions are shown in Figure 4. A list of aging mechanisms in cable joints and terminations is shown in Tables 2 and 3.
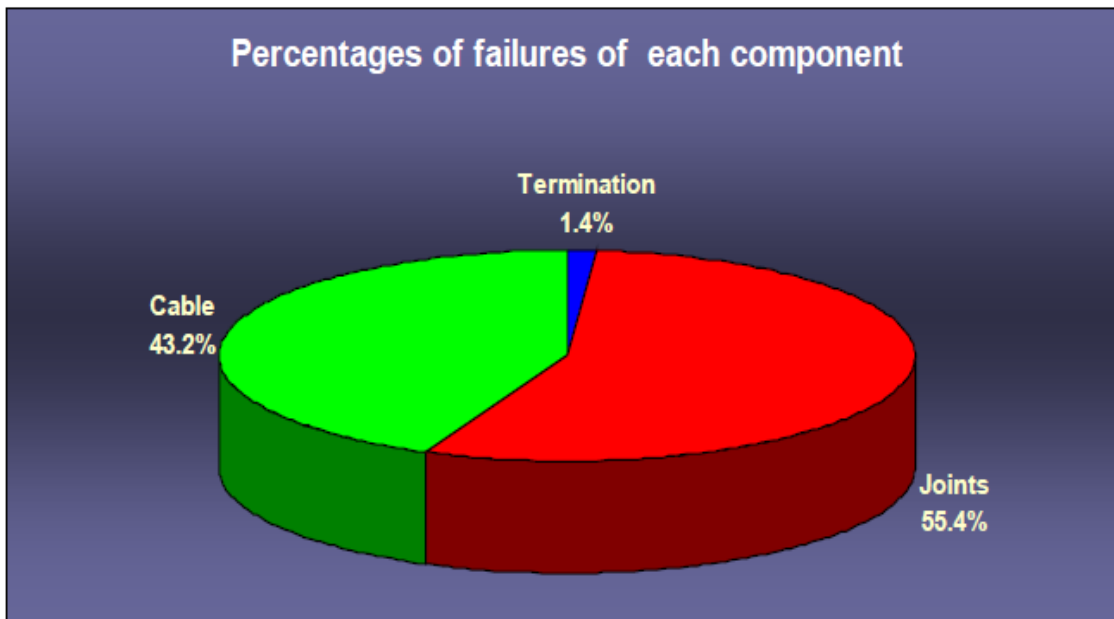
Fig. 3 Percentages of failures for cables, terminations and joints in North America MV (15 kV-35 kV) cable system [4].
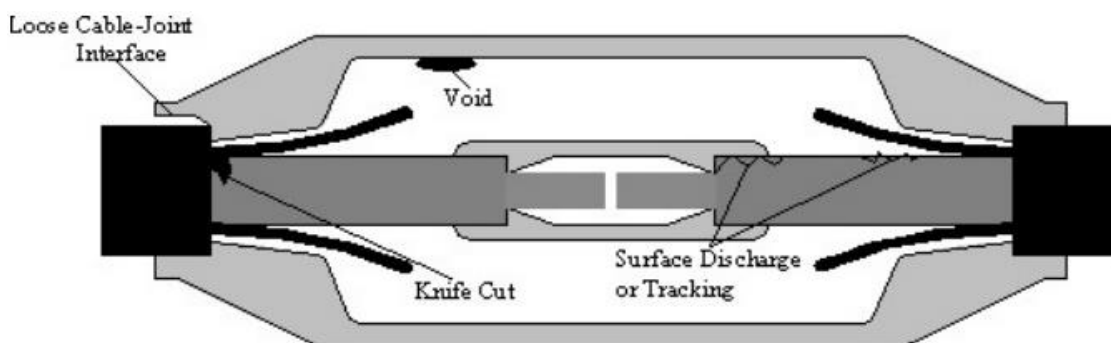
Fig. 4 Typical Cable Joint Defects [3].

The temperature of the soil around the cable changes seasonally due to the weather conditions such as rain, ambient temperature, solar radiation and etc. An increase of the soil temperature creates a kind of hot-spot around the joint consequently increasing the temperature inside the joint. As a result a combination of that hot-spot with the rise of the

soil temperature can lead to the breakdown of the joint insulation and consequent failure [38].

| Type of Deterioration	Aging Process	Accessory Type	Typical Causes	Example
Dry Electrical	Voids / Delaminations → Partial discharge → Insulation degradation → Decrease in dielectric strength	Joint, termination, separable connector	Manufacture defects, natural aging, poor workmanship	Void
Electrical Interface	Contamination / Improper interface pressure / Moisture ingress → Flashover → Insulation degradation; Partial discharge → Decrease in dielectric strength	Joint, termination, separable connector	Moisture ingress, poor workmanship	Tracking
Electrical External	Contamination / Oxidation → Surface tracking → Insulation degradation → Increase in dissipation factor at the accessory → Decrease in dielectric strength	Termination	Pollution, Ultra Violet (UV) degradation	Tracking
Thermal	Abnormal Temperature → Reaction Products (ions) → Insulation Degradation → Increase in dissipation factor at the accessory → Decrease in dielectric strength; Oxidation / Dielectric deterioration	Joint, termination, separable connector	Excessive conductor current for a given environment and operating conditions, failed connectors	Hot Conductor

Table 2 Aging mechanism for extruded cable joints and terminations [3]

Type of Deterioration	Aging Process	Typical Causes	Example
Oil Starvation	Oil migration → Oxidation → Changes in paper characteristics; Partial discharge; Localized dielectric heating → Decrease in dielectric strength	Extreme elevation changes, lead (Pb) breach: cracks and corrosion	Well impregnated paper / Poorly impregnated paper
Thermal	Abnormal temperature → Reaction products (ions) → Insulation degradation; Oxidation; Insulation Deterioration → Decrease in dielectric strength	Excessive conductor current for a given environment and operating conditions, poor connection design for installation	Hot Conductors / Oxidized Insulation
Localized Electrical Stresses	Localized stresses → Oxidation → Changes in dielectric characteristics; Partial discharge → Decrease in dielectric strength	Tearing or separation of cable paper due to poor workmanship	Tearing of cable paper
Oil Contamination from Paper to Extruded Cable in Transition Joints	Oil contamination → Swelling / Chemical cracking → Insulation degradation → Decrease in dielectric strength	Poor accessory design, poor workmanship	PILC / XLPE / Oil Contamination

Table 3 Aging mechanism for PILC cable joints [3]

15

High current loads and particularly high cyclic loads are considered to be another cause for a larger number of failures in underground cable joints. High loads cause fatigue to cable joints in many ways but the main factor leading to failure is the mechanical stress in the joint produced by cable conductor under high loads. The investigation performed by Dutch power network owners together with KEMA to identify the cause of the breakdown in their power networks confirmed that considerable number of failures was related to causes of mechanical nature in networks operated at high cycling current loads [39][40].

High current cycling loads cause severe extension and contraction stresses to the connector of the conductors. If the connector used is not fully appropriate for the type of conductor, the connection between conductor and connector will loosen. The high resistance of the joint and high currents produced a significant amount of heat [41]. This as a result leads to the creation of voids in insulation around the joint which would weaken the insulation material and lead to failure of the joint [39].

A considerably large amount of failures in cable joints are related to mechanical forces acting on the joints due to the cyclic heating effects. These cyclic heating effects are due to the cyclic current loads which cause mechanical forces on the cable conductor as they expand when heated. This longitudinal force can be calculated by:

$$F = EA\alpha\Delta\theta \quad (1)$$

where E is the Young's modulus [Nm^{-2}] of the conductor material, A the conductor cross section [m^2], α the thermal expansion coefficient [$\degree C^{-1}$] and Δθ the temperature increase with respect to the ambient temperature of the cable [42].

The failures of accessories are most commonly caused by human imperfection factors. A summary of some of the failure is presented in Table 4.

Failure causes	Visual Indication
Improper stress grading	Failure spot near the insulation screen/shield terminus
Insufficient clearance between shield terminus and conductors	Failure of the insulation along the surface between screen terminus and conductor lug
Semi conducting layer missing over stress control cone ,partly or completely	Failure of insulation
Cut in insulation at the end of semi conducting layer	Direct puncture of cable insulation in the region around termination screen

Improper jointing of conductor	Overheating of joint insulation around the conductor joint
Missing metallic shield or floating shield	Degradation and failure of joint insulation
Improper protective covering of termination	Erosion and tracking at the surface of insulation and termination
Improper sealing of joint	Deterioration of joint due to ingress of moisture
Presence of knife cuts and traces of semi conducting material on the surface of the cable insulation	Rapid deterioration and failure of insulation
Overloading of the cable accessory	Change in colour, softening or charring of insulation over conductor joint and near the lug.

Table 4 Failure causes and visual indication for cable accessories [43].

2.6.1 Diagnostic and Condition monitoring methods for cable joints and terminations

The possibility of diagnosing the health of electrical components is of great demand for Network Operators. In the case of underground electrical components there always exists an unknown state of degradation and therefore it is of a vital importance for Network Operators to have an indication of asset health [12].

A continuous monitoring system of an optical gas sensor is used in Japan to detect concentration of the gas dissolved in the oil up to 5ppm (parts per million). In order to extract the gas dissolved in the oil, a gas cell with a function of separating dissolved gas from the oil was used and installed in the oil ports of an oil-filled cable joint. It was proven that at an early stage of degradation of an oil-filled cable, small electrical discharges occur which generate gases such as hydrogen (H_2), acetylene (C_2H_2), ethylene (C_2H_4), methane (CH_4) and ethane (C_2H_6) [44]. Further discharges cause carbonization of the insulation paper generating C_2H_2. An investigation was made for 75 joints dismantled after faults and it had been verified that C_2H_2 and CH_4 are gases which can provide an early stage of deterioration by continuously monitoring them [45]. The above approach is costly due to the very expensive equipment needed to operate, difficult to implement and cannot be applied in a large scale.

Recently developed diagnostic and condition monitoring systems are based on GPRS data transmission. Meng and Hu [46], developed a monitoring device to monitor real-time the temperature of a cable joint via a digital temperature sensor. When the temperature exceeds a pre-set limit value an alarm signal is sent automatically via GPRS

communication module to the control centre. Furthermore, a judge system is running to check the state of the cable joint through the historical temperature data analysis of the joint, in order to prevent the occurrence of an accident. The device is self-powered through a super capacitor which takes advantage of the principle of electromagnetic induction from the AC voltage of the high voltage cable. Chang et al. [47] used the same arrangement but they combined the GPRS communication protocol with ZigBee in order to achieve transmission of data for longer distances up to 400 m. Their monitoring unit is powered with a set of electronic components connected to a Current Transformer which is connected with the underground cable. Mitsubishi Cable Industries created two systems for online condition monitoring to find hot-spots in underground joints. The first one measures the temperature of the joint using a series of thermocouples (TCs) along the cable joint connected with a PC and the second one uses an optical fibre sensor connected as well to a PC [48]. Diagnostic software to monitor the health of the underground cable joint was developed in the Hydro Quebec Research Institute. Many factors such as critical joint temperature, current load, ambient temperature, cable size, type of cable joint and historical data previously collected are taken into the account to perform the diagnostic of the cable joint [9]. The first two systems are very complex to implement, they have high installation costs and specific operational knowledge is required. Furthermore both systems can only be applied inside transmission underground tunnels. The judgement alarm system might give wrong alerts as it is only taking into account local temperature fluctuations by the cable joint without considering loading demands and weather conditions. The judgement temperature is related to an overheating faulty temperature limit which does not avoid the failure from happening. On the other hand the technique of sending data via GPRS seems to be a useful approach of capturing data from remote locations. Despite the fact that the systems are able to monitor the health of an underground joint they are unable to predict the upcoming failures which are of a great importance for a reliable power network system. The idea of monitoring the temperature of a cable joint through a series of thermocouples (TCs) is cost effective and relatively reliable technique which can be used for large scale implementation.

Partial discharge (PD) monitoring units for cable joints have been developed in recent years. Continuous online PD monitoring systems are able to obtain long-term data relating to gradual deterioration under normal operational stress, from which the characteristics of the PD signal can be extracted to increase the possibility of detecting defect prior to

insulation failure [6]. Hydro-Quebec has developed a portable PD analyser for detection, localization and interpretation of PD in cable accessories such as cable joints. The device is a narrow band AM receiver with a small capacitive probe which through an automated software can detect, discriminated and localize PD among RF signals. The device localizes different defective joints in the Montreal underground network and can carry out remote on-line detection, from a range of 100 metres to a few kilometres, accessories with abnormal PD activity [8]. KEMA has created an on-line tool measuring partial discharges in cables and cable joints. The system is capable to find the origin(s) of PDs from a complete cable connection by using only two inductive sensors, each at one cable termination. The installation of the sensors can be performed while a cable is in service. Data is monitored continuously and collected results are transferred and stored in a centralized Control Centre where results are analysed and interpreted. Results from there are made visible on a secured web-site for the network owners. Field results collected from 100 installed systems detected weak spots by the cable joints which made it possible to replace them before a breakdown occurred [7]. The above systems, based on the PD monitoring, consider only one of many possible degradation mechanisms. Furthermore monitoring the reliability of a whole power network using the above systems is high in cost and difficult to maintain. A huge amount of data is captured and has to be analysed making this technique very time consuming. Nevertheless it might be of a great use if it is possible to reduce the amount of captured data by enabling PD monitoring units when an abnormal temperature on the cable is spotted.

Over the past years there have been a number of failures reported within cable terminations. The biggest number of failures are reported to occur near the termination sealing ends where in some cases the monitored temperatures increase by up to 10 °C [10]. Factors such as poor workmanship [49], high frequency stresses caused by an increased usage of power electronic devices [50][51] and circulating currents on the cable support structure [52] cause the temperature increase by the termination sealing ends. A thermal infrared camera was used for diagnostic purposes in order to identify exactly where the point of failure was [10] on a cable termination. Nevertheless the failure of the cable termination could not be avoided as the failure was detected too late. According to Electric Power Research Institute (EPRI) most cable problems are associated with increased heat generation. This heat generation will lead to the creation of local hot-spots. Hence EPRI suggests that infrared thermography can be used periodically to inspect the

health state of power cable accessories such as joints and terminations [11]. Hydro-Quebec has developed a thermal imaging program based on an infrared imaging camera and the software mentioned in [9] for diagnostics of the condition of underground cable joints and terminations in manholes. They succeeded in reducing the number of failures to cable accessories, such as joints and terminations, by 20 %. That proves that monitoring the accessory surface temperature can give vital information for the state and condition of the accessories. Due to its inspection maintenance nature this technique is repeated every year on accessories where the surface temperature is close to a pre-defined normal reference temperature of the investigated accessory, every six months when their temperature is slightly abnormal and when seen as abnormal the decision is to replace the accessories straight away. Over the that time period of 6-12 months there is no monitoring of the accessories which might be a period of time where a failure can occur [53][54] . On the other hand thermal cameras require skilful and experienced operators who have the knowledge and understanding to distinguish a possible hot-spot as the readings might be affected by weather factors (e.g. air ambient temperature, wind speed), solar reflections, solar radiation and emittance variation [55]. Furthermore the above mentioned diagnostic technique is not reliable enough to identify and prevent a possible failure prior to its occurrence due to the periodical inspection survey that is usually performed. Hence the need of a predictive method that is able to identify degradation at the early stage of the formation is highly relevant.

The use of prognostic capabilities enables the determination and prediction of future health condition of assets [56] [57] while diagnostic techniques can just identify the final stage of an upcoming failure [58] sometimes without leaving enough time to schedule maintenance to prevent faults. Hence implementation of predictive maintenance techniques [59] is vital due to the increasing complexity of power network systems [60]. Different approaches can be used for the implementation of data driven prognostic systems [61]. The most commonly used prognostic technique is predicting the estimated remaining life time of an asset prior to the occurrence of the failure [58] [62][63]. Although the technique of remaining useful life (RUL) looks appealing, in reality it can give just an approximate insight on the condition of the assets as it lacks accuracy and most importantly the confidence to determine the initial stages of degradation activity and thus might not give enough time for operator to take the necessary precautions. RUL prediction systems assume that the deterioration happens at a constant rate which in

reality cannot be valid as sudden changes in real field can accelerate aging drastically and therefore might significantly reduce the estimated remaining useful life of the asset.

It has been found in the published literature that there are a number of approaches and techniques for diagnostic and condition monitoring of cable joints and terminations but there is a lack of reliable prognostic approaches for these accessories.

2.7   Summary

It has been found that factors such as electrical, mechanical, thermal, environmental and combinations of them are the main reasons for underground cable aging. Thermomechanical aging is a major factor affecting the lifetime of the underground cables. Daily load cycles cause cyclical heating and cooling of the cable which cause movement and hence bending of the underground cable which leads to damage and failure, particularly at the cable joints and terminations. In some cases it may cause formation of microvoids which respectively under wet or dry environmental conditions will result in water or electric trees. High ambient temperatures can cause drying out and movement of the soil and consequent mechanical damage to the cable. During the high cable loading demands high temperatures might cause cable overheating and thus breakdown of insulation which will lead to failure of the cable and cable joints or terminations.

Joints and terminations of the cable are installed manually and very often under poor weather conditions. Thus their health and lifetime maybe directly related to human factors. Such factors include poor workmanship, lack of appropriate stress control or inappropriate fitting of the accessories under constant exposure to high loads and thus thermomechanical stresses will accelerate the aging and reduce lifetime.

Different diagnostic and condition monitoring techniques for cable joints and terminations have been developed over the last decade. Some of them are based on optical gas sensors, temperature sensing with GPRS data transmission, partial discharge diagnostics and condition monitoring units and finally temperature monitoring techniques for cable joints and terminations.

It can be concluded that the extension of condition monitoring and diagnostics of cable joints and terminations to prognostic indicators is of importance as these accessories

appear to be the weakest point in underground cable systems. By observing the health and operational condition of underground joints and terminations, improved reliability of power networks can be achieved as well as reduction in costly repairs.

An increased temperature of the underground cables has proved to be the most common aging effect initiating different aging mechanisms such as electrical, thermomechanical, environmental factors or combinations of them. Therefore by continuously monitoring the temperature of the investigated cable accessories, such as cable joints and terminations and by developing thermal prognostic techniques it may be possible to avoid catastrophic failures by taking actions prior to their incidence.

Chapter 3 gives a better understanding of how the magnitude of the potential fault within the cable might reflect on the surface temperature of it as well as it investigates the possibility of developing the thermal prognostic models using machine learning regression techniques such as Support Vector Regression (SVR), Artificial Neural Network (ANN), Multiple Linear Regression (MLR) and Gradient Boosting (Mboost). Each of the above mentioned algorithms is used to predict the likely surface temperature of the cable in the air-filled trench and their performance is compared in order to choose the one with the best performance to continue with the further development of the models.

Chapter 3 Design of a Thermal Prognostic model

This Chapter investigates the feasibility of identifying abnormal temperature changes on the cable surface using a thermal cable model created in COMSOL. Four machine learning regression techniques based on Support Vector Regression (SVR), Artificial Neural Network (ANN), Multiple Linear Regression (MLR) and Gradient Boosting (Mboost) are introduced and discussed. Benchmarking between them based on their accuracy to predict the cable temperature in an air-filled trench was performed. The SVR showed better performance and thus was chosen to be further investigated for the development of the thermal prognostic models described in Chapter 4, 5 and 6. Hence a more in depth theoretical background of the SVR and the development techniques of it are discussed.

3.1   Thermal cable model in COMSOL

As it has been mentioned before a great number of faults in cable systems are related to heat generation. EPRI suggests four temperature stages of concern in their survey. The first one is the advisory stage where the rise of the temperature is between 0.5°C and 8°C above a reference temperature, the second stage is the intermediate stage where the temperature increase is between 9°C and 28°C, the third is the serious stage where temperature is between 29°C and 56 °C and the last stage is the critical stage where the temperature is above 56°C above the reference temperature [11]. The reference temperature is considered to be the normal operating temperature of the investigated cable system or accessory.

In order to investigate in more detail the magnitude of an internal fault inside a cable related to the change of surface temperature of a cable, a simple thermal model was developed to simulate temperature rise as a function of thermal power supplied by a fault. A 5m long cable was designed in COMSOL based on a cable manufactured datasheet which all the details can be found in Appendix 1. An internal hot-spot was introduced in the middle of the cable under constant loading condition. Four different hot-spot profiles of 2.5W, 5W, 7.5W and 10W where used. Figure 5 shows the surface temperature distribution on the cable with the introduction of hot-spots.

With reference to Figure 5, a significant rise of temperature of the cable surface can been seen a several meters away from the source, if the source is large enough. An increase of temperature at 0.25 m away from the location of the fault for the 2.5W, 5W 7.5W and 10 W was respectively 1.5, 3, 4.5 and 6 degrees Celsius. This increase corresponds to 0.60℃ per W. The same temperature increase was recorded for a constant and cyclic loading. An important factor to investigate further was the time needed for the cable surface located 0.25 m away from the centre of the cable to increase by 1˚C.
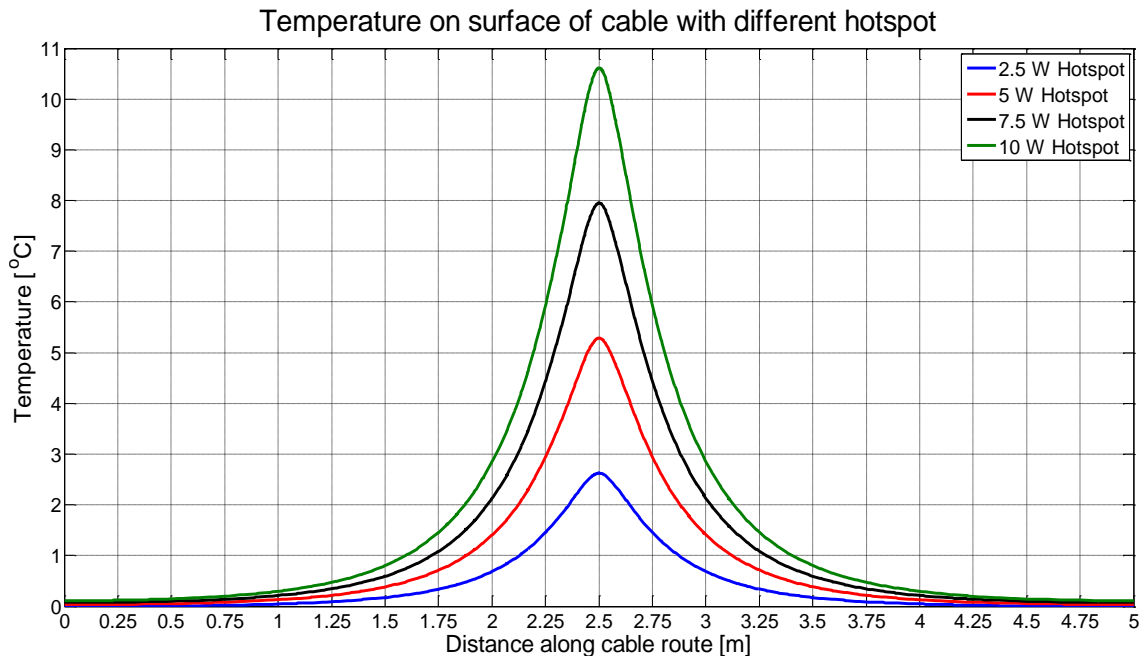
Fig. 5 Cable temperature distribution under the influence of the hot-spots.

The Figure 6 shows the relationship between the temperature increase and the time.
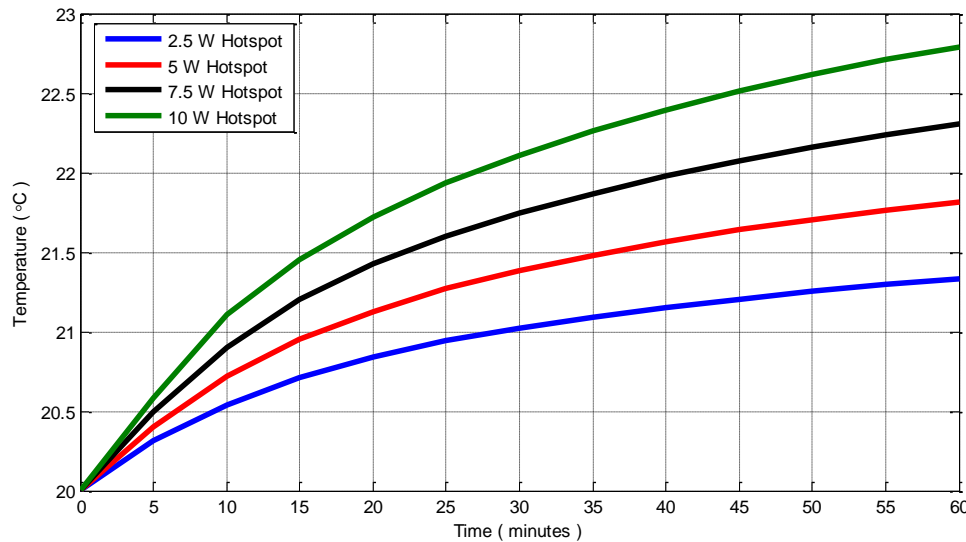
Fig. 6 Relation between temperature increase and time at 0.25 m away from the

center of the cable.

24

It can been seen in Figure 6 that for a 2.5 W hot-spot around 30 minutes is needed to see an increase of the surface temperature by $1°C$. As the power of the hot-spot increases the time needed for the cable surface temperature to increase by $1°C$ is reduced. Hence a 30 minutes prediction horizon is an ideal time gap that can be used by the thermal prognostic models to identify an increase of temperature by $1°C$. Furthermore the increase of $1°C$ was chosen as a measure of comparison as most of the existing monitoring units have a minimum accuracy $\pm 1°C$ [64][65][66]. Therefore if it is possible to identify abnormal temperature behaviour on the joint surface or cable terminations it is likely to be indicative of a fault.

3.2   Machine Learning Algorithms: Artificial Neural Network (ANN), Support Vector Regression (SVR), Multiple linear regression (MLR) and Gradient Bosting (Mboost)

Machine Learning is a branch of artificial intelligence which is based on the construction and study of systems that are able to learn from training data and produce a model which is able to determine and find a solution for an underlined problem. In this section machine learning algorithms are introduced and briefly discussed.

Linear regression attempts to model the relationship between a scalar dependent variable y and one or more independent variables x. In the case where more than two independent variables are used to describe the relationship between input data and output data then the model is called multiple linear regression (MLR) [67]. Linear regression is one of the oldest types of regression [68] and due to its simplicity has been used in a variety of prediction problems such as in water quality [69], mass of solid waste generation [70], estimation of time-frequency electrophysiological responses in neuroscience [71], prediction of swell potential of clayey soils [72] in geological sciences as well as in management for capital structures [73]. The MLR performs well in situations where there is a clear relation between input data and output data as it is shown in the case of oilfield output forecasting [74]. In the cases where there is a more complex and nonlinear relationship between input and output data ANN outperforms MLR [70] [72].

The concept of the Gradient Boosting is to combine multiple models alongside with weights into a single prediction model [75] [76] [77] [78]. Two Gradient Boosting machine algorithms were ranked in the top 5 algorithms in a GEFCom load forecasting

competition in 2012 [79] [80]. They were also successfully used by the pharmaceutical industry to predict the biological activity of molecules [81], in transportation research to predict freeway travel time [82] as well as in finance to predict insurance losses [83]. Gradient boosting machines can affectively solve a variety of non-linear problems but have several drawbacks such as memory and time consumption as well as being difficult to design [84].

An ANN is a widely used data modelling tool that simulates the way how the neurons work in the human brain. The method of non-linear mapping which transforms data from R^I to R^K, where I and K are the dimensions of the input and output space, is used to express complex functions [85]. An ANN is based on interconnected nodes which are simply processing elements. Weights are connected with each of the inputs to a given neuron. This connection controls the strength of the input data. By manipulating these weights an ANN is able to create a model where the data is presented as patterns of input-output pairs [86].

The ε-Support Vector Regression aims to determine a function that has a maximum ε deviation from the targets output values and at the same time is not complex. As long as the errors do not exceed the deviation parameter ε, they are not taken into account but errors larger than ε are penalized [87].

Artificial Neural Networks aim to minimize the empirical risk error over a given set of data and try to fit the data as closely as possible. This results in a solution function which works very well on a known training data but poorly on unknown data. This is known as overfitting. In the SVR the issue of overfitting is less common because the algorithm is trying to minimize both the empirical risk error and the generalization error (model complexity) [88]. The less complex model results in better fitting of unknown data. Another advantage of the SVR algorithm over ANNs is that it always converges to a solution. ANN can work better with massively large data sets while SVR is limited by speed and memory constraints [89].

The Support Vector Regression algorithm has shown better performance and generalization ability in a variety of problem solving such as short-term temperature prediction [89], daily maximum temperature prediction [90], protein structure prediction in bioinformatics [91], financial forecasting [92], structural engineering [93] than ANN.

3.3 Benchmarking of Predictive Techniques

Four different machine learning algorithms were used and compared to identify which one has a better performance. A variety of regression techniques based on Support Vector Regression (SVR), Artificial Neural Network (ANN), Multiple Linear Regression (MLR) and Gradient Boosting (Mboost) have been used to determine the most appropriate one and the implementation stages are shown in Appendix 2. Figure 7 shows the temperature prediction using the four different algorithms based on data collected from an air filled trench. The first 8 days were used for training and the last 4 days for testing as it is a common practice to use 2/3 of the dataset for training and 1/3 for testing [94]. Figure 8
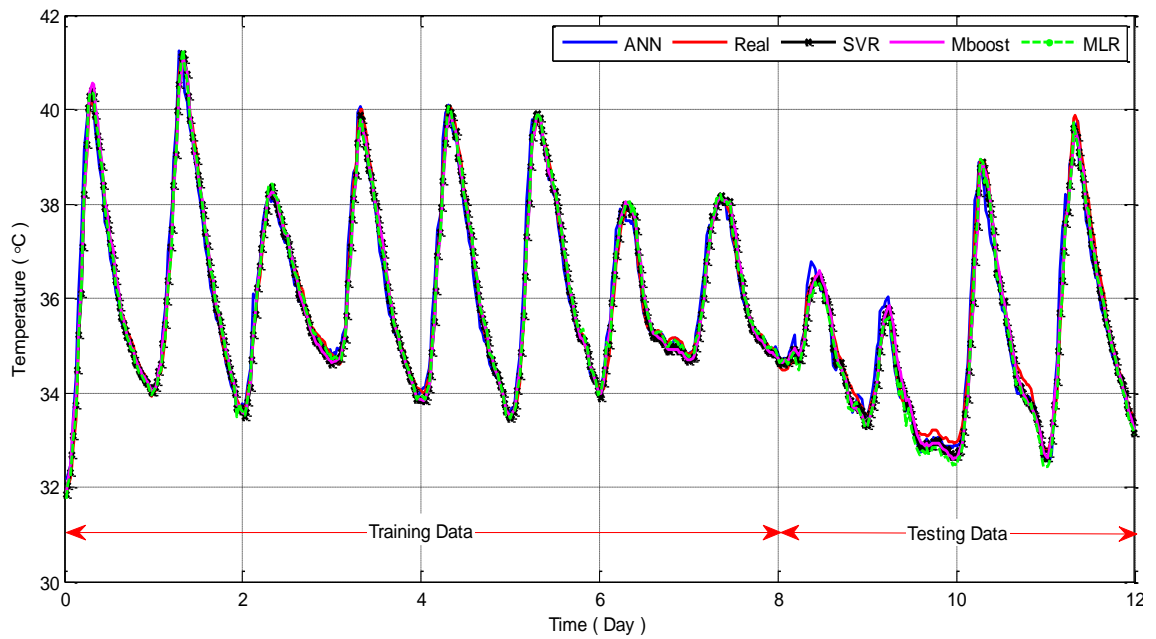
Fig. 7 Temperature prediction comparison between ANN, SVR, Mboost, MLR with the real temperature.
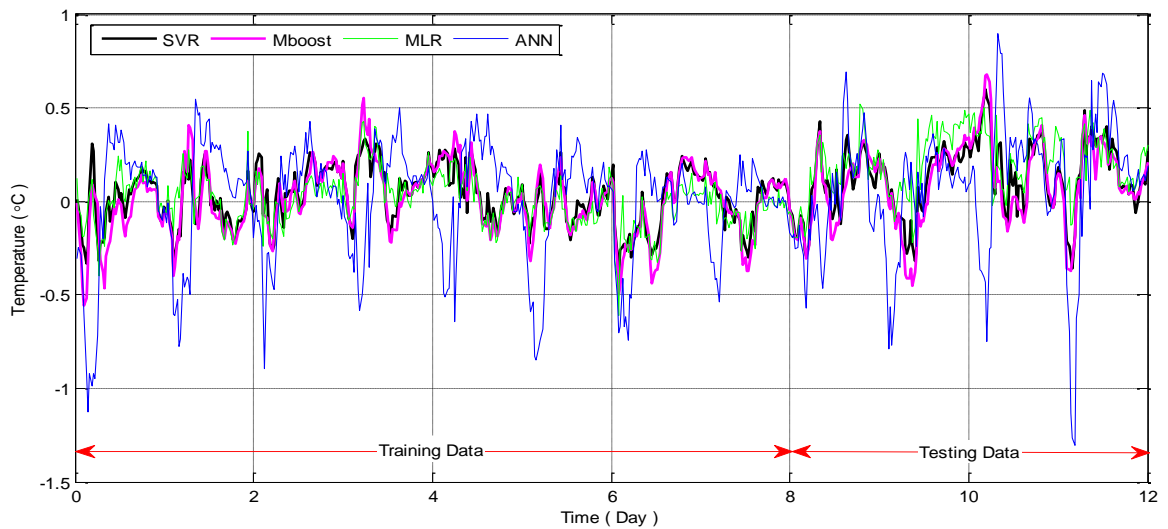
Fig. 8 Temperature prediction error for ANN, SVR, Mboost and

27

shows the temperature prediction error graph where the difference between the real-time measured temperature and the model output prediction temperature for each of the 4 benchmarked algorithms is presented. The performance of the algorithms is summarized in Table 5, by calculating the mean absolute percentage error (MAPE) as defined by [95]:

$$MAPE = \frac{100}{n} \sum_{i=1}^{n} \left| \frac{y_a(i) - y_p(i)}{y_a(i)} \right| \qquad (2)$$

where y_a the real value of TCs temperature, y_p is the predicted value of TCs temperature and n is the total number of samples.

Algorithms	Error (MAPE %)	Parameters
SVR	0.66	C = 16384 γ = 9.7656e^{-4}
MLR	0.70	
Mboost	0.73	Iteration = 700 nu = 0.15
ANN	1.20	Layers = 9

Table 5 Benchmarking results for air filled trench.

From the obtained results it can been seen that SVR showed the best performance. The MAPE for SVR was 0.66% while for ANN, which showed the worst performance, it was 1.20%. MLR and Mboost showed satisfactory performance as well but not as good as the SVR. It can be clearly seen from Figure 8 that ANN produces an overestimated model compared to the other three algorithms. Furthermore ANN training is always a time consuming process because of the algorithm's nature. Every time the ANN is trained the weights are initialized randomly which each time results in a different prediction output model. In order to achieve the best prediction output, the ANN was trained 10 times and the model with the lowest MAPE error was selected. Hence due to its better performance, less training time is needed and the simplicity of its use, it was decided to continue further investigation and development of the prediction models using the SVR algorithm. SVR is able to avoid overfitting problems, creates less complex models that always converge to a solution. The test was performed in order to choose the machine learning algorithm to continue with the further development of thermal prognostic model techniques which aim to identify potential hot-spots on the cable surface in a variety of environments such as soil and air as described in Chapters 4 and 5. A benchmarking between the algorithms is performed as well in Chapter 5 to verify the performance of SVR in the soil

environment as well as to validate the choice of SVR for the field experiments in Cyprus described in Chapter 6.

3.4   Support Vector Regression and SVR Development

Support Vector Regression (SVR) is a machine learning algorithm which uses a non-linear mapping to transform data into a high dimensional feature space where linear regression is performed [88]. SVR has the advantage that not only does it fit the training data in order to find a solution but also keeps the highest possible degree of generality when new unseen data is introduced [89].

The ε-SVR is used to predict the values by solving the following optimization problem [87]**:**

$$\text{minimize} \quad \frac{1}{2}\,\|w\|^2 + C\sum_{i=1}^{l}(\xi_i + \xi_i^*)$$

$$\text{subject to} \quad \begin{cases} y_i - w^T\varphi(x_i) - b \;\leq\; \varepsilon + \xi_i \\ w^T\varphi(x_i) - y_i + b \;\leq\; \varepsilon + \xi_i^* \\ \xi_i, \xi_i^* \geq 0 \end{cases} \tag{3}$$

where x_i is a feature vector of the input space with dimension N, y_i is the output value to be estimated, b is a parameter of bias, w is a weight vector which controls the smoothness of the model, φ(x) is a function used to map training samples x_i to a higher dimensional feature space, penalty factor C controls the trade-off between complexity of the function and the frequency with which errors are allowed and ξ_i and ξ_i^* are slack variables which compute the error for overestimating and underestimating the true output value y_i. The parameter **ε** determines the maximum deviation from the target output value y_i. Figure 9 shows the situation graphically. This above optimization problem can be transformed into the dual problem, as mentioned in [96] and its solution is given by:

$$max_{\alpha,\alpha^*}\left[-\frac{1}{2}\sum_{i,j=1}^{l}(\alpha_i - \alpha_i^*)(\alpha_j - \alpha_j^*)K(x_i, x_j) - \varepsilon\sum_{i=1}^{l}(\alpha_i + \alpha_i^*) + \sum_{i=1}^{l}y_i(\alpha_i - \alpha_i^*) \right]$$

$$\text{subject to} \quad \begin{cases} \sum_{i=1}^{n}(\alpha_i - \alpha_i^*) = 0 \\ 0 \leq \alpha_i, \alpha_i^* \leq C, i = 1, \dots, n \end{cases} \tag{4}$$

Having estimated α, α* and b, using a suitable quadratic programming algorithm, the SVR based regression function solution is given by:

$$f(x) = \sum_{i=1}^{Nsv} (\alpha_i - \alpha_i^*) K(x_i, x) \qquad (5)$$

where Nsv denotes the number of the Support vectors. The kernel function $K(x_i, x)$ is used to avoid the complicated calculations of the inner products of the mapped inputs in the feature space φ(x). The bias parameter b is calculated automatically and accommodated within the Kernel [97] [98].
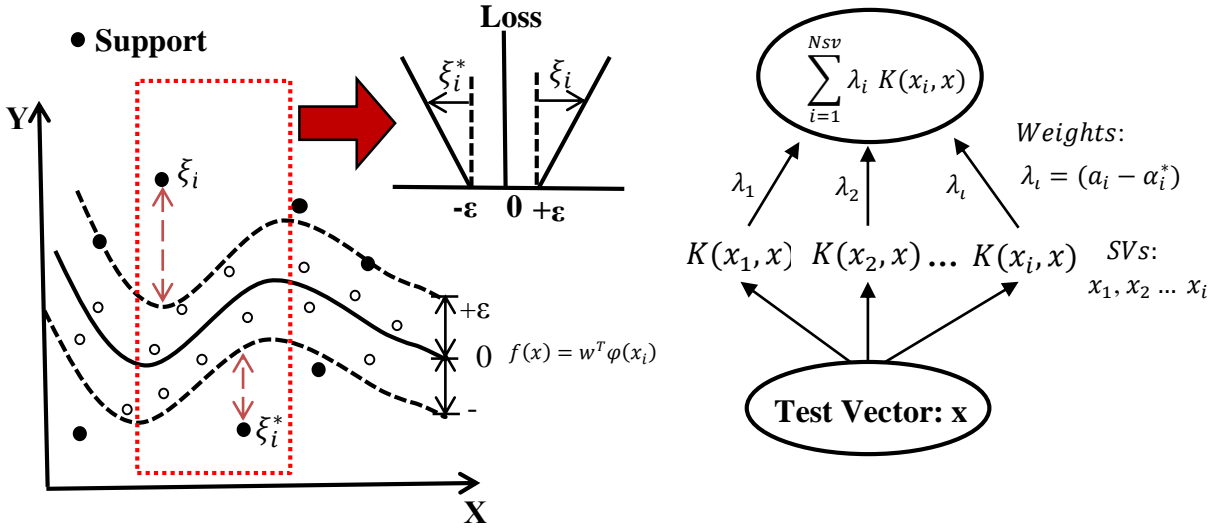

Fig. 9 The parameters for the SVR algorithm

The vector w is described in terms of the Lagrange multipliers α_i and α_i^*. Only some of the coefficients $(a_i - \alpha_i^*)$ are non-zero and the corresponding input vectors x_i are called support vectors (SVs). The SVs can be thought of as the most informative data points that compress the information content of the training set. The coefficients α and α* can be seen as forces pushing and pulling the regression estimate $f(x)$ towards the measurements y_i.

Lagrange multipliers α_i and α_i^* will be non-zero values for training points "above" and "below" an ε-tube. Because no training data can be on both sides of the tube, either α_i or α_i^* will be non-zero. For data points inside the tube, both multipliers will be equal to zero.

30

The final answer of the $f(x)$ as shown in Equation 5 is as an approximation function of N sum of Gaussian RBF functions which have as their center the Support Vectors. The parameter γ controls the width of the Gaussian RBF function while the parameter C which is related with the Lagrange multipliers α and α* controls the amplitude of it.

3.4.1 Kernel Selection

The kernel function is used to allow operation in the input space instead of the potentially high dimensional feature space. Hence as was mentioned before the inner product does not need to be computed in the feature space. There are different types of kernel functions such as Gaussian Radial Basis Function, Exponential Radial Basis Function, Multi-Layer Perceptron, Fourier Series, Splines and etc. There is no a straightforward way to select a kernel function yet, but the most effective for general use has been found to be the Gaussian Radial Basis [99]. Hence the Gaussian - Radial Basis Function (RBF) is used in this research which is defined as:

$$K(x_i, x) = e^{(-\gamma \|(x_i - x)\|^2)} \qquad \gamma > 0 \qquad (6)$$

where parameter γ controls the width of the Gaussian-RBF kernel function of the model.

3.4.2 Data Preparation

Input data has to be scaled before being imported in the SVR in order to avoid features with larger numeric values being dominant to those with smaller values. Furthermore scaling makes the computation easier during the application of the kernel function. In this model the data was scaled from [0,1] as follows:

$$X_{scale} = \frac{X_i - X_{min}}{X_{max} - X_{min}} \qquad (7)$$

where X_i is the original data, X_{scale} the scaled data, X_{max} and X_{min} are the maximum and minimum values of X_i.

3.4.3 Grid-Search and Cross-Validation

The penalty factor C and the kernel parameter γ have to be decided by the user of the LIBSVM [100] MATLAB toolbox in order for the regression model to be developed. The

aim is to identify a good pair of C and γ so that the classifier can accurately predict unknown data. To identify the most appropriate C and γ two algorithms are combined together, Cross-Validation and Grid-Search. The training data are split into K segments with equal size in K-fold cross-validation and then each segment is predicted by the remaining K-1 segments sequentially. For each of the iterations of the Grid-Search, a combination of C and γ values are tested and the one with minimum Cross-Validation error is selected. C and γ pairs are change based on the grid-search algorithm which suggest exponentially growing sequence for C (2^{-5}, 2^{-3}... 2^{15}) and γ (2^{-15}, 2^{-13}... 2^{5}).

3.4.4 Choosing SVR parameter C, γ and ε

The user has to select in ε-SVR the tuneable parameters C, γ and ε, which is not a straightforward procedure as all of them play a significant role to achieve a good generalization performance.

The parameter C as was mentioned earlier, controls the trade-off between complexity of the function and the frequency with which errors are allowed. From Equation 3 it can be seen that if C has a large value more emphasis is placed on the empirical error $\sum_{i=1}^{l}(\xi_i + \xi_i^*)$ while if C is small, more emphasis is placed to the generalization error $\frac{1}{2} \|w\|^2$. That is why parameter C has to be tuned in such a way that it will offer a balance to the model.

The parameter γ controls the width of the Gaussian-RBF kernel. When γ is small, the Gaussian function is wide and hence the parameter C can has higher values. On the other hand when γ is large, the Gaussian function is narrow and thus C cannot have very large values. The combination of C and γ controls the input range of the training data and therefore these two values are considered to be best tuned together as mentioned in Section 3.4.3.

The parameter ε controls the width of the ε-insensitive zone of the loss function which is used to fit the training data. It depends on the deviation of the target output value in the training set. A large value of ε will result in fewer Support Vectors and therefore to a less complex- under fitting regression model. On the other hand small values of ε will increase the number of Support Vectors resulting in a complex- over fitting regression model. As ε is associated with the deviation of the output value from the training data, choosing ε to

have certain accuracy will result in improved accuracy results. The temperature data collected in the experiments has a precision of two decimal places hence the value of $\varepsilon=0.01$ has been selected.

3.5   Summary

From the thermal simulation model created in COMSOL it can be concluded that internal faults in the cable may generate heat and increase the cable surface temperature several meters away from the location of the fault, if the fault is large enough. It has been found using the simulation model that for the 2.5 W internal fault, smallest power fault, the increase of the cable temperature by $1^{\circ}C$ can be detected approximately 30 minutes after the occurrence of the fault. Hence a 30 minutes prediction horizon is used for the development of the thermal prognostic models described in Chapters 4, 5 and 6.

In terms of prediction of future behaviour, the SVR was selected to be investigated rather than MLR, Mboost and ANN as it shows better performance during the temperature prediction for a cable in an air filled trench. Furthermore SVR is able to avoid overfitting problems, develop less complex models which are always converged to a solution. An in-depth analysis of SVR was performed and the SVR development steps were investigated in more detail.

The developed methodology was later implemented during the constant and cyclic load experiments in air-filled trench and the on 33 kV closed loop cable termination to establish initial thermal prognostic models as well as to verify viability of the chosen methods for monitoring of cable accessories that are likely to be affected by the hot-spot activity through a series of sensitivity tests as it is further described in Chapter 4.

Chapter 4 Implementation of Thermal Prognostic Models for the Air Trench and 33 kV Cable Termination in Air

Two different experiments were used to investigate the feasibility of different approaches for monitoring underground cables, in the areas where hot-spots are more common to occur, such as joints and terminations. The first experiment was performed in an air filled trench while the second was performed in a 33 kV closed loop cable termination in air. In both experiments the operation of power cables were simulated using a programmable control system able to simulate a wide range of cable loading. The surface temperature of the cables were continuously monitored by a series of TCs as well as the weather conditions such as solar radiation, wind speed and air temperature. It is hypothesised that an increase of the local cable temperature is indicative of accelerated aging of the cable insulation due to thermomechanical, electrical and environmental factors.

Thermal prognostic models have been established using a Support Vector Regression (SVR) algorithm which predicts the likely temperatures along the cables 30 minutes into the future, according to weather conditions and known loading. A series of different sensitivity tests as well as the pre-processing data analysis for the input feature data were performed in order to investigate which input parameters are crucial for the development of a generalized and robust thermal prognostic model. Anomalies of temperature measurements along the cable compared to predicted temperatures can indicate possible degradation activity in the cable.

4.1   Experimental Design and Development for Air filled Trench

A model surface trough was used to develop a thermal prognostic model which aims to predict the likely temperature impact on a cable at burial depth according to weather conditions and known loading. Initial experiments were performed in an air filled trench to investigate the relationship between weather conditions and the constant power demand as well as to investigate if the standard T-type thermocouples (TCs) are sensitive enough to detect the existence of the increased cable surface temperature produced by a hot-spot.

4.1.1   Trench Instrumentation

The cable trough experiment consisted of two 3.95 meter trenches one filled with small grain sharp sand and the second is unfilled. Simulated cables are constructed by a heater tape wrapped around a length of aluminum pipe. The tape has a nominal power of 400 W, thus for a pipe of 3.95 meters the maximum heat loss is approximately 100 W per meter. The surface temperature of the cable is continuously monitored using 22 TCs placed on the cables at various positions within the unfilled trench. The abovementioned trough have been constructed and used in a previous research project for the investigation of cable ratings of underground cables in unfilled and soil filled trenches hence more details can be found in [101].

Figure 10 shows the position of the TCs layout in the unfilled though. All the TCs are connected to the Campbell Scientific datalogger CR1000 via a 32 channel multiplexer. The datalogger record the temperatures every 1 minute giving an average value every 5 minutes.
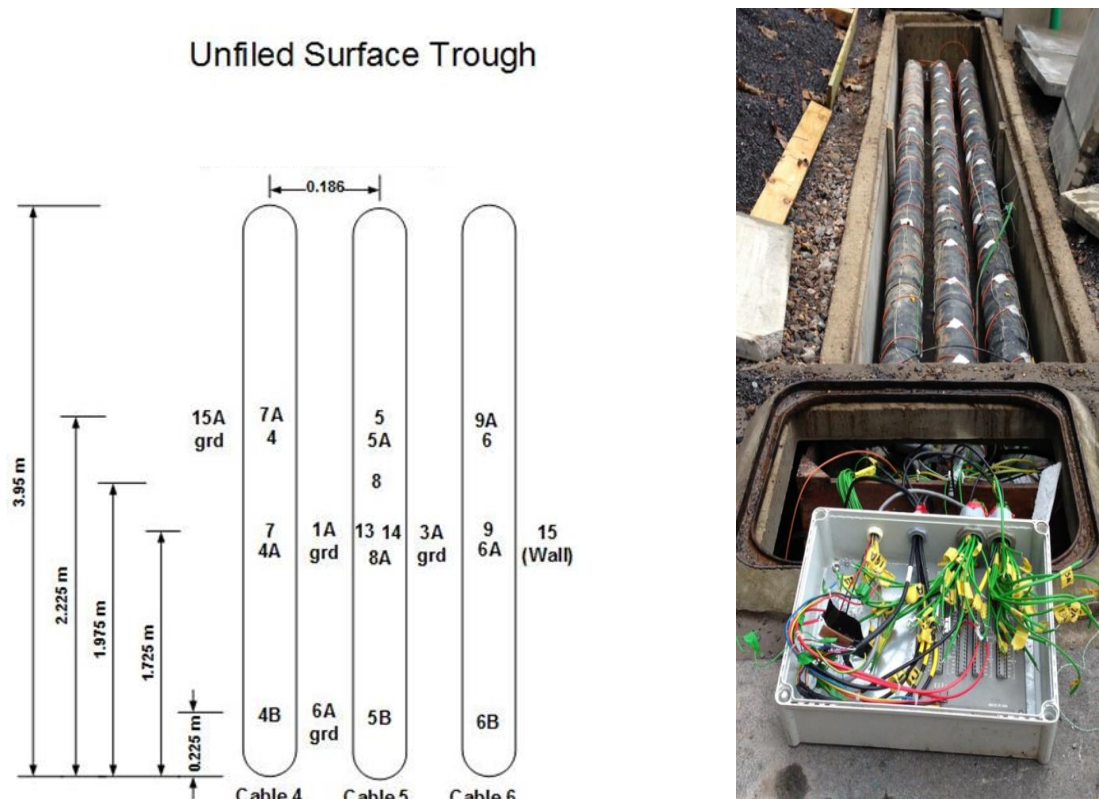
Fig. 10 Layout of TCs in the unfilled surface trough.

A weather station installed on the roof of Tony Davies High Voltage Laboratory is used to collect measurements of weather conditions. Table 6 below shows the weather condition factors that are monitored by the Campbell Scientific datalogger CR10.

Factors	Unit	Measurement Interval	Averaging Interval
Air Temperature	˚C	1 minute	5 minutes
Solar Radiation	Wm^{-2}	20 seconds	5 minutes
Wind Speed	ms^{-1}	20 seconds	5 minutes

Table 6 Recordings of the Weather Data

4.1.2   Control System

A computer program is used to operate various pre-set load/time profile patterns to control the heat output to the simulated cables shown in Figure 11. The controller sets the voltage supply to the heater tape whilst reading the current and voltage flowing through the tape as shown in Appendix 3. A variable transformer (Variac) is connected to each simulated 3-phase cable and a stepper motor is connected to the Variac in order to control its output voltage. The control system is based on the Data Acquisition system of National Instrument (NI) USB-6008. The NI USB-6008 provides connection to eight analog input (AI) channels, two analog output (AO) channels, 12 digital input/output (DIO) channels, and a 32-bit counter with a Full-Speed USB interface. Current transducers are used to convert the real time current in the cable (0-2 A) into a voltage output (0-10 V DC) and voltage transducers to convert the output voltage from the Variacs (0- 240 V AC) into a lower voltage (0-10 V DC) . The output signals from both transducers are read real-time by the NI USB-6008 device which collaborates with a Control Algorithm written in LabVIEW to send the appropriate digital signals to the stepper motors and adjust the corresponding power profile demands. The schematic diagrams for the stepper motors, voltage and current transducers in relation with the NI USB-6008 are shown in Appendix 3.
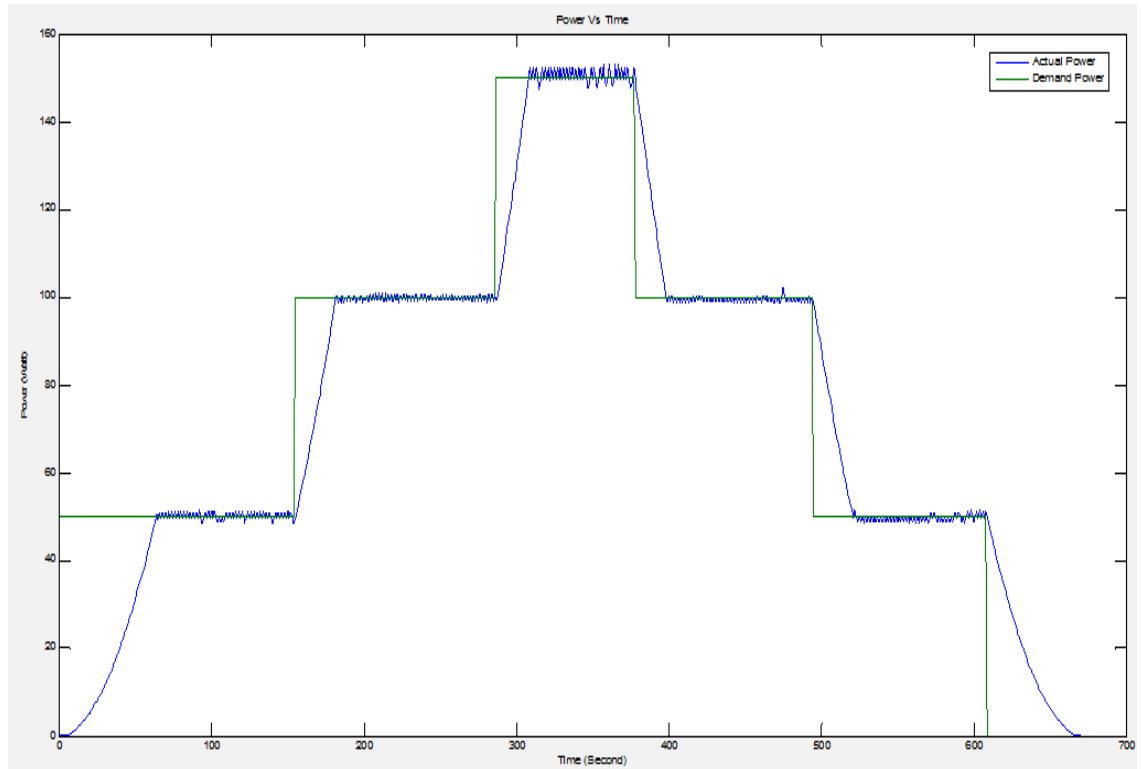
Fig. 11 Cyclic power demand profile

As the heater tapes are essentially resistances, the actual power is calculated in real-time by multiplying the readings from the voltage transducer and current transducer values. According with the power demand value the NI USB-6008 sends a digital signal to the stepper motor in order to rotate it clockwise or anticlockwise to increase or decrease the power output from the corresponding Variac and adjust the demanding power. A schematic of the controller system and the program flowchart is shown in Figures 12 and 13.
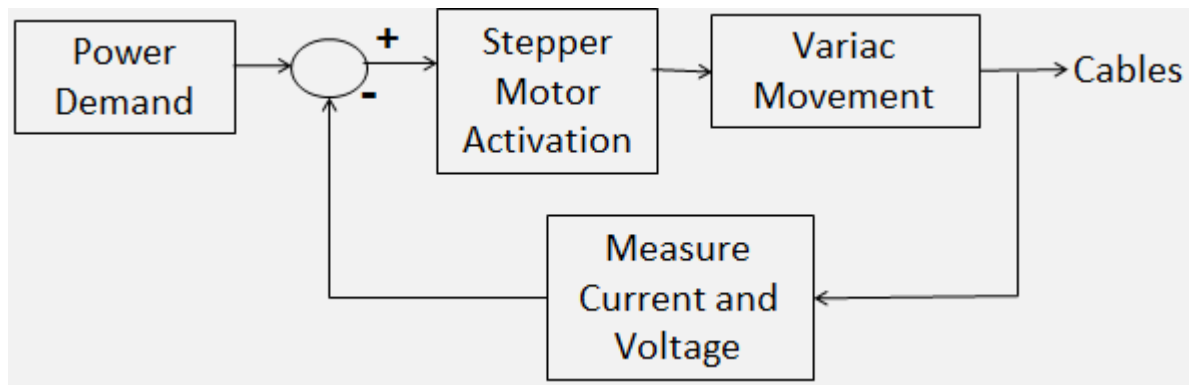
Fig. 12 Simulated Cable power output control system

37
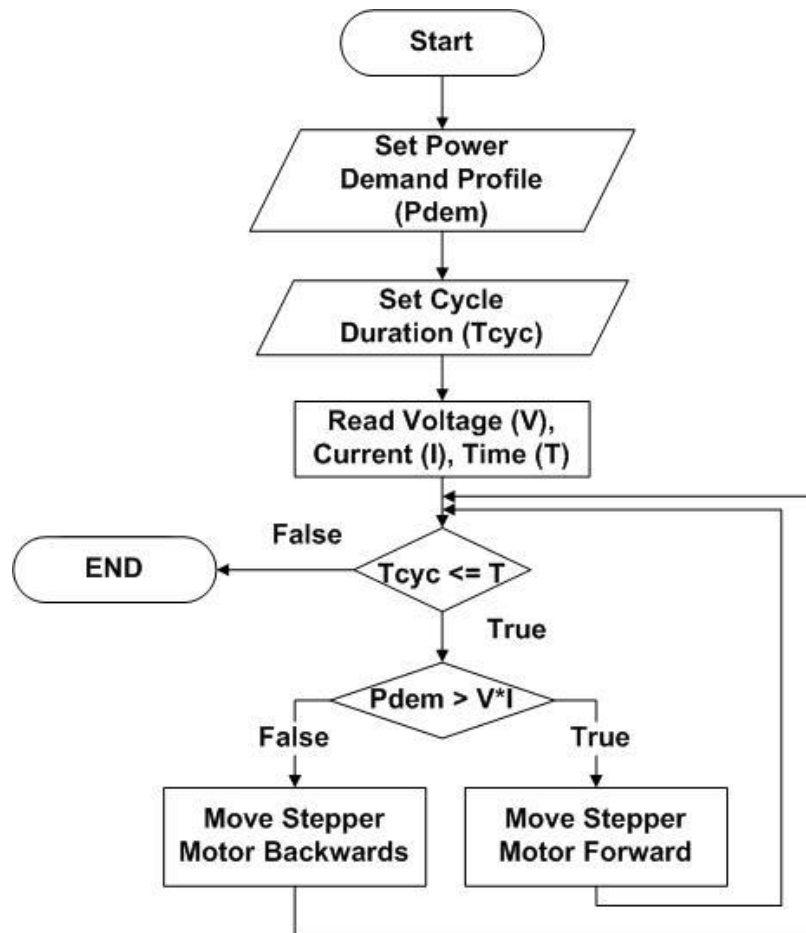
Fig. 13 Flowchart of the power demand algorithm program

4.2 Sensitivity tests and Pre-Processing

An analytical approach was made during the implementation of the thermal prognostic model for the air filled trench in order to investigate different parameters that have to be taken into the account prior to the development of a robust and generalized model. The performed investigation includes the optimal time needed to average the input data, which weather parameters are needed, the amount of input data needed, how many hours ahead a model can predict and finally whether it is possible to monitor specific areas of an underground cable, where hot-spots are more likely to occur, such as joints and terminations.

Weather data and cable surface temperature data were taken from 7th - 28th of August 2013. The weather data used initially were solar radiation, air ambient temperature and wind speed. TC 6B (positioning can be seen in Figure 10) is used as an input variable for SVR training as it is the TC with the lowest temperature reading. The cables were loaded

with a constant power demand of 100W which for a cable of around 4 m it has an output heat loss of 25 Wm^{-1}.

4.2.1   Sensitivity test for time averaging of the input data

Four different averaging minutes intervals (30 minutes, 15 minutes, 10 minutes and 5 minutes) have been taken in order to identify which is the best averaging sample time that has to be used in order to predict the temperature for the cable surface temperature at position of TC 13 (positioning can be found in Figure 10) in a prediction time horizon of 30 minutes. Four different models based on averaging time were built and the corresponding performance was calculated. All models were trained and tested with the same proportion of data (8 days training and 4 days testing) while the MAPE was calculated. This stage is very crucial as it calculates the prediction accuracy of the model obtained from the unknown data and reflects the performance on classifying and independent data set. For each model the optimum combination of C and γ was found. Obtained results are presented in Table 7.

Time	C	γ	Error (MAPE)
30 minutes	32768	$4.8828*10^{-4}$	0.84%
15 minutes	8192	0.002	0.89%
10 minutes	8192	$4.8828*10^{-4}$	0.92%
5 minutes	8192	$1.2207*10^{-4}$	0.95%

Table 7 Best SVR testing accuracies and optimized parameters.

The model based on averaging input data every 30 minutes showed best performance. By averaging the data every 30 minutes it was possible to filter and remove any electromagnetic interference from the thermocouple measurement readings and hence to achieve a smoother input data for the SVR. Reducing the averaging sampling time made the random fluctuation of the real data values higher thus making it difficult for the SVR to produce a generalized model. For a 30 minutes ahead prediction SVR has to calculate one data point for the case of the 30 minutes model, two data points for 15 minutes model, three data points for 10 minutes model and six data points for 5 minutes model. The reduction of the sampling averaging time will cause a more complex system as the SVR has to perform more calculations while training and testing time will increase as well. Furthermore 30 minutes averaging sampling time proved to be sensitive enough to monitor the increase of abnormal temperature on the cable surface even when the external

cable heater failed and caused the temperature to increase up to 135 degrees Celsius over a period of 1 hour.

4.2.2   Sensitivity test for weather parameters

A study was undertaken in order to identify which weather parameters are the most dominant and need to be taken into account during the development of the thermal prognostic model. Four different models were built, trained and tested with the same proportion of data, 8 days training and 4 days testing, while MAPE was calculated. The prediction horizon of 30 minutes and the TC 13, located 1.725 m from the beginning of the middle cable 5, were chosen. Model 1 includes the parameters of solar radiation and the cable surface temperature of a point far away from the location of TC 13 which in this case is TC 6B. Model 2 includes the parameters of air ambient temperature and the cable surface temperature of TC 6B. Model 3 includes the parameters of solar radiation, air ambient temperature and the cable surface temperature of TC 6B. And finally model 4 includes the parameters of solar radiation, air ambient temperature, wind speed and the surface temperature of the TC 6B. For each model the optimum combination of C and γ was found. Obtained results are presented in Table 8.

Model	C	γ	Error (MAPE)
1 (SC)	16384	$4.8828*10^{-4}$	1.05%
2 (AC)	16384	$9.7656*10^{-4}$	1.10%
3 (SAC)	16384	$9.7656*10^{-4}$	0.96%
4 (SACW*)	16384	$2.4414*10^{-4}$	1.03%

* Where S=Solar, A= Ambient, W= Wind and C= Cable surface

Table 8 Best SVR testing accuracies and optimized parameters for sensitivity test of weather parameters

The Figure 14 shows the temperature prediction error, which is defined as the measured temperature minus the predicted temperature, between the Model 2 (worst) and Model 3 (best).
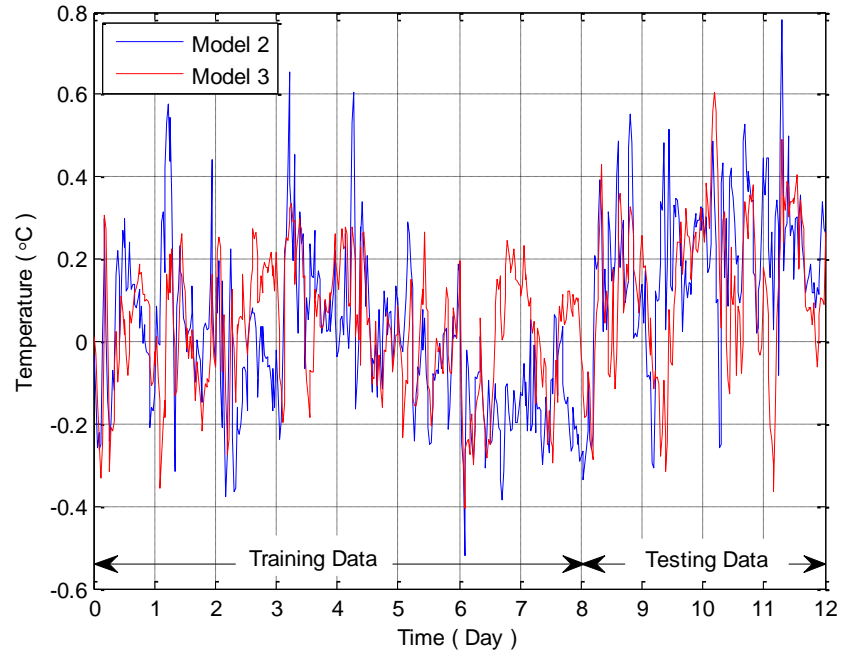
Fig. 14 Temperature prediction error for Model 2 and Model 3 for TC 13.

The maximum temperature prediction error defined as:

$$Max\ Temp\ Prediction\ Error = |3 * \text{std(model error)} + \text{mean (model error)}| \quad (8)$$

was for Model 2 ±0.51℃ and for Model 3 ±0.39℃. The error difference is not that significant because the models are developed with small amounts of training data but as the amount of training data increases the error difference will become greater. Hence it is better to choose the model with the lowest error deviation, which in this case is Model 3. The overall temperature uncertainty error is of the order of ±0.6℃, which is due to data logger temperature uncertainty (±0.1℃) and the T-type thermocouple (±0.5℃).

Clearly solar radiation and air ambient temperature are required in order to build an SVR model that predicts cable surface temperature with reasonable accuracy less than ±1℃. Solar radiation and air ambient temperature provide enough and crucial information for the development of a robust model. Hence all the further models were developed taking into account only solar radiation and air ambient temperature.

4.2.3   Sensitivity test for the amount of input data features

A further investigation was performed to identify the amount of the input feature data needed in order to achieve the best results. During constant loading conditions the temperature of the cable can change due to the variation of air ambient temperature and solar radiation values. It was found, in the recorded data for August 2013, that peak air ambient temperature occurred two hours after peak solar radiation. Therefore according with the above observation it can be deduced that changes in solar radiation affects the variation of the air ambient temperature in the cable trough sometimes later which directly relates to subsequent variations of the temperature of the surface of the cable.

In order to proceed with further investigation it was of a great importance to determine the time intervals between the occurrence of the peak solar radiation, peak air ambient temperature and the time intervals before any measurable affect on the temperature of the surface of the cable. Analysis of the whole data set showed that the time gap from the moment of the peak solar radiation to the peak of the cable temperature is of the order of 4 hours. The time gap between peak solar radiation and peak air ambient temperature is 2 hours.

Each 4 hours interval contained patterns that the SVR used to build the relationship and the generalization function for the input feature data against the output data. The averaging time taken was 30 minutes as it was previously shown to have the best performance. Solar radiation, air ambient temperature and cable temperature at the location of TC 6B were also used to develop the model. The same length of training and testing data was used as before (8 days training and 4 days testing). Figure 15 shows the number of columns taken and the corresponding MAPE error. The number of columns correspond to 30 minutes intervals. The optimum pair of C and γ were determined as it is described in Section 3.4.3.

 It can be concluded that the best MAPE error is at 8 columns which correspond to 4 hours of input data. The SVR method was able to build a robust model using the number of patterns that were contained in the 4 hours' time gap calculated previous. For more complex systems it is better to consider multiples of initially calculated time gaps to identify the corresponding MAPE error as input feature data will contain more patterns and therefore the SVR will be able to derive the corresponding generalized function easier.
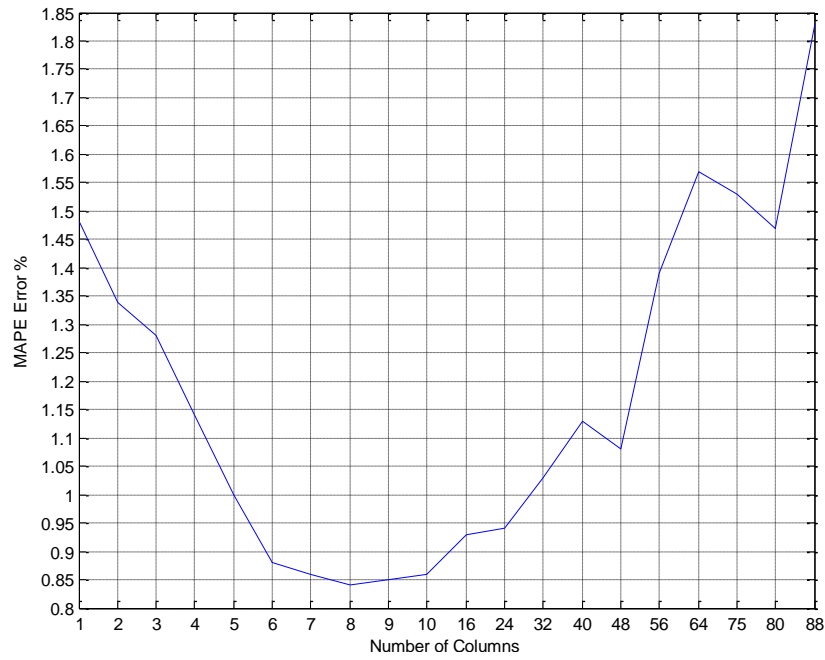
Fig. 15 Sensitivity test between number of input data needed and
corresponding MAPE error.

4.2.4   Sensitivity test for hours ahead prediction

It is necessary to understand how many hours ahead a model is able to predict a value by comparing a model with the same parameters of C and γ and with a model using tuned C and γ as a function of the hour ahead prediction. The same length of training and testing data is used as before (8 days training and 4 days testing). The averaging time taken was 30 minutes as it has proven before to have the best performance. Solar radiation, air ambient temperature and cable temperature were used as well to develop the model. Eight input feature data columns were used. The Figures 16 and 17 show the two different approaches for C and γ.

By having the same values of C and γ the model was able to predict the temperature of TC 13 up to two hours ahead, with very good accuracy, with MAPE error less than 2 %. By tuning the parameters C and γ the MAPE error can be reduced but the model is still able to produce satisfactory prediction results for up to two hours ahead. But tuning the parameters C and γ increases the computational effort as well as well as the complexity of the system. Therefore it is suggested to keep the same C and γ for a prediction of up to two hours ahead, as it is more efficient and less complex to be developed from the existing model.

43
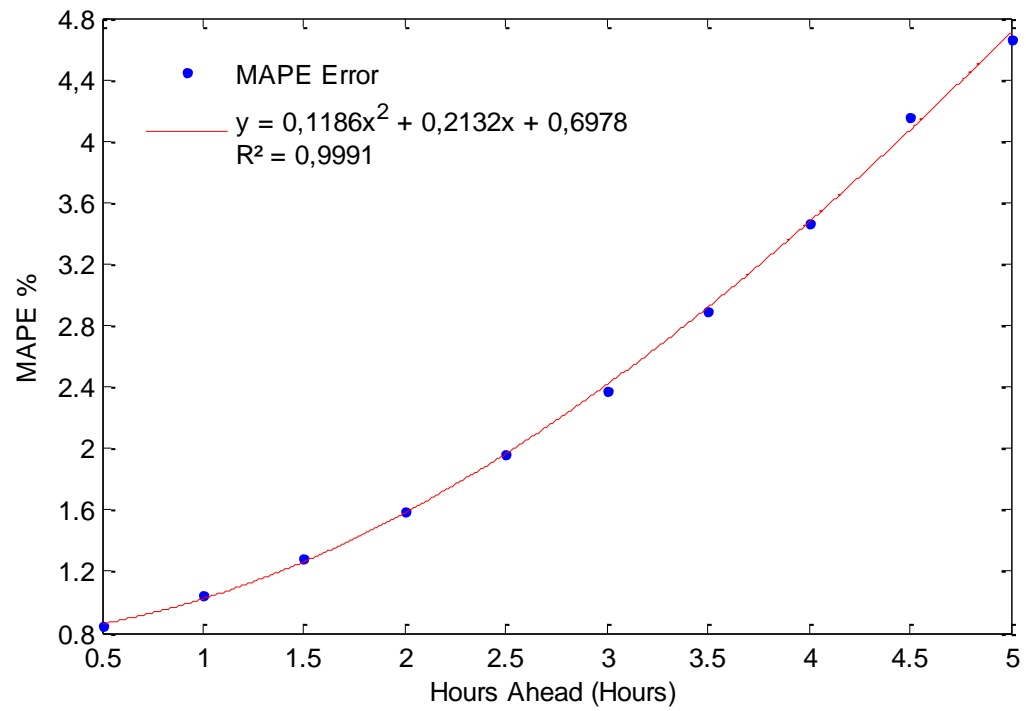
Fig. 16 Keeping the same C and γ parameters

Fig. 17 Tuning C and γ parameters

44
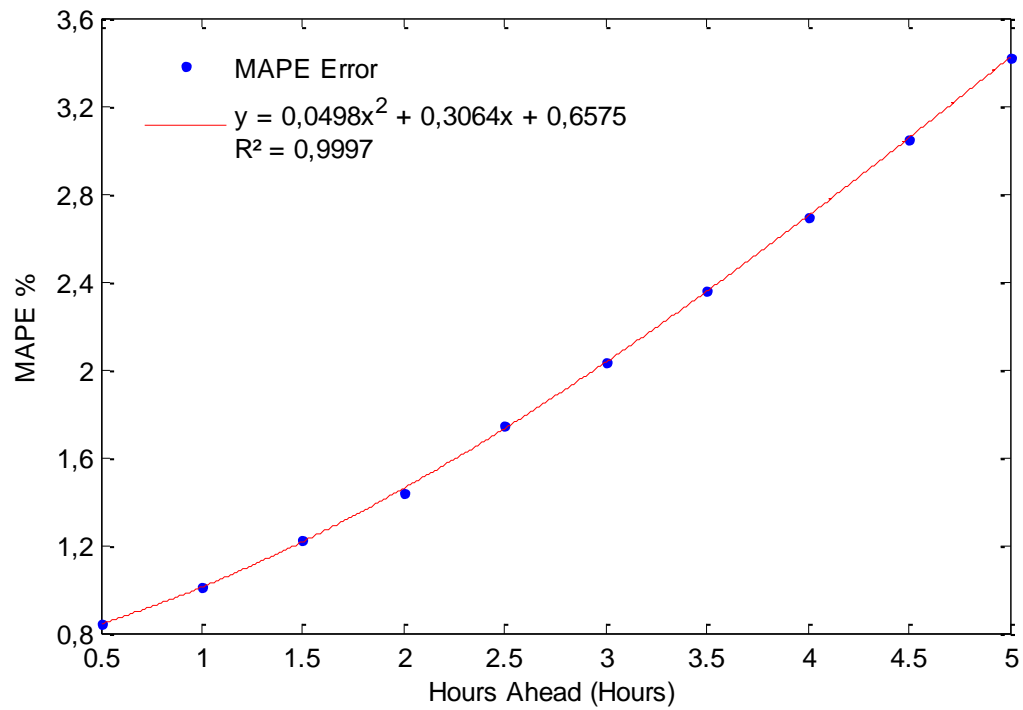
4.2.5   Pre-processing feature data

All the input feature data such as solar radiation, air ambient temperature and the surface temperature of TC 6B were averaged every 30 minutes. Figures 18-20 show the half hour intervals of one day for the input features with their corresponding 1 standard deviation.
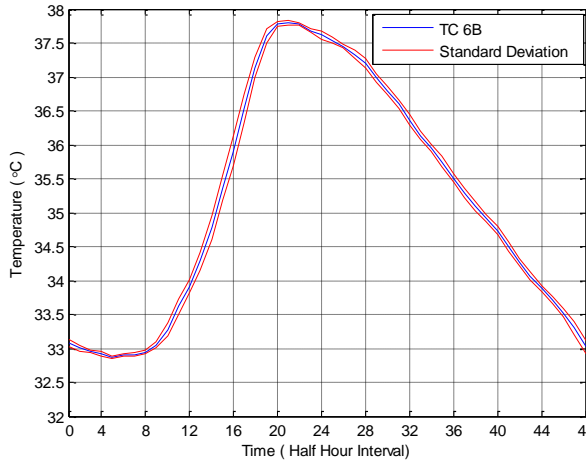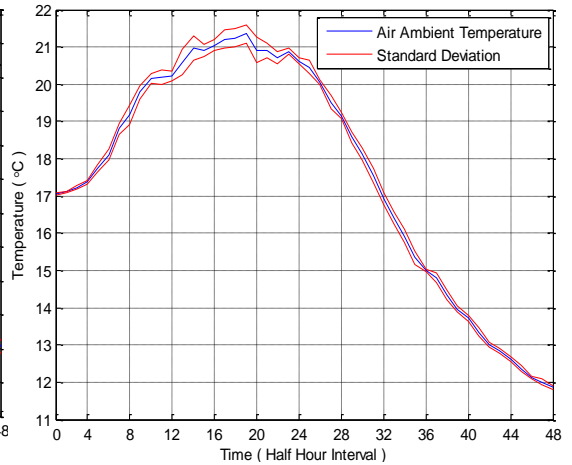

Fig. 18 Mean and standard deviation for TC 6B.   Fig. 19   Mean and standard deviation for air ambient temperature.
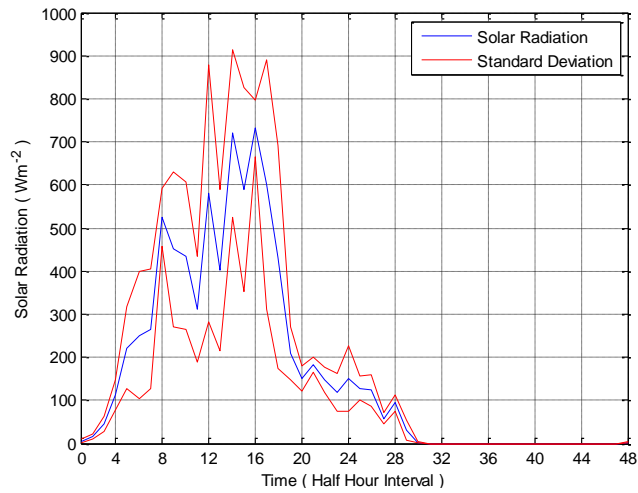
Fig. 20   Mean and standard deviation for solar radiation.

For every 30 minutes data averaging interval, 6 data points of 5 minutes measurement intervals were used. The red line in the graphs shown in Figures 18-20 indicates the standard deviation of these 6 data points while the blue line stands for their averaged value. It can be clearly observed that the standard deviation for the air ambient temperature and the TC 6B is small. That means that the error corresponding to the data point of the half an hour interval is small, as the fluctuation of the 5 minutes measurements in that period of half an hour did not cause a large uncertainty for the average value. In

contrast for the case of the solar radiation the uncertainty corresponding to every half an hour data point is large because of the disturbed nature of the solar radiation due to intermittent cloud cover.

After averaging the data, the input features are scaled from 0 to 1 as it is mentioned in Chapter 3. An example of the scaling input features array used for the development of thermal prognostic model by the SVR is shown in Figure 21.The input features of solar radiation, air ambient temperature and temperature of TC 6B are scaled from 0 to 1.
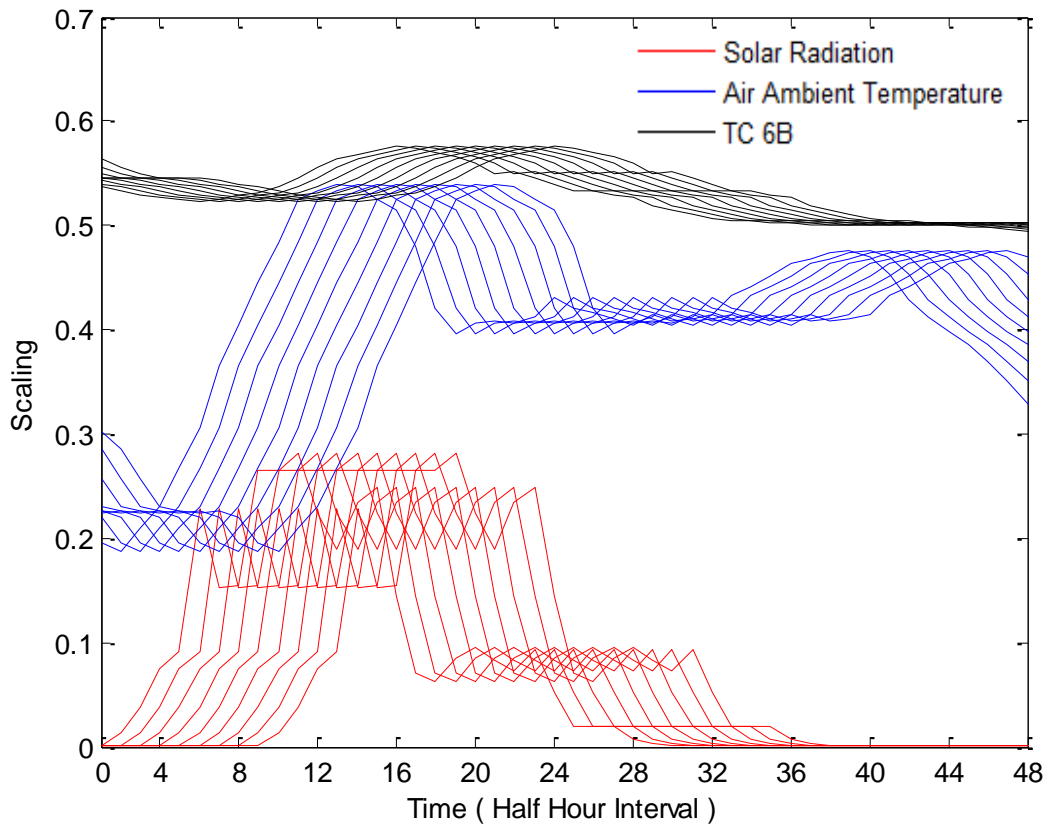
Fig. 21   Scaled input feature data

4.2.6   Sensitivity tests and pre-processing summary

From the sensitivity tests performed on data obtained from the trough experiment it was concluded that 30 minutes averaging time proved to be optimal for the development of robust and generalized models. Solar radiation and air ambient temperature were found to be the most dominant weather parameters that have to be used as an input data during the development of the thermal prognostic model. Calculating time intervals between the occurrence of the peak solar radiation, peak air ambient temperature and the time interval

46

when it affects the temperature of the cable surface provide the key information about the amount of input data needed for the development of the model. The model is able to provide satisfactory prediction results up to 2 hours ahead. Hence the above facts were used during the development and implementation of the thermal prognostic models. Furthermore the pre-processing data analysis showed that the solar radiation has the largest standard deviation error due to the disturbed nature of it.

4.3   Hot-Spot Experiment in the Air filled trench

During the air filled trench experiment a constant power demand profile of 100W was loaded in the simulated cables producing an output heat loss of 25 Wm^{-1}. During the loading, condition artificial hot-spots were introduced to the cable, using an external heat source, in order to investigate if the thermal prognostic model is sensitive enough to detect the existence of temperature anomalies along the cable, produced by the hot-spots. A hot-spot power profile of 10W was performed. The external heater had a surface area of 100 cm^2 hence the hot-spots heat density was 0.1 Wcm^{-2}.The experiment aimed to investigate whether it is possible to monitor specific areas of an underground cable, where hot-spots are more likely to occur, such as joints and terminations.

4.3.1   Constant Load

The external heat source was monitored by TC 8 which is positioned in the middle of Cable 5 as is shown in Figure 10. TC 6B was used as an input variable for SVR training as well as the solar radiation and the air ambient temperature. The TC 6B was chosen as it is one of the most distantly located TCs from where the heat source lies.

A thermal prognostic model was developed based on the outcomes of the sensitivity tests performed, mentioned in the section 4.2. The first 8 days were used to train the SVR model while the next 4 days were used for testing it and to choose the optimal pair of C and γ. After the 12th day the model ran unchanged. On the day 13th of the experiment the hot-spots were introduced. The hot-spot cycle was 4 hours on at 10W and 2 hours off.

The model was used to identify the abnormal temperatures produced by an external heat source with power output of 10W. Figure 22 shows the prediction made while the hot-spots were enabled.
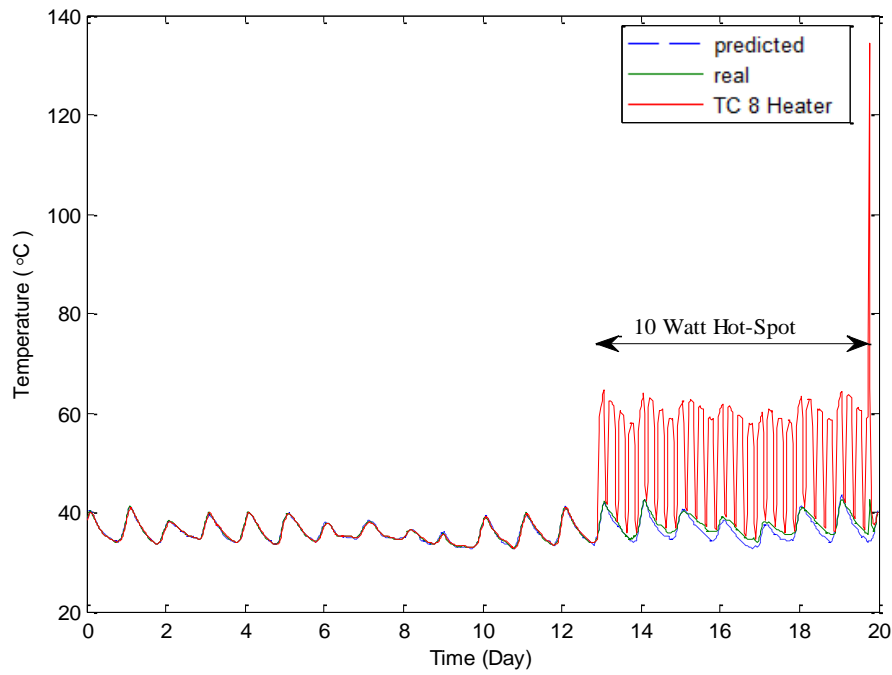
Fig. 22   Predicted temperature and real temperature for TC 13 under
the influence of hot-spots, MAPE=2.78 %.

Figure 23 shows the temperature difference between the measured temperature of TC 13 and the predicted temperature by the model of TC 13. It can be clearly seen that when
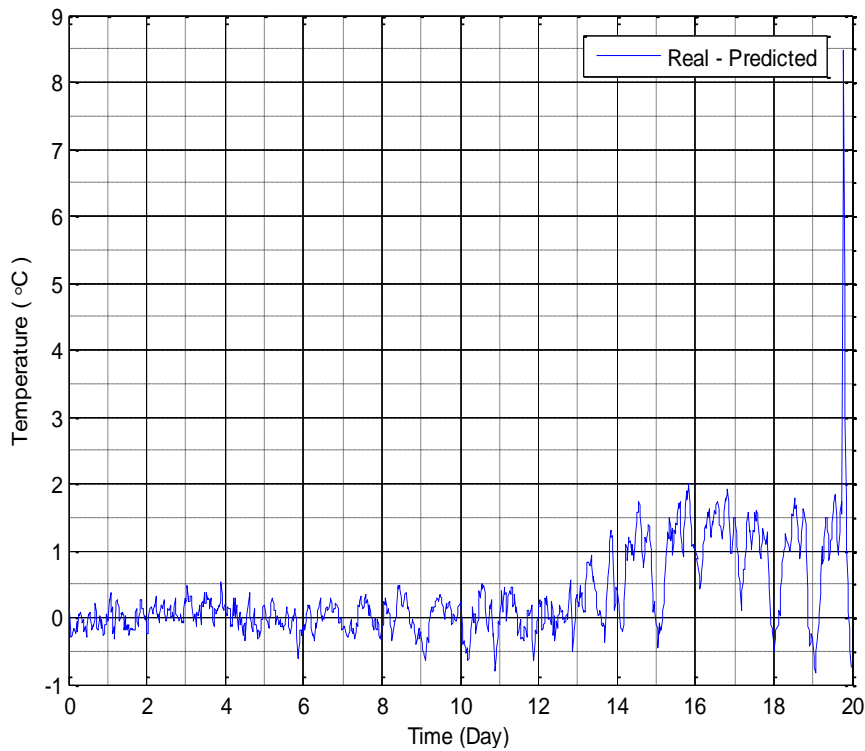

Fig. 23 Temperature prediction error for TC 13 under the influence of hot-spots.

the hot-spots cycle starts on the day 13th of the experiment and onwards the positive temperature prediction error has increased more than 1 ℃ during the nigh-time. During the night-time due to the much lower temperature time constant the detection with confidence was possible.

The thermal prognostic model has an accuracy of ± 1°C. Hence in the event when the real temperature is higher than the predicted temperature by at least 1°C, the positive part of the temperature prediction error, it can be assumed as an indication of an upcoming failure of the system.

The techniques used for the development of the model such as the scaling of the input data, the selection of the parameters C and γ, the way that the input data were selected and prepared, the sensitivity tests performed to tune the model verified that the chosen methodology was feasible and realistic.

The air-filled trench prognostic model was able to detect abnormal increase of temperature on the cable, produced by the external heat source. TC 13 which is located 0.25 m away from the location of the hot-spot was able to detect the change of the temperature due to the existence of the heater by TC 8.

4.4   33 kV thermal cycle experiment

This section investigates a method of developing a reliable thermal prognostic indicator system for cable terminations. An experiment was set up where a closed loop 33 KV cable is tested under current loading patterns. Real-time measurements (air ambient temperature, temperature of the cable terminations and loading demand) taken close to the cable are used to update the prognostic model based on the SVR algorithm. The model predicts the likely temperatures of cable terminations 30 minutes into the future. Anomalies of the measurements along the cable are compared with predicted values in order to identify possible degradation activity in the cable terminations.

As before, it is assumed that an increase of local cable temperature, i.e. a hot-spot, is indicative of degradation of the cable insulation due to thermomechanical, electrical and environmental factors.

4.4.1   Experimental Design and Setup

A closed loop of 10 meters 33 kV cable, under different current loading patterns, was used to generate data needed to develop the thermal prognostic model. Two ends of the cable are electrically connected to create a loop. Single-point-bonding is used to prevent any circulating earth currents. The sheath voltage is proportional to the sheath resistance which varies directly as the length of cable circuit. Hence the length of cable circuit is much shorter in the lab test than in the field, thus any sheath voltage is minimal.

Two current transformers (CT1 and CT2) and a motorized variac unit were used to generate the current loading profiles. The motorized variac is used to control the input current to the primary windings of the CTs. The CTs generate a magnetic field due to their primary current. This magnetic field then induces a much higher current in the secondary side which is formed by the single short circuit turn of the test cable.

A LabVIEW control system program, the flowchart of which can be seen in Figure 24, was developed in order to vary the input current to the CTs and to simulate different load profiles. A data acquisition device, NI USB-6008, collaborates with the control system program written in LabVIEW by receiving and sending analog signals. A Rogowski coil is used to measure the current passing through the cable conductor in real-time. This current is input to the NI USB-6008 which updates the LabVIEW control system program. Afterwards the LabVIEW control system program sends the appropriate signals to the motorized variac and adjusts the corresponding load profile demand in the cable to be close to the expected current value via the NI USB-6008.

The surface temperature of the cable was continuously monitored using 7 thermocouples (TC) placed on the cable at various positions as is shown in Figure 25. Four thermocouples (FA1, FB1, FC1 and FD1) are located 2 meters away from each other. The other three thermocouples (T1, T2 and T3) are located at the termination section. The thermocouples are connected to the Campbell Scientific datalogger CR1000. The datalogger records the temperatures every minute giving an average value of local temperature every 30 minutes.
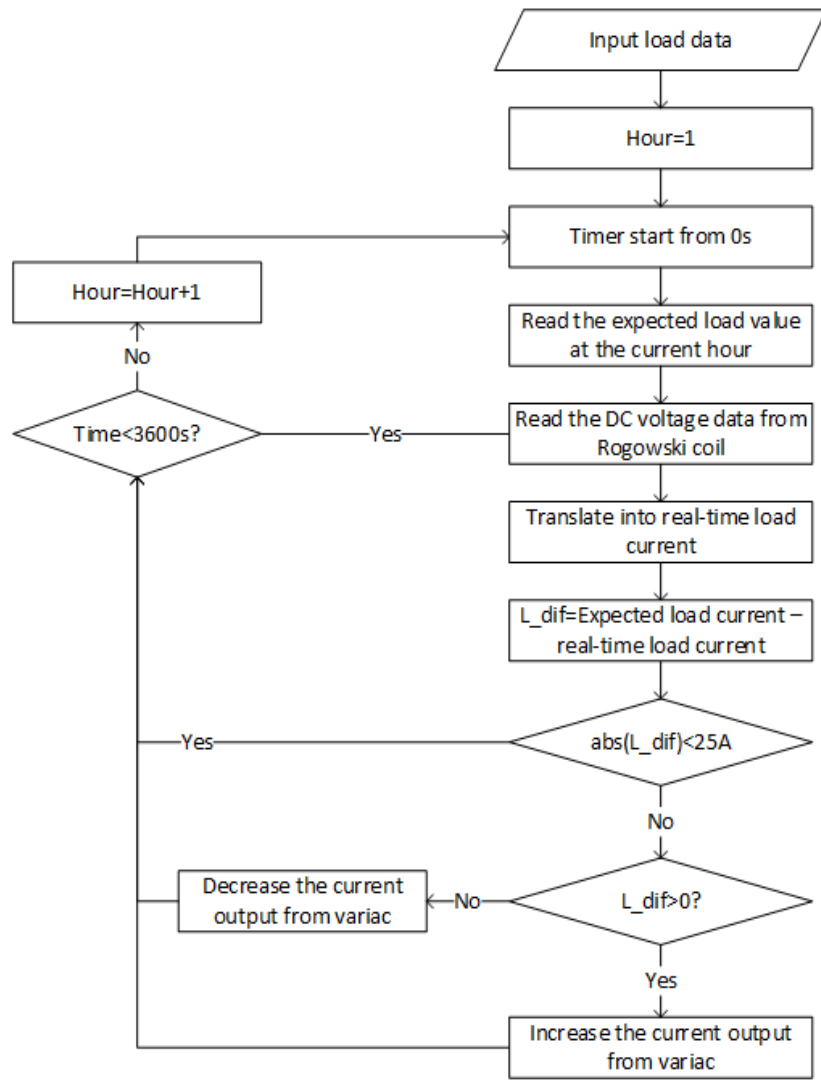
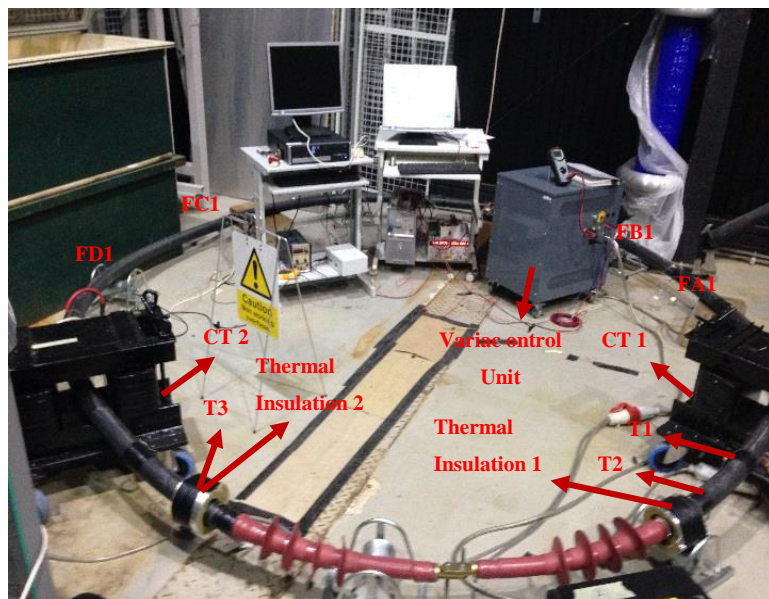Fig. 24 Flowchart of the LabVIEW control system.

Fig. 25 Experimental Setup of 33 kV

51

During this experiment a daily load current cycle, as shown in Figure 26, was loaded in the 33 kV cable producing an increase in temperature on the surface of the cable. The experiment was run for two weeks, with the same current load. The first week of the
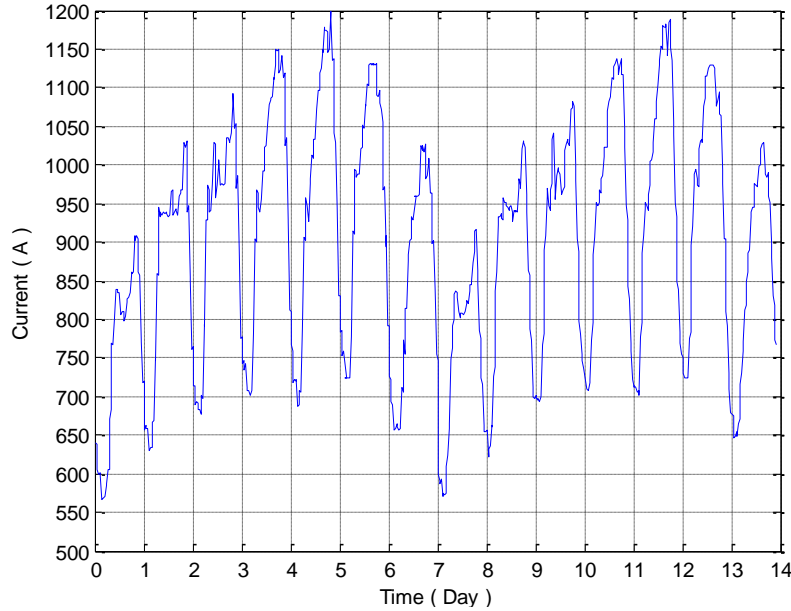

Fig. 26 Experimental current daily

experiment was used to gather data in order to build the thermal prognostic model while the second week was used to test the performance of the model. During the second week of loading artificial hot-spots were introduced to the cable, by adding fiberglass insulation sections, in order to investigate if the thermal prognostic model is sensitive enough to detect the existence of the temperature anomalies along the cable produced by local hot-spots. The two thermal insulation sections were added close to the end of the termination, where failures are more likely to occur. The first insulation was added by the end of the termination, located 0.10 meters away from TC T2 and 0.35 m from TC T1. The second insulation was added above the TC T3, 0.10 meters away from the end section of the termination.

4.4.2 Experimental results for the cable in air base on the SVR thermal prognostic model

TC FC1 is used as an input variable for SVR training as well as the air ambient temperature in the Tony Davies High Voltage Laboratory (TDHVL) and the current load profile of the experiment. The relationship between the peak of the air ambient

52

temperature and the cable temperature was 2 hours. Hence 4 input feature columns where used for the development of the models as the environment was not harsh.

The data scaling, preparation, kernel selection as well as the grid-search technique and cross-validation method used were as previously described in Chapter 3. The LIBSVM toolbox in MATLAB has been used for the development of the thermal prognostic model.

4.4.3   Results

Three different models were built to detect temperature increases by the location of the TC T1, T2 and T3 after the introduction of the hot-spots produced by the fiberglass insulation sections by the end of the terminations.

The hot-spots were introduced on the second week of the experiment. The first 5 days of the experiment were used to train the SVR algorithm, the next 2 days to test its performance using MAPE and to identify the optimum combination of C and γ. Finally in the last week the models, developed the week before, were left to run under unknown data and under the influence of local hot-spots.

Figures 27, 28 and 29 show predictions made for the testing and unknown data for TC T1, T2 and T3 without and with the influence of hot-spots.

The prediction made for the testing data of TCs T1, T2 and T3 shows good results with prediction MAPE less than 1.3%. After the introduction of the hot-spots from the day 7 until day 14 of the experiment, the MAPE for TC T1, T2 and T3 increased to 3.50%, 7.71% and 14.46% respectively. It can be observed that all of the TCs were able to identify the increase of temperature caused by the nearby hot-spots.
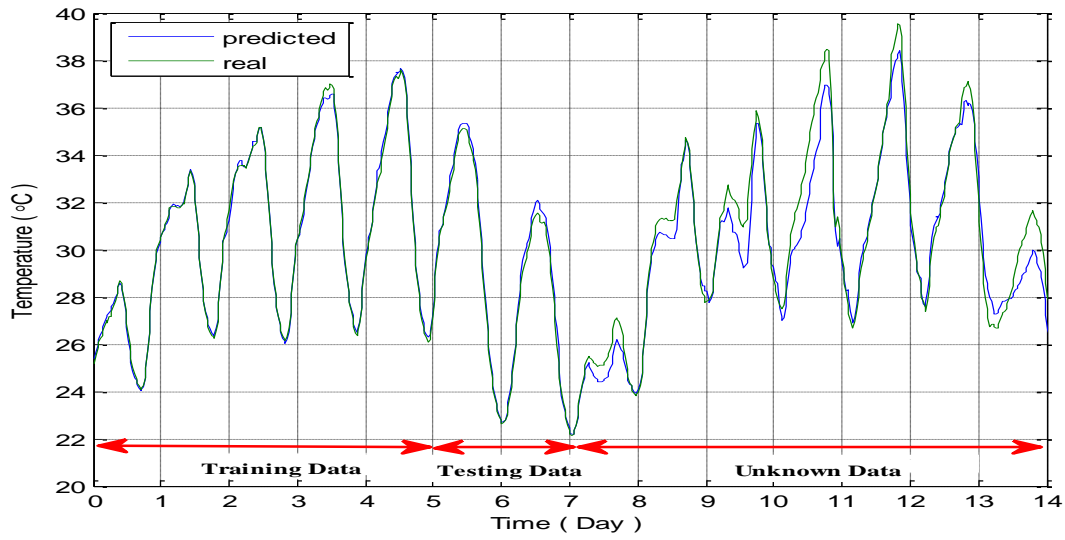
Fig. 27 Comparison between predicted temperature on Testing Data (MAPE= 1.11%) and Unknown Data (MAPE=3.50%) with the real temperature of TC T1.
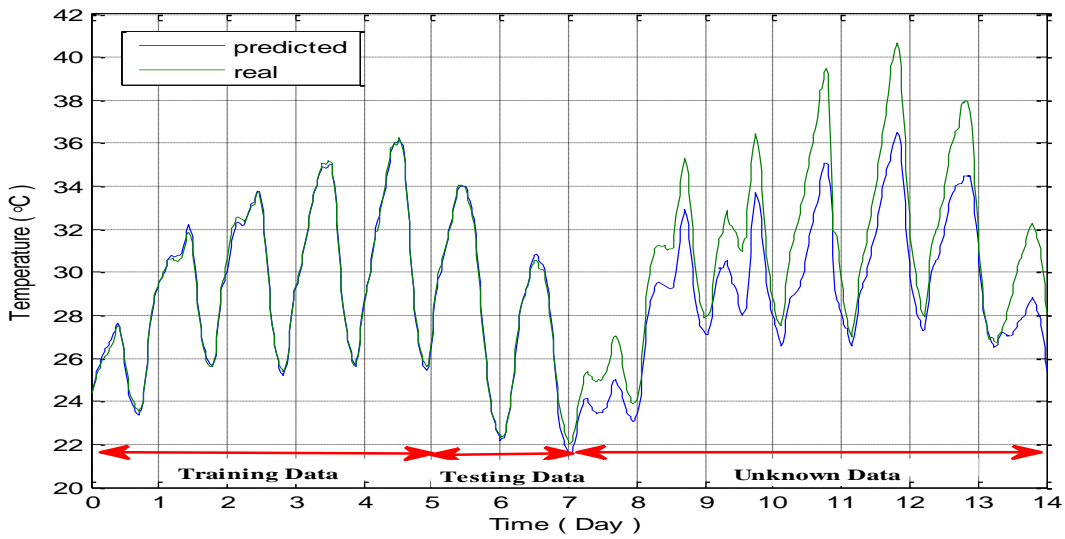

Fig. 28 Comparison between predicted temperature on Testing Data (MAPE= 0.89%) and Unknown Data (MAPE=7.71%) with the real temperature of TC T2.
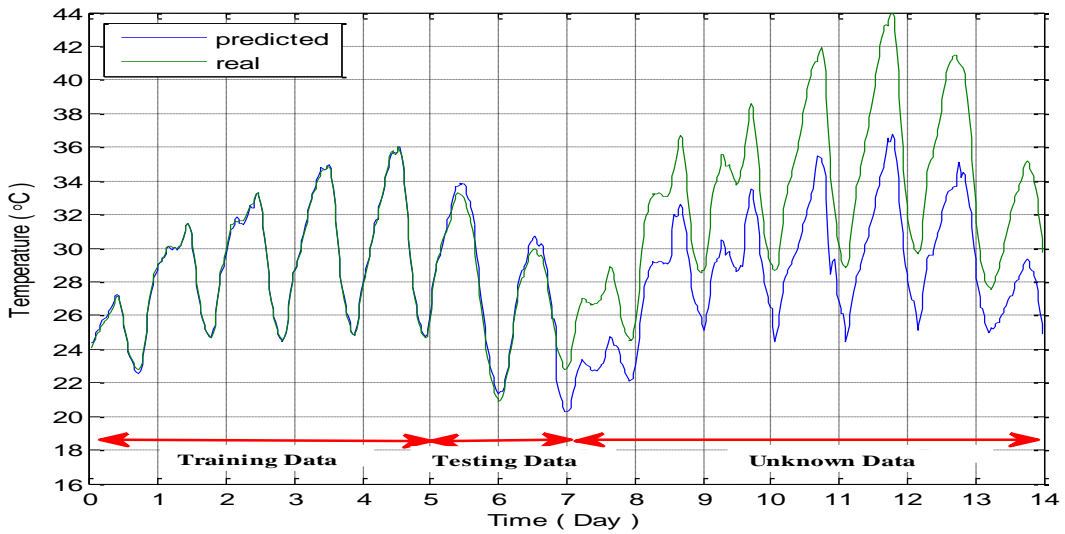

Fig. 29 Comparison between predicted temperature on Testing Data (MAPE= 1.26%) and Unknown Data (MAPE=14.46%) with the real temperature of TC T3.

Figures 30, 31 and 32 show the temperature prediction error made for the same TCs while the hot-spots were disabled and enabled. TC T2 which is 0.10 m away from the first hot-spot, thermal insulation 1, identified an increase of temperature of the order of 4.42 °C while TC T1 which is located further away from the hot-spot, at the distance of 0.35 m, could as well identify an increase of temperature of 2.54°C. TC T3 which is located just below the second hot-spot, thermal insulation 2, had a temperature increase which reached 8.22°C.
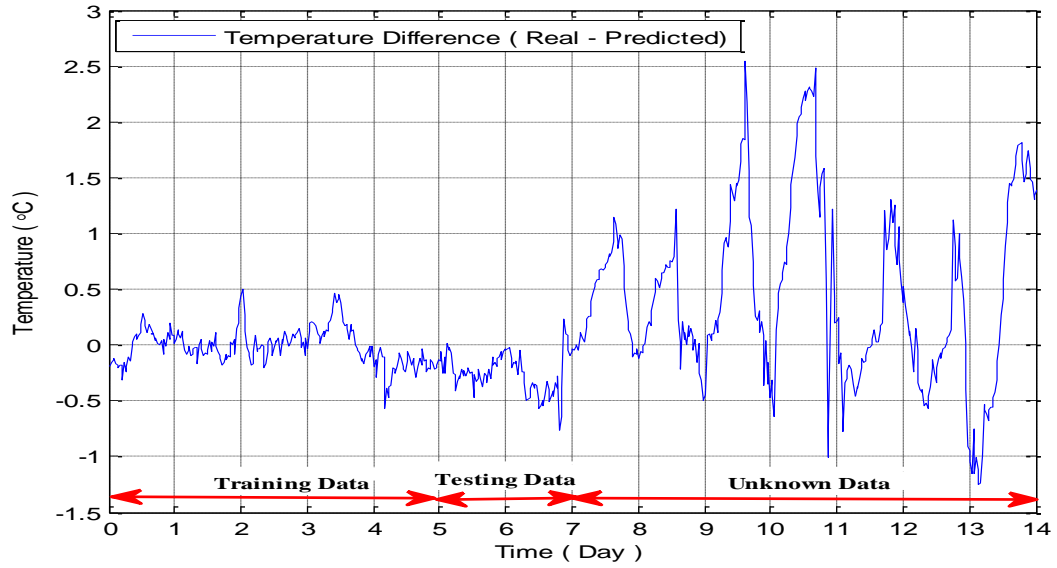
Fig. 30 Temperature prediction error for TC T1
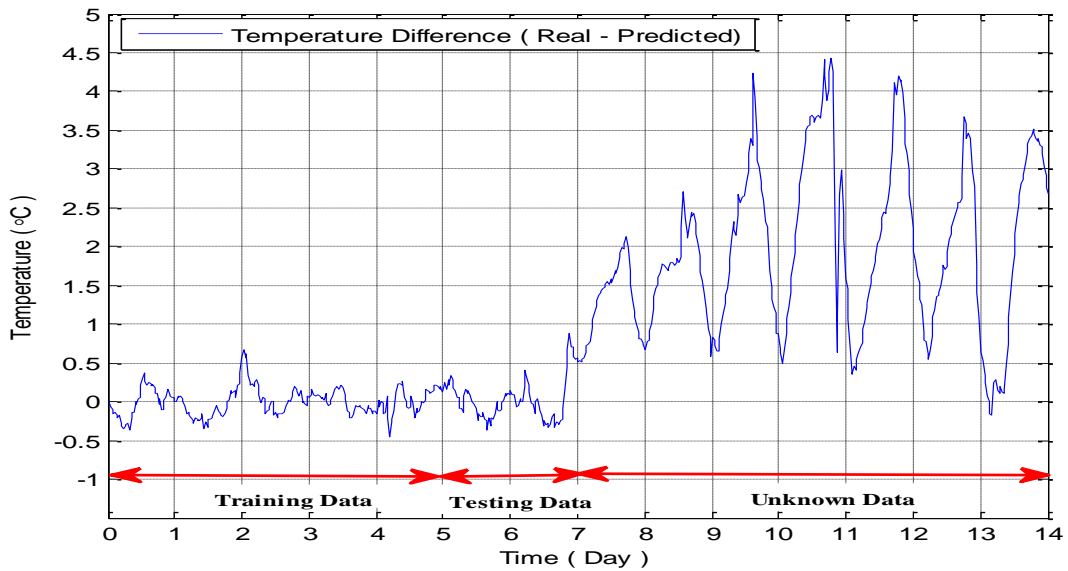
Fig. 31 Temperature prediction error for TC T2
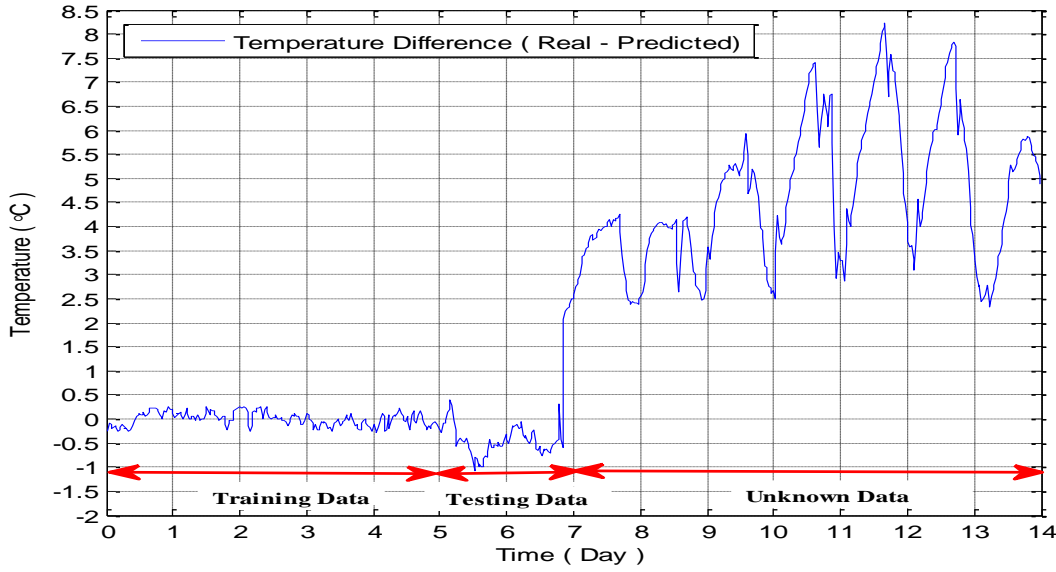
Fig. 32 Temperature prediction error for TC T3

The temperature prediction error for TC T2 and T3 is well above 1°C as these TCs are located near or below the hot-spots. TC T1 positioned 0.35 m away from the location of the first hot-spot was able to identify the presence of hot-spots with the highest temperature magnitude falling during the daytime but could not detect the hot-spots during the night-time due to the lower air ambient temperature.

Hence it can be concluded that the most effective distance for the thermal prognostic model to identify the location of the hot-spots is within a radius of up to 0.35 m. A distribution of TCs close to the area of interest is good enough for the model to identify and predict a possible failure process at an early stage within the cable terminations.

4.5   Summary

The 30 minutes averaging time proved to be the best averaging interval for a prediction horizon of 30 minutes ahead because the model has to predict only one data point ahead which makes the model less complex and more robust. Solar radiation and air ambient temperature showed to be the most dominant weather parameters that influenced the surface cable temperature and hence they are used as input data during the development of the model. The time gaps between the occurrence of the peak solar radiation, peak air ambient temperature and the time gap when the above affects the surface temperature of the cable contain patterns that can be used by SVR to develop a generalized model. For more complex systems a larger amount of input data is needed for the SVR to build the relation between input data and output data. The methodology of multiple time intervals

56

can help to identify the optimal number of the input data needed by the SVR. Reducing the size of input feature data will create a generic model while large amounts of data will create a specific model. The model can provide satisfactory prediction results up to 2 hours ahead. The pre-processing data analysis shows how the input data was averaged and scaled prior to the insertion to the SVR model.

Both the air-filled trench experiment and the 33kV thermal cycle experiment prognostic models were able to detect abnormal increases of temperature on the cable surface, produced by the external heat source. It was verified that the TC are sensitive enough to detect temperature anomalies as far as 0.35 m away from the location of the heat source. Hence TCs placed close to the area of interest, such as joints and termination in an air environment, can be used to develop prognostic models which can identify and predict a possible failure process at an early stage by the cable terminations and joints.

The proposed methodology during the sensitivity tests proved to be suitable to develop robust and generalized models for both experiments. The two experiments were performed in a different environments, more complex for the air-trench experiment and less complex for the 33 kV thermal cycle experiment. The analysis of the relationship between peak solar radiation, peak air ambient temperature and peak temperature of the cable surface provides vital information for the development of the models. Less input feature data were used for the 33 kV thermal cycle because the surface temperature of the investigated cable was influenced only by the air ambient temperature inside the TDHVL. While the cable surface temperature during the air-filled trench experiment was influenced by the solar radiation as well as the air ambient temperature, thus the model required more input feature data.

After the implementation of the established thermal models in the air-filled trench and the termination it was decided to test the performance of them in a more complex environment. Thus cyclic and constant load experiments were performed in backfill trench and are described in Chapter 5. The following chapter as well further investigates the performance of the previously mentioned machine learning regression algorithms for the case of backfill trench and the accuracy of the established models that predict the likely cable temperature 30 minutes into the future in order to verify robustness of the thermal prognostic system in a more complex environment prior to the implementation of it in the real field experiment.

Chapter 5 Implementation of Thermal Prognostic Models for the Backfill Trench

Two experiments constant load and cyclic load, were setup up in the backfill trench to investigate the possibility of identifying abnormal surface cable temperature measurements in an underground cable system. An ability to identify anomalies in cable surface temperature can help to target the cable degradation activity, commonly occurring by the cable joints, at an early stage prior a catastrophic failure. It is assumed that a sign of an upcoming cable joint failure is closely related with abnormal temperature due to a combination of electrical, thermomechanical and environmental factors.

The SVR algorithm was used to develop thermal prognostic models for the soil filled trench which can predict the likely temperature along the cable 30 minutes into the future. Weather conditions such as solar radiation, air ambient temperature as well as known cable loading conditions were used to develop the thermal models. Other machine learning algorithms were investigated and benchmarking was performed. The accuracy of the thermal prognostic model as well as the verification of model parameters selection were investigated.

5.1 Hot-Spot Experiment in the Soil filled trench

Based on results obtained for experiments in air, a thermal prognostic model was established using the Support Vector Regression (SVR) Algorithm which predicts the likely temperatures along the cable 30 minutes into the future, according to weather conditions and known loading. Anomalies of temperature measurements along the cable compared to predicted temperatures can indicate possible degradation activity in the cable. The surface temperature of the cable was continuously monitored as well as the weather conditions such as solar radiation and air ambient temperature. The experiment was used to investigate the feasibility of different approaches for monitoring of underground cables, where hot-spots are more likely to occur, such as joints and terminations. It is assumed that an increase of the local cable temperature is a sign of aging of the cable insulation caused by thermomechanical, electrical and environmental factors. Various machine learning algorithms were benchmarked as well as a system error analysis and a verification technique for the selected model parameters was performed.

5.1.1   Soil trench input experiment

The surface temperature of the 3 simulated cables is continuously monitored using 15 TCs placed in the sand filled trench. Figure 33 shows the position of the TCs in the sand surface trough. The surface temperature for each TC as well as the weather conditions are monitored with the same dataloggers as it described in Chapter 4.

During the loading condition artificial hot-spots were introduced to the cable surface, using an external heat source monitored by TC S8 which is positioned in the middle of the Cable 2. Two different loading conditions were investigated, the first with constant loading and the second with cyclic loading.

Three different hot-spot power profiles of 5, 10, 15 Watt were generated using the external heat source, in order to investigate if the thermal prognostic model is sensitive enough to detect the existence of the temperature anomalies along the cable produced by the hot-spots. The external heater had a surface area of 100 cm^2 hence the hot-spots heat density was 0.05 Wcm^{-2}, 0.1 Wcm^{-2} and 0.15 Wcm^{-2}.

The same sensitivity tests as described in Section 4.2 have been used. In order to proceed with further investigation it was of a great importance to determine the time difference between the occurrence of the peak solar radiation, peak air ambient temperature and when these effects influence the temperature of the cable in the soil. Analysis of the whole data set showed that the time gap from the moment of the peak solar radiation to the peak of the cable temperature is about 8 hours. Each 8 hour interval contains patterns that SVR uses to build the relationship and the generalization function for the input feature data against the output data. The averaging time taken was 30 minutes as it has shown to have the best performance. Solar radiation, air ambient temperature and cable temperature by the position of TC S2 were used to develop the model to predict the temperature of the TC S11 with reference the Figure 33. Each column corresponds to 30 minutes interval. Training data for 20 days and 8 hours and testing data of 3 days where used to develop the regression model using the LIBSVM MATLAB toolbox. The amount of input columns was varied in order to determine the best amount of input data needed for the development of the model. For each new number of columns the best combination of C and γ was selected with the corresponding MAPE error. Figure 34 shows the number of columns taken and the corresponding MAPE error
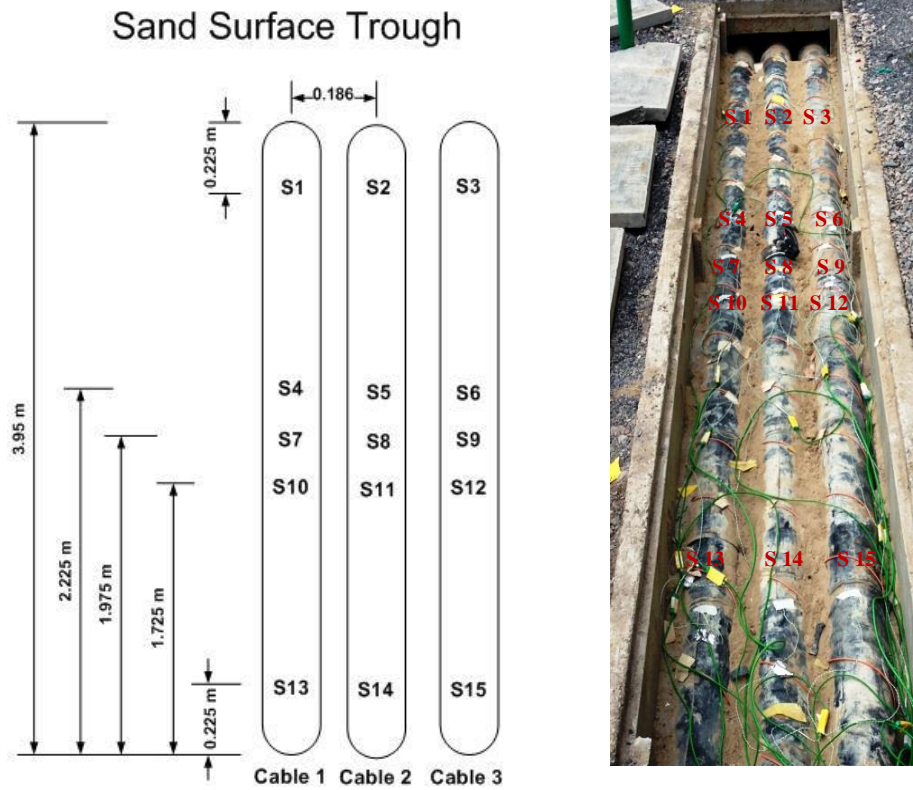
Fig. 33 Position of TCs in the sand surface trough.
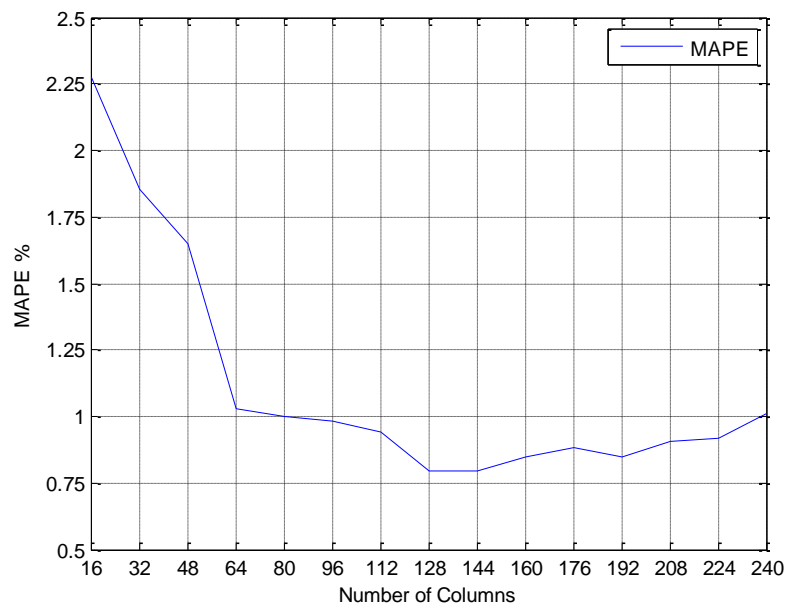

Fig.34 Sensitivity test between number of input data needed and
corresponding MAPE error.

From Figure 34 it can be seen that the soil constant load experiment is much more complex than the air trench constant load experiment. Even though the time gap between the peak solar radiation and the peak air ambient temperature is the same as previously described in Section 4.2.3, the time interval between air ambient temperature peak and

peak of the surface cable temperature is greater due to the larger thermal time constant of the soil. That as a result has increased the time interval between the peak of solar radiation to the peak of the cable surface temperature to 8 hours rather than 4 hours for the air trench case. Hence the system is more complex and more input data are needed. As it was previously suggested in Section 4.2.3 the technique of multiplying intervals was used to identify the appropriate amount of input data features needed for the development of the model.

5.1.2   Constant load experiment

Based on the SVR input experiment, a thermal prognostic model was developed. The temperature measured by TC S2, solar radiation and air ambient temperature were the input parameters to the SVR model which predicts the temperature of the TCs buried in the sand surface trough. The load demand input was not taken into the account for this model, as the constant value of it does not add any feature to the model but only increases the complexity of the whole system. Initially the model was trained for 20 days and 8 hours, tested for 3 days and the corresponding MAPE was calculated. This stage was crucial as it calculated the prediction accuracy of the model obtained from the unknown data. After the testing period of the experiment the hot-spots were enabled until day 39 of the experiment after which they were switched off for a period of 3 days. The hot-spot cycle was the same as in the air-filled trench; 4 hours on and 2 hours off.

In order to investigate the performance and the reliability of the thermal prognostic model two points were selected. The TC S11 was the first point as it is close to the hot-spot location, 0.25 m, and the second point of interest was TC S15 which is located farthest from the hot-spot, 1.5 m away. Figure 35 shows the prediction made for the TC S11 before and after the introduction of the hot-spots. The prediction made for the unknown testing data of TC S11 showed good results with a prediction MAPE 0.89%.
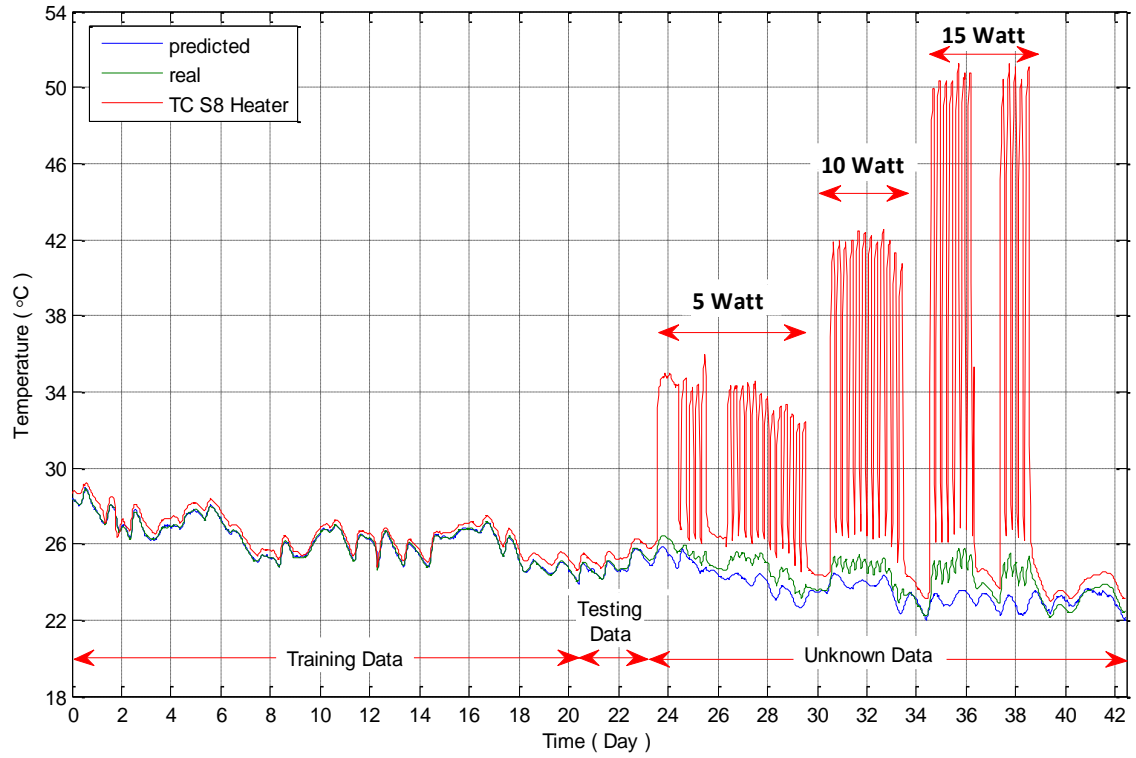
Fig. 35   Comparison between predicted temperature on Testing Data (MAPE=0.89%) and
Unknown Data (MAPE=8.28%) with the real temperature of TC S11.

After the introduction of the hot-spots from day 23 until day 39 of the experiment, the MAPE for TC S11 increased to 8.28%, which was more than 9 times greater than before. When the real temperature is higher than the predicted temperature, giving a positive temperature prediction error graph, it can be assumed that this is an indication of a potential upcoming failure of the system.

A better understanding of the influence of the hot-spots on the TC S11 can be seen in Figure 36. The temperature prediction error for TC S11 increased when the hot-spots were on. When the hot-spots were off, on the days 26, 30, 34, 37, 39 and onwards, it can be seen that the predicted temperature matched the real temperature. Hence the TC S11 was affected by the hot-spots. On day 12 a power shut down occurred in the TDHVL which caused power loss in the simulated cables for a period of an hour. The temperature of the cables dropped instantaneously causing the thermal model to over predict for that period, as it can be seen in Figure 36 the power cut resulted in the negative temperature error spike in the temperature prediction error graph. The second point which shows signs of over prediction was between the days 39 and 40 due to the drying out of the soil around the TC S11 which was caused by the prolonged exposure to the heat produced by the hot-spots. The thermal resistivity of the soil is 1.2 K m/W prior to drying and 3 K m/W in the

dry state. Therefore the dry region increased the thermal time constant of the soil and hence more time was needed for the area around TC S11 to cool down. It should be noted that this is also indicative of the failure modes associated with thermal run away. In this case the increased local thermal resistance of the backfill can cause the cable to overheat leading to damage of the insulation.
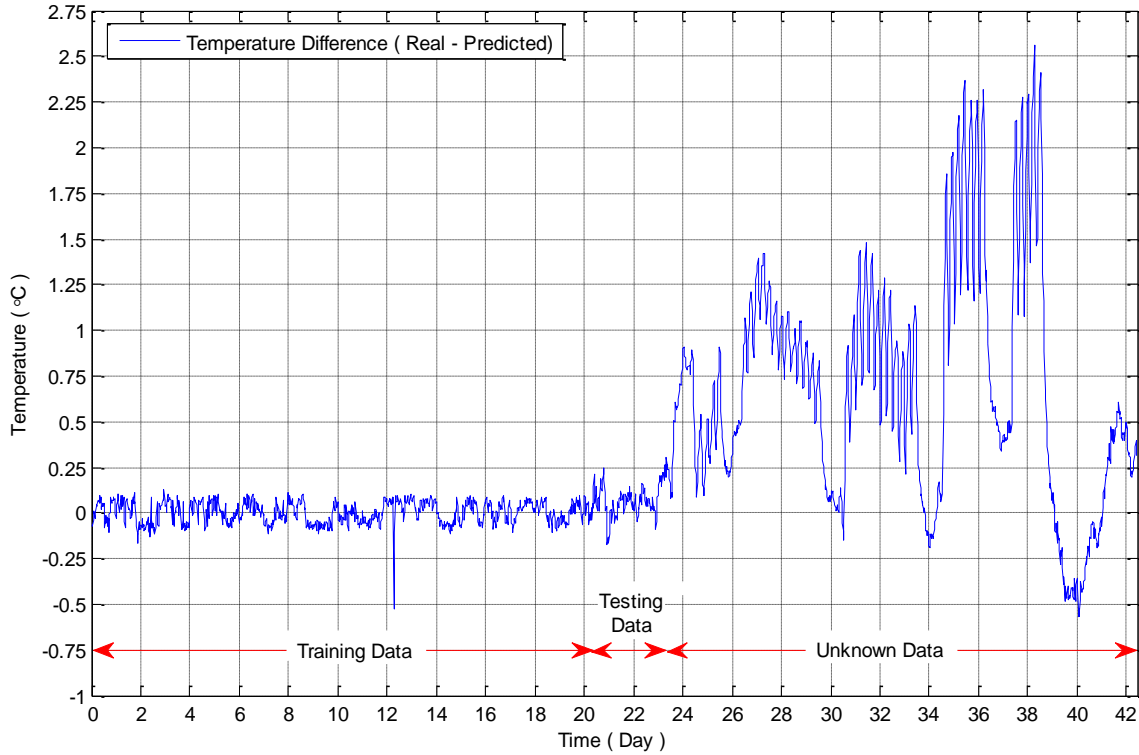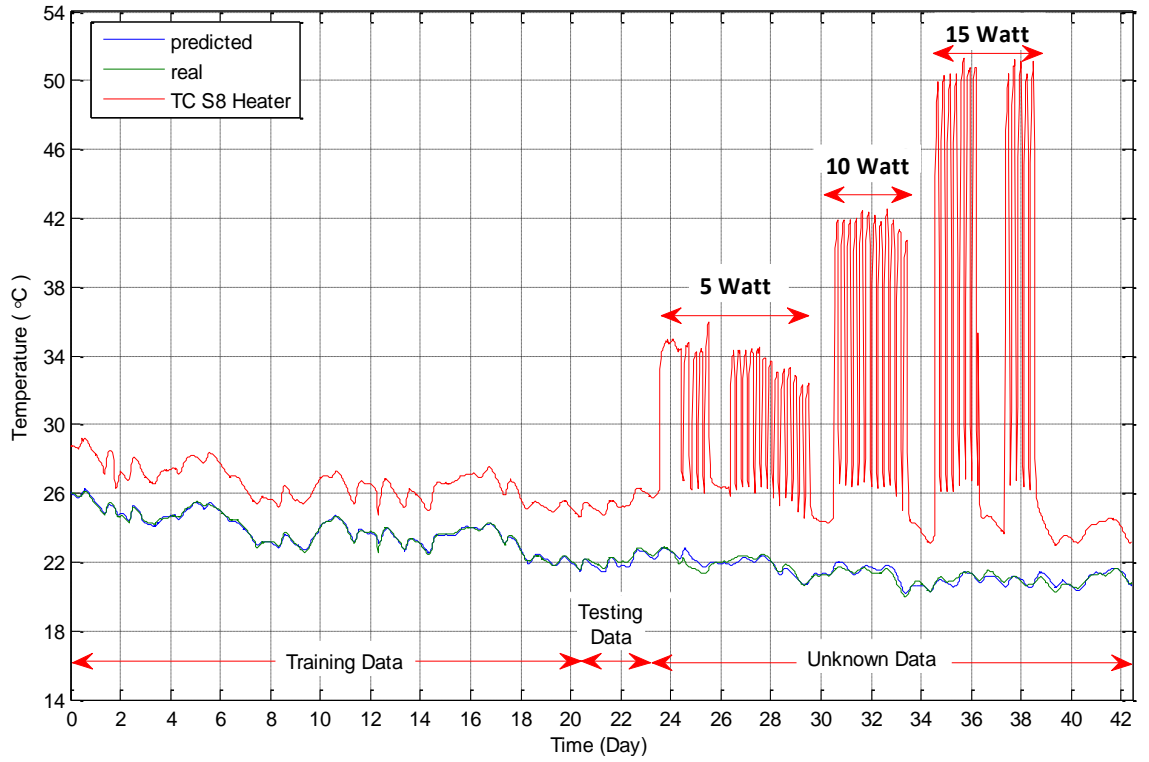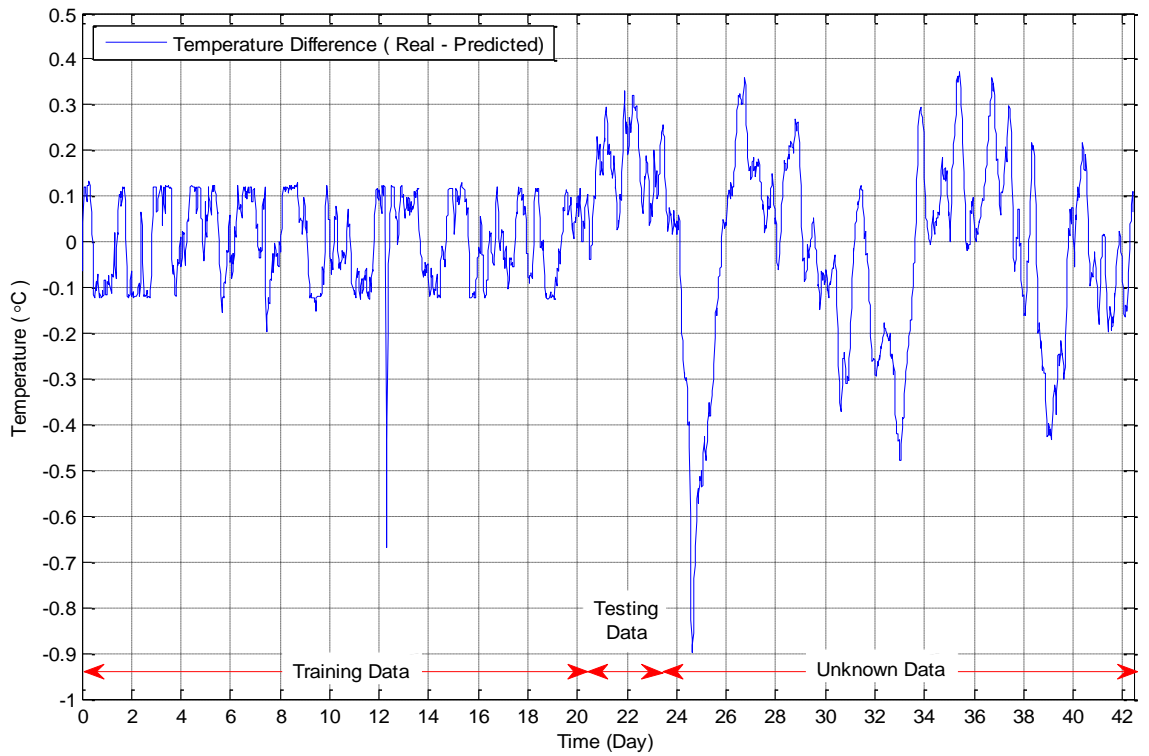

Fig. 36 Temperature prediction error for TC S11

The MAPE of TC S15 during the introduction of the hot-spots was 1.43%, which was close to its previous testing value of 0.91%. Thus the prediction error of the TC S15 was within the boundaries of less than 2% and was not affected by the introduction of the hot-spots as it can be seen in Figure 37. Figure 38 shows the temperature prediction error for TC S15 with the hot-spots on and off. The same negative spike on day 12 caused by the power shut down in the TDHVL can be seen in Figure 38. During the interval between days 24 -26 heavy rain caused the temperature of the TC S15 to be reduced. The above caused the model to over predict the temperature of the cable surface by the position of TC S15.

Fig. 37   Comparison between predicted temperature on Testing Data (MAPE=0.91%) and Unknown Data (MAPE=1.43%) with the real temperature of TC S15.

Fig. 38 Temperature prediction error for TC S15

Figure 39 shows the distribution of the maximum temperature prediction error for different locations on the cables.
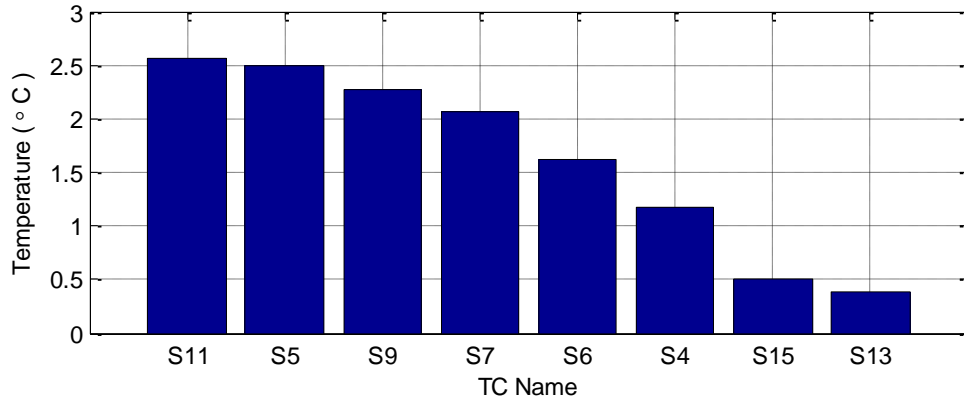
65

Fig. 39 Maximum temperature prediction error.

The TCs close to the hot-spots such as S11, S5, S7 and S9 had the highest temperature prediction error. The influence of the hot-spots, produced by the heater positioned above TC S8, was reduced for the TCs located farther such as TCs S6 and S4. However TCs S6 and S4 could still identify the anomalies of the temperature produced by the hot-spots despite the fact they have a smaller temperature prediction error than the TCs S11, S5, S7 and S9. The most distant TCs such as S15 and S13, positioned 1.5 m away from the heater location, were not capable to detect temperature anomalies of the system as the sensitivity of the system is around $\pm$ 1 ℃. Hence it was concluded that the most effective distance for the thermal prognostic model to identify the location of the hot-spots is again within a radius of up to 0.30 m.

5.1.3 Benchmarking for Constant load experiment

The ANN, MLR and Mboost prediction approaches were tested, as previously described in Section 5.1.1, to identify the best amount of input data needed for the development of the regression model for each of the algorithms. The performance of each individual algorithm was determined as before using the MAPE error. This step is required in order to tune and identify the best parameters needed during the testing period before the introduction of the hot-spots activity. The total amount of days before the introduction of hot-spots was 26 days and the amount of testing data was fixed to be 3 days for all of the algorithms before the introduction of the hot-spots. Hence as the amount of input data was different for each algorithm, it resulted in a slightly different durations of training data. A graph showing the number of columns used against the corresponding MAPE error is presented in Figure 40.
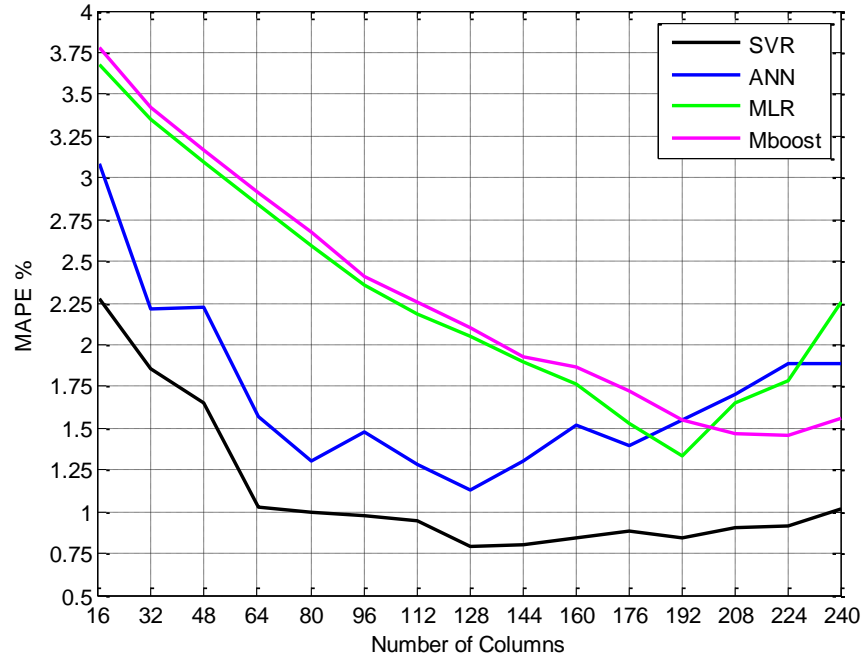
Fig. 40 Sensitivity test between number of input data needed and corresponding MAPE error for ANN, Mboost, MLR and SVR.

SVR and ANN used 20 days and 8 hours for training data and hence the actual period before the introduction of hot-spots is 23 days and 8 hours. For MLR the training period was 19 days and the actual period before the introduction of hot-spots was 22 days while for Mboost the training period was 18 days and 8 hours and the actual experiment period was 21 days and 8 hours. All the training data sets did not include, as mentioned before in Section 5.1.2, the 1 hour interval of the power shut down in the TDHVL. The investigated algorithms were tested to determine whether they were able to identify the introduction of the hot-spots during the constant loading experiment. The performance of each algorithm before the introduction of the hot-spots, after the introduction of the hot-spots, the number of hot-spots that they could identify as well the number of input features and the parameters needed is summarized in Table 9. The SVR showed the best performance as it was able to identify 39 out of 42 hot-spots which corresponded to 92.9% accuracy. ANN and MLR were able to identify 27 and 25 hot-spots respectively but even though the MLR had a worse performance, it showed a better generalized prediction model during the hot-spot periods. ANN on the other hand created an overestimated prediction model. It is can be seen in Figures 42, 44 and 46 that during the last days after

Algorithms	Hot-spots	MAPE% (Before)	MAPE% (After)	Input Features	Parameters
SVR	39/42 (92.9%)	0.89	8.28	128	C = 16384 $\gamma = 6.1035*10^{-5}$
MLR	25/42 (59.5%)	1.34	7.21	192	
Mboost	20/42 (47.6%)	1.45	6.42	224	Iteration = 700 nu = 0.15
ANN	27/42 (64.3%)	1.13	6.62	128	Layers = 9

Table 9 Benchmarking between ANN, Mboost, MLR and SVR for constant load

the introduction of the hot-spots both SVR and MLR still had a prediction output which was close to the real values while ANN and Mboost had overestimated predictions. Mboost had the worst performance as it could identify only 20 out of 42 hot-spots. The Figures 41-46 below show the prediction output of the different algorithms models with their corresponding temperature difference prediction error graphs.
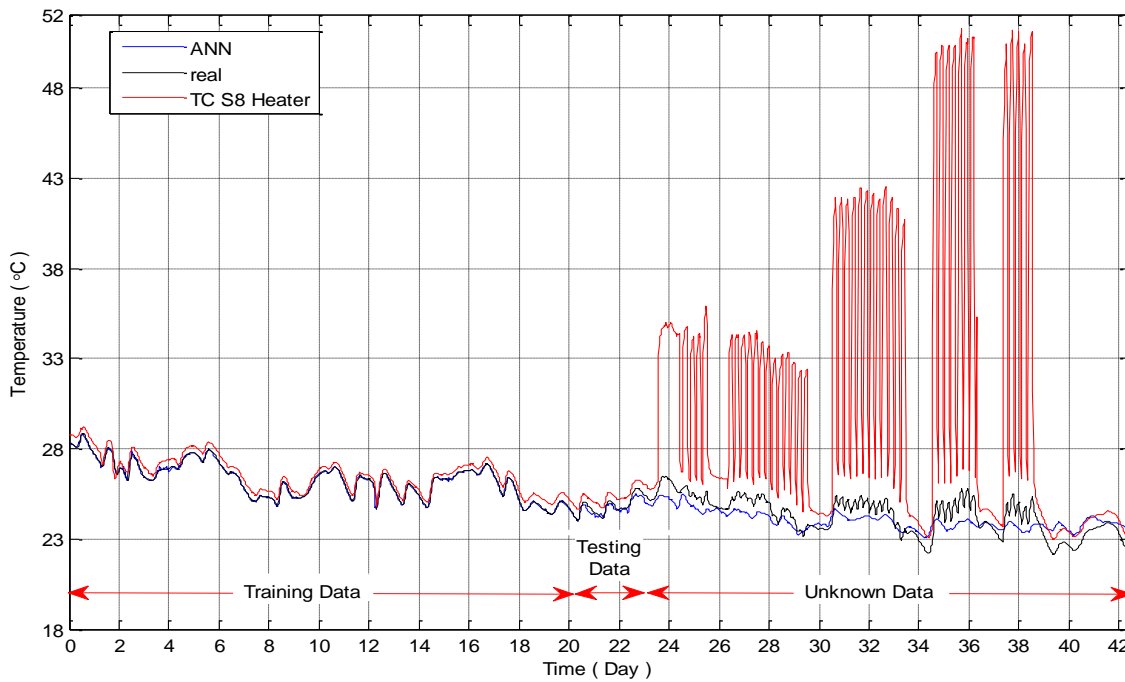
Fig. 41 Comparison between predicted temperature on Testing Data (MAPE=1.13%) and Unknown Data (MAPE=6.62%) with the real temperature of TC S11using ANN.

With reference to Figure 42, the temperature prediction error graphs of SVR and ANN it can be seen that ANN produces an overestimated prediction model by almost 1.5℃ from day 39 and onwards. During the power shut down on day 12, the ANN instead of finding a temperature reduction it identified a possible hot-spot which was obviously incorrect.
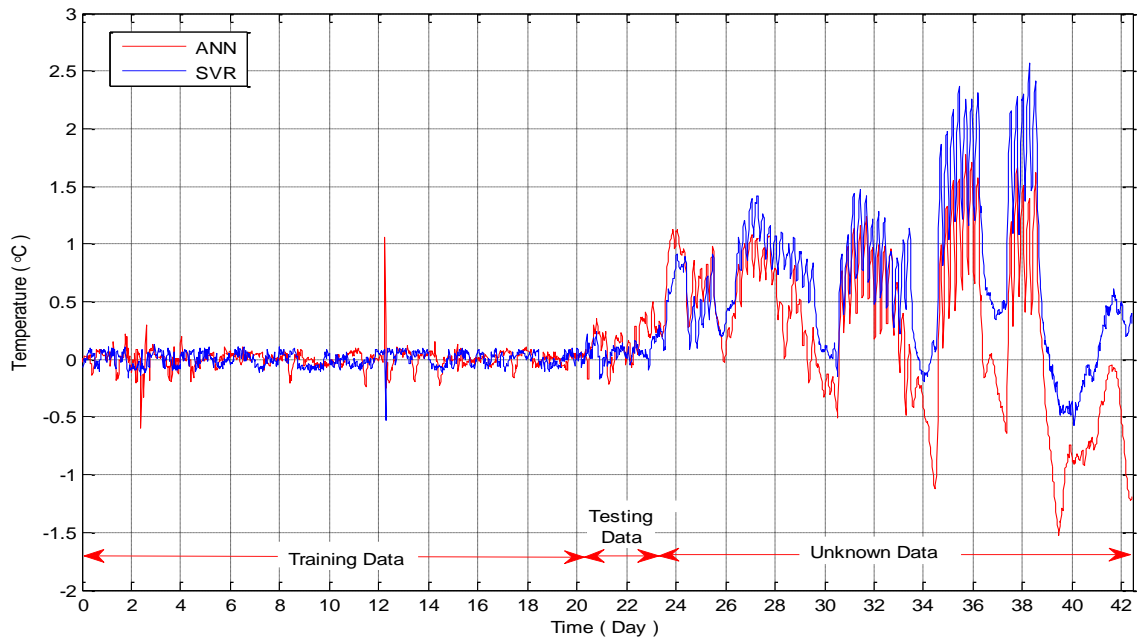
Fig. 42 Temperature prediction error for TC S11 using ANN and SVR.

Even though ANN could identify 27 out of 42 hot-spots and had the second best hot-spots performance it underestimated the amplitude of the hot-spots due to the overestimated model produced. Hence the actual amplitude of the hot-spots is greater in reality which
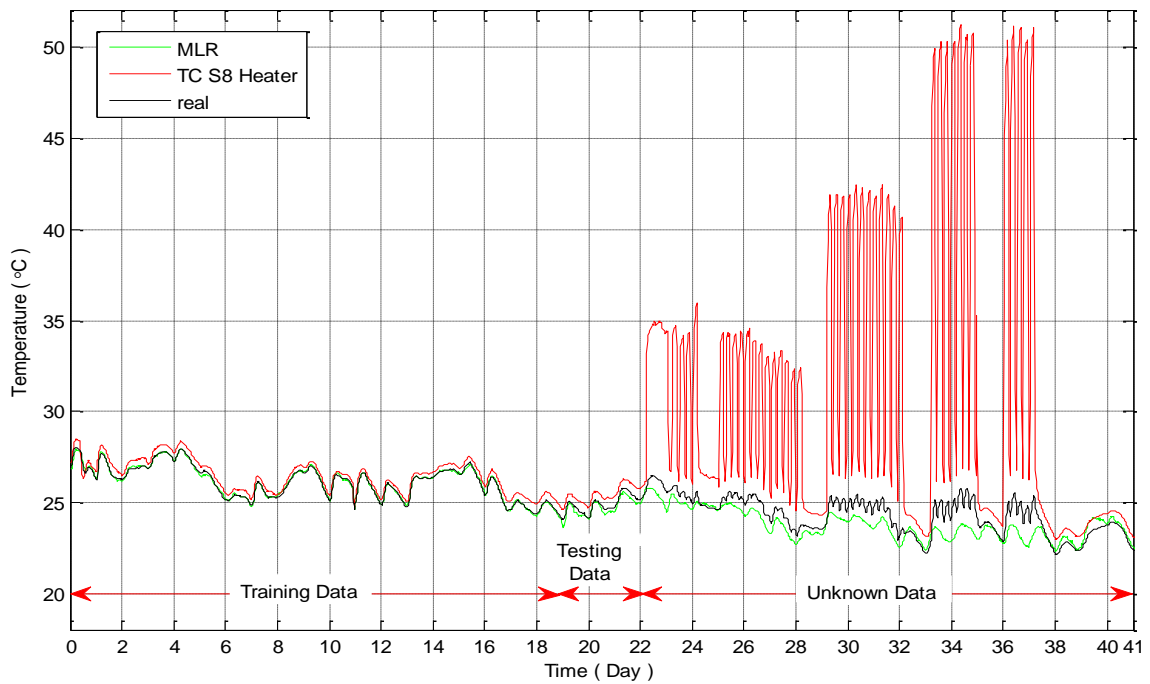

Fig. 43   Comparison between predicted temperature on Testing Data (MAPE=1.34%) and
Unknown Data (MAPE=7.21%) with the real temperature of TC S11 using MLR.

means that in a real online condition monitoring environment it might produce serious problems and set false alarms. Figures 43 and 44 present the performance of MLR which

like SVR showed much better performance compared to ANN and Mboost during the end of the hot-spots introduction period. It was able to identify the power shut down and it could identify the hot-spots. Mboost like ANN produced an overestimated model and performed poorly during the end of the hot-spots introduction period as can been seen from Figures 45 and 46.
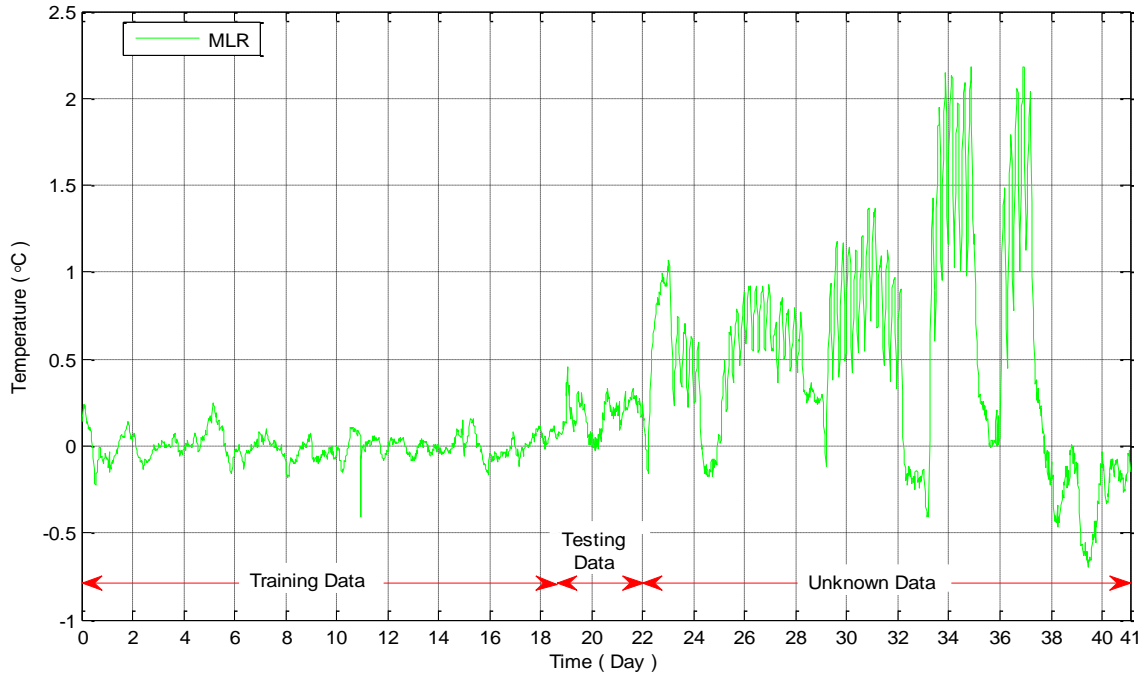
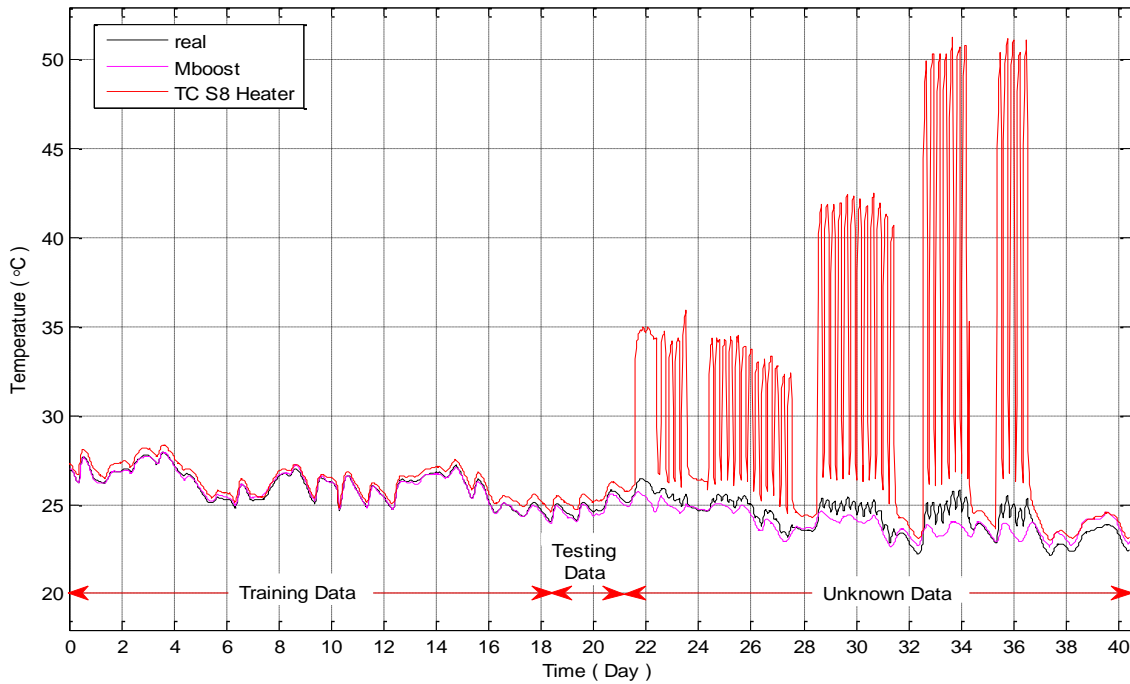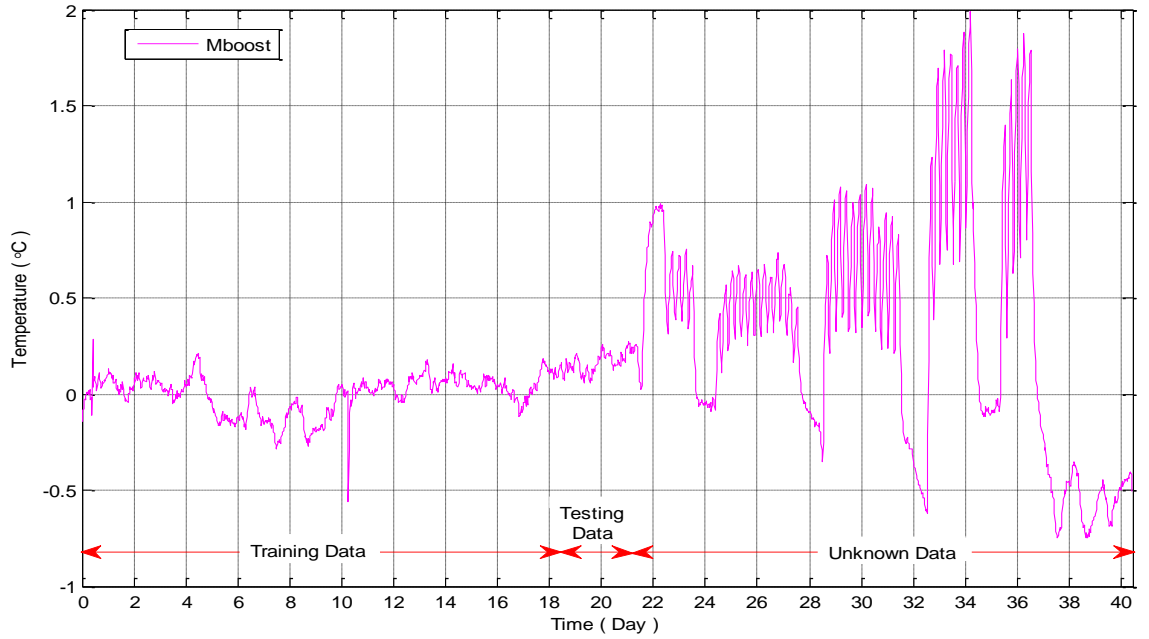Fig. 44 Temperature prediction error for TC S11 using MLR.

Fig. 45   Comparison between predicted temperature on Testing Data (MAPE=1.45%) and

Unknown Data (MAPE=6.42%) with the real temperature of TC S11 using Mboost.

70

Fig. 46 Temperature prediction error for TC S11 using Mboost.

Taking into the account the performance of the benchmarked algorithms, SVR was not only able to identify a greater number of hot-spots but it also created a generalized prediction model which was not subject to overestimating problems unlike both ANN and Mboost.

5.1.4 Cyclic load experiment

A new experiment was set up from 25/06/2014 – 28/8/2014, where a daily cycle of 16 hours of high load (200 W from 06:00 until 22:00) and 8 hours of low load (100 W from 22:00 – 06:00) were performed. This data, as well as the corresponding weather conditions, such as ambient temperature and solar radiation, were input to the SVR algorithm. Hot-spots of 5 W, 10 W and 15 W were introduced to the daily cycle experiment after day 25. Hot-spots were applied on the minimum and maximum points of the daily cycle in order to check the performance of the SVR model and test if it is able to detect abnormal changes corresponding from these hot-spots for a period of 4 hours on and 2 hours off.

The data was divided again into two groups: a) 27/06/2014 - 18/07/2014 training data and b) 18/07/2014 – 20/07/2014 unknown testing data. To identify the most appropriate C and γ two algorithms were combined together, Cross-Validation and Grid-Search and the corresponding MAPE error was calculated. This stage was crucial as it calculated the

prediction accuracy of the model obtained from the unknown testing data and reflected on the performance of the temperature prediction model.

The input data for the SVR was solar radiation, air ambient temperature and the temperature of the distant TC S2 and the daily load demand. The TC S2 was chosen as it is one of the most distantly located TCs on the same cable where the heat source was. The same sensitivity test as previously mentioned in Section 4.2 has been used. Analysis of the whole data set showed that the time difference from the moment of the peak solar radiation to the peak of the surface cable temperature is about 7 hours.

Each 7 hour interval contains patterns that the SVR uses to build the relationship and the generalization function for the input feature data against the output data. The averaging time taken was 30 minutes as with previous models. Solar radiation, air ambient temperature and cable temperature were used as well to develop the model. Figure 47 shows the number of columns taken and the corresponding MAPE error.
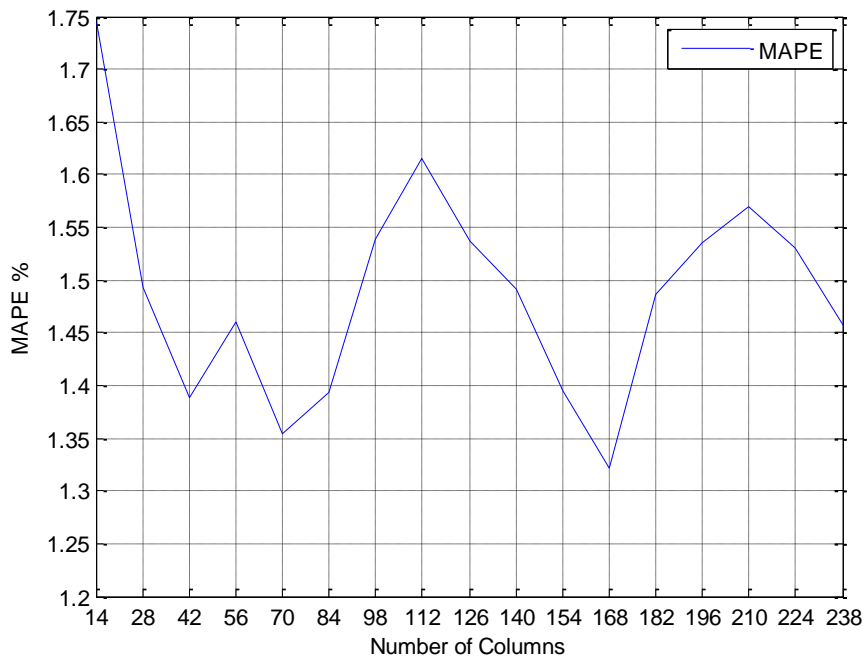

Fig. 47 Sensitivity test between number of input data needed and
corresponding MAPE error.

TC S11 and TC S15 were once again compared as previously for the constant load experiment. Figure 48 shows prediction made for the TC S11 before and after the introduction of the hot-spots. The prediction made for the unknown testing data of TC S11 showed good results with prediction MAPE 1.32% which is less than 2%. From day

72

22 and onwards where the hot-spots were enabled the MAPE increased to 9.43%, 7 times more than before.
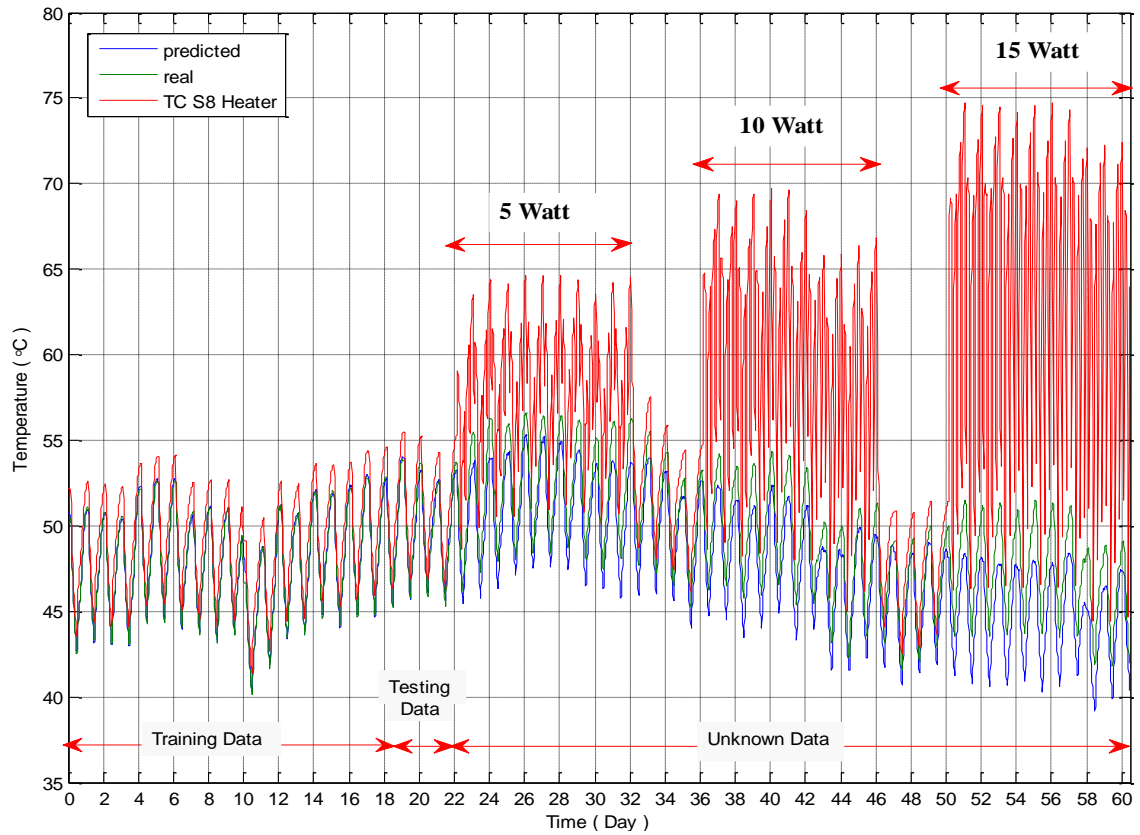

Fig. 48 Comparison between predicted temperature on Testing Data (MAPE=1.32%) and
Unknown Data (MAPE=9.43%) with the real temperature of TC S11.

A better understanding of the influence of hot-spots on the TC S11 can be seen in Figure 49. It can be observed that the TC S11 was affected by the introduction of hot-spots. The temperature prediction error for TC S11 was increased when the hot-spots were on. When the hot-spots were off, on days 33-35 and 47-49 the prediction temperature error reduced but still not as much as expected due to the dry out of the soil around TC S11. On day 10 of the experiment a heavy rain caused a flooding above the surface soil trench which caused the temperature of the TC S11 to reduce dramatically by more than 1.5 °C. That resulted in the model over predicting the temperature of the cable surface at the position of TC S11.
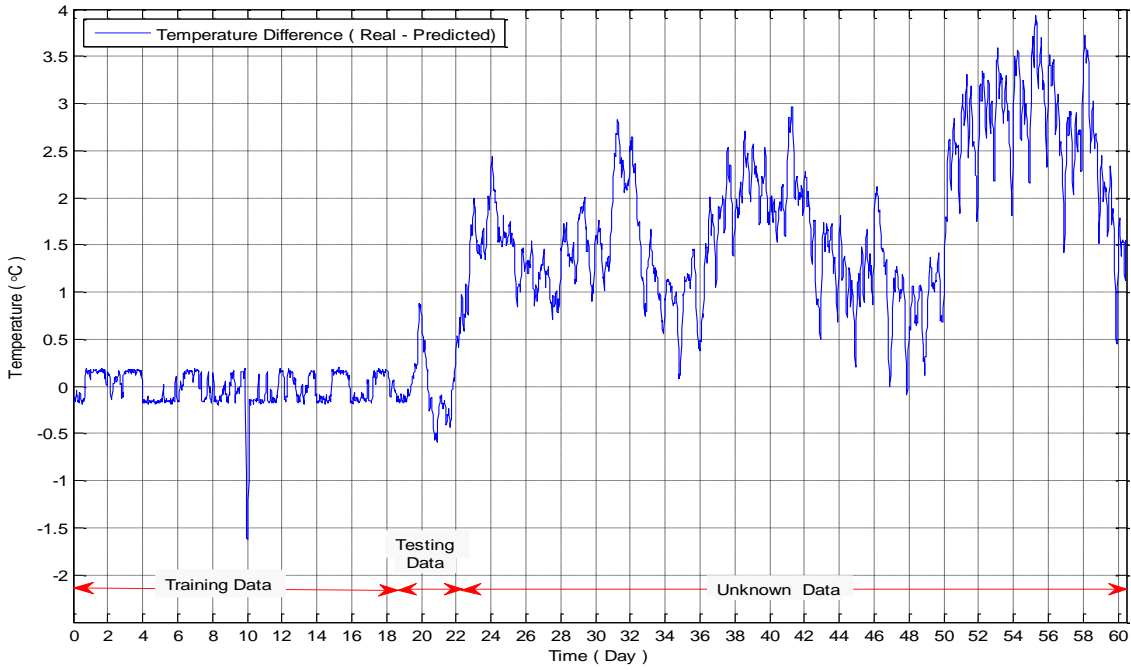
Fig. 49 Temperature prediction error for TC S11

The MAPE of TC S15 during the introduction of the hot-spots was 1.36%, which was close to its previous testing value of 1.24%. Thus the prediction error of the TC S15 was within the same boundaries as before, less than 2% and was not affected by the introduction of the hot-spots as can be seen in Figures 50 and 51.
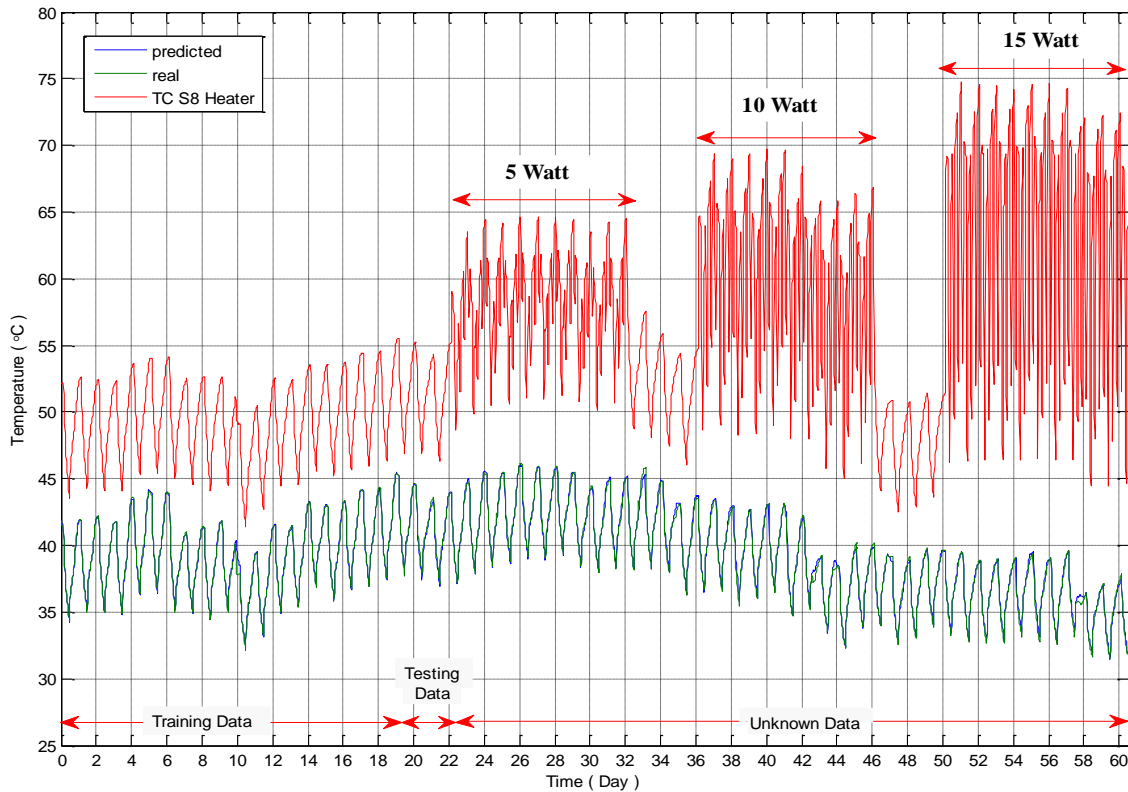

Fig. 50 Comparison between predicted temperature on Testing Data (MAPE=1.24%) and Unknown Data (MAPE=1.36%) with the real temperature of TC S15.

74

The large negative prediction spike in Figure 50 was due to the flooding which occurred during that day.
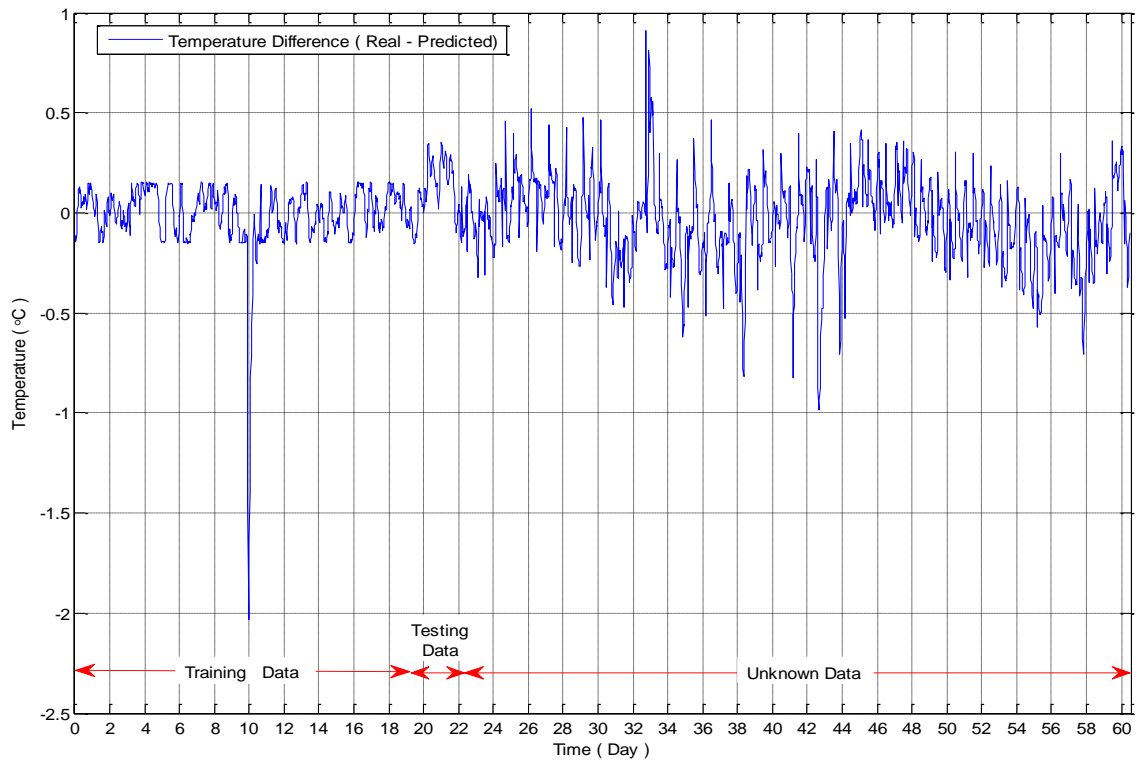

Fig. 51 Temperature prediction error for TC S15

Figure 52 shows the distribution of the maximum temperature prediction error along the cable.
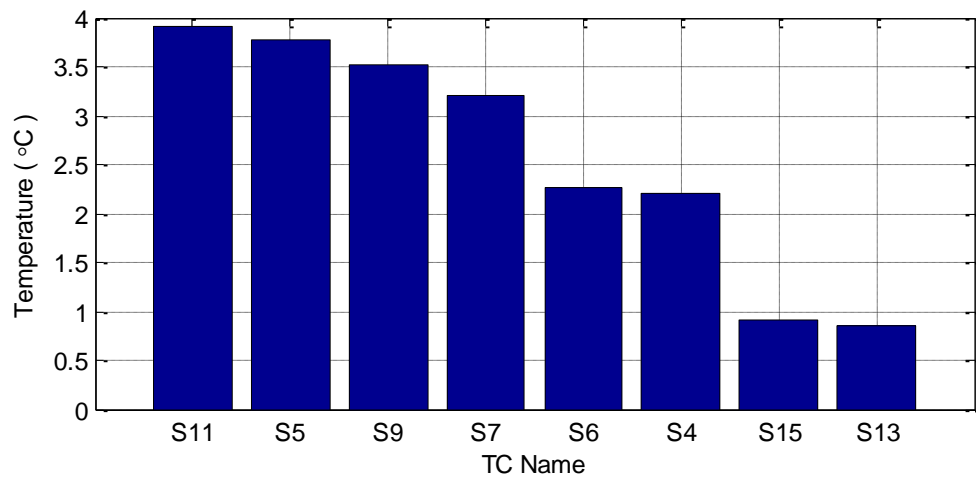

Fig. 52 Maximum temperature prediction error.

With reference to Figure 52, the TCs positioned close to the heat source and within a radius up to 0.30 m such as S11, S5, S7, S9, S6 and S4 had temperature prediction error larger than 2 °C. It can be confidently stated that they were able to identify the anomalies of the temperature produced by the heater positioned above TC S8. The most distant TCs

such as S15 and S13, positioned 1.5 m away from the heater location, were not capable of detecting temperature anomalies of the system as the sensitivity of these was around $\pm 1^\circ$C. It can be concluded once again that the most effective distance for the thermal prognostic model to detect the location of the hot-spots in the soil trench is in the radius of up to 0.30 m.

5.1.5   Benchmarking for Cyclic load experiment

As previously described in Section 5.1.1 determination of the ideal amount of input data required was performed for all the benchmarked algorithms. Figure 53 shows the best number of input data needed for SVR, MLR, Mboost and ANN. After this step all models were developed and tested for 3 days in order to select the best parameters to tune the models
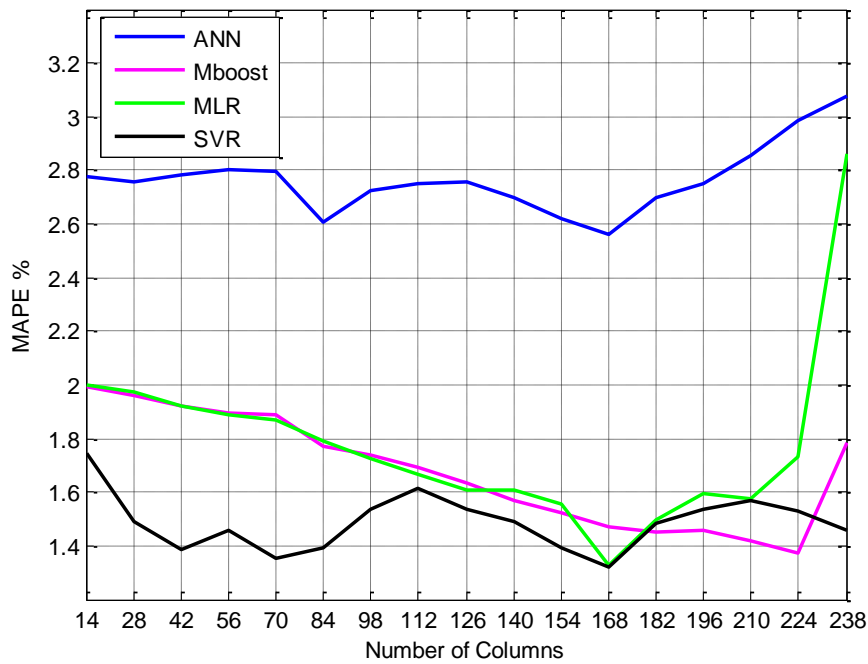

Fig. 53 Sensitivity test between number of input data needed and
corresponding MAPE error for ANN, Mboost, MLR and

and to check their performance. The total amount of days before the introduction of hot-spots was 25 days and 16 hours. SVR, MLR and ANN were trained for 19 days and 4 hours while Mboost was trained for 18 days. The training data sets did not include a 6 hour period of the flooding caused by heavy rain as mentioned before in Section 5.1.4. The performance of all the investigated algorithms is summarized in Table 10 below.

Algorithms	Hot-spots	MAPE% (Before)	MAPE% (After)	Input Features	Parameters
SVR	116/122 (95.1%)	1.32	9.43	168	C = 16384 $\gamma = 3.0518*10^{-5}$
MLR	115/122 (94.3%)	1.33	9.32	168	
Mboost	114/122 (93.4%)	1.37	8.12	224	Iteration = 700 nu = 0.15
ANN	93/122 (76.2%)	2.56	12.12	168	Layers = 7

Table 10 Benchmarking between ANN, Mboost, MLR and SVR for cyclic load experiment.

The SVR once again showed the best performance. It could identify 116 out of 122 hot-spots which corresponded to 95.1% accuracy. MLR and Mboost produced satisfactory results as well, identifying 115 and 114 hot-spots respectively. ANN performed poorly comparing the other three algorithms by identifying only 93 hot-spots out of 122. Figures 54 - 58 below show the prediction model for each algorithm separately as well as their temperature difference prediction graphs. Figure 56 shows the temperature prediction error difference of MLR, ANN and SVR.
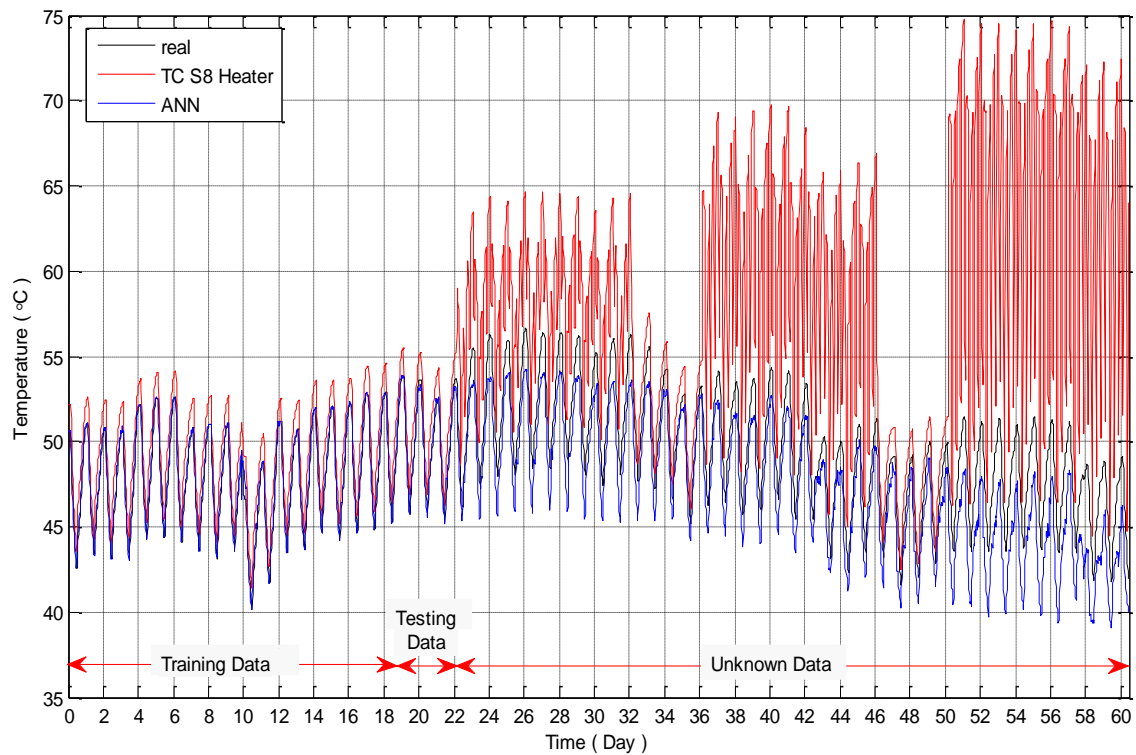

Fig. 54 Comparison between predicted temperature on Testing Data (MAPE=2.56%) and Unknown Data (MAPE=12.12%) with the real temperature of TC S11 using ANN.
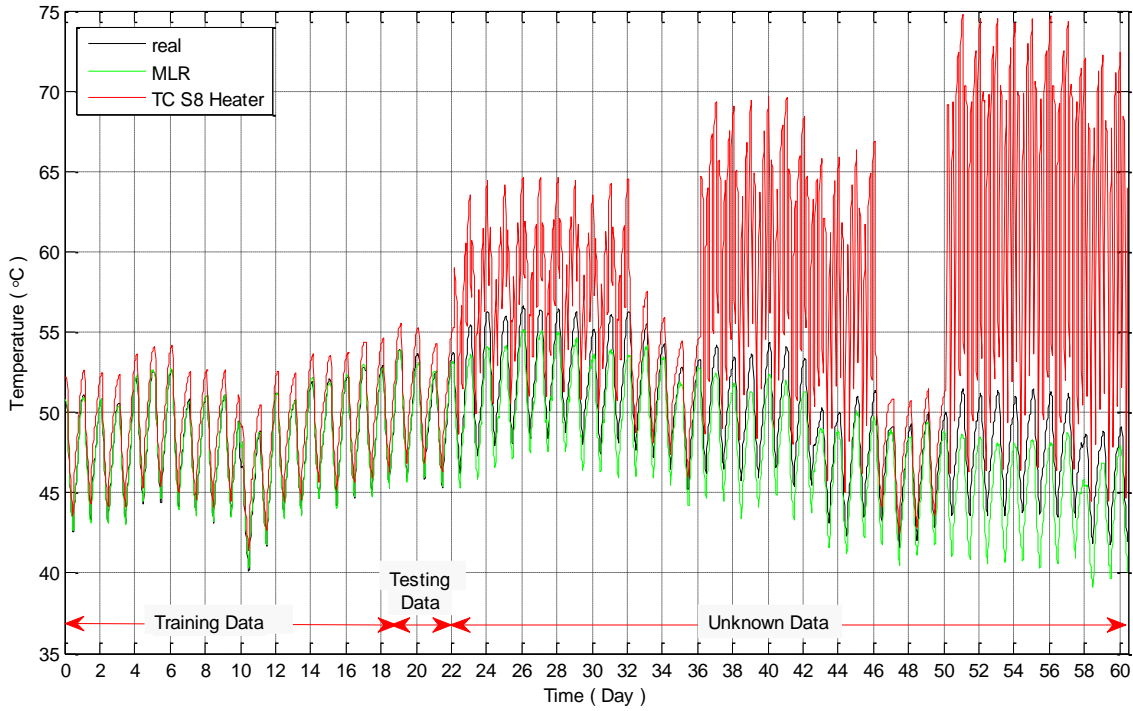
77

Fig. 55   Comparison between predicted temperature on Testing Data (MAPE=1.33%) and
Unknown Data (MAPE=9.32%) with the real temperature of TC S11 using MLR.

The temperature difference errors for SVR and MLR have similar results. Both could identify similar numbers of the hot-spots, have predicted similar hot-spots amplitudes and both could identify the flooding. ANN on this occasion produced an underestimated model resulting in overestimated amplitude of the hot-spots and identified the flooding
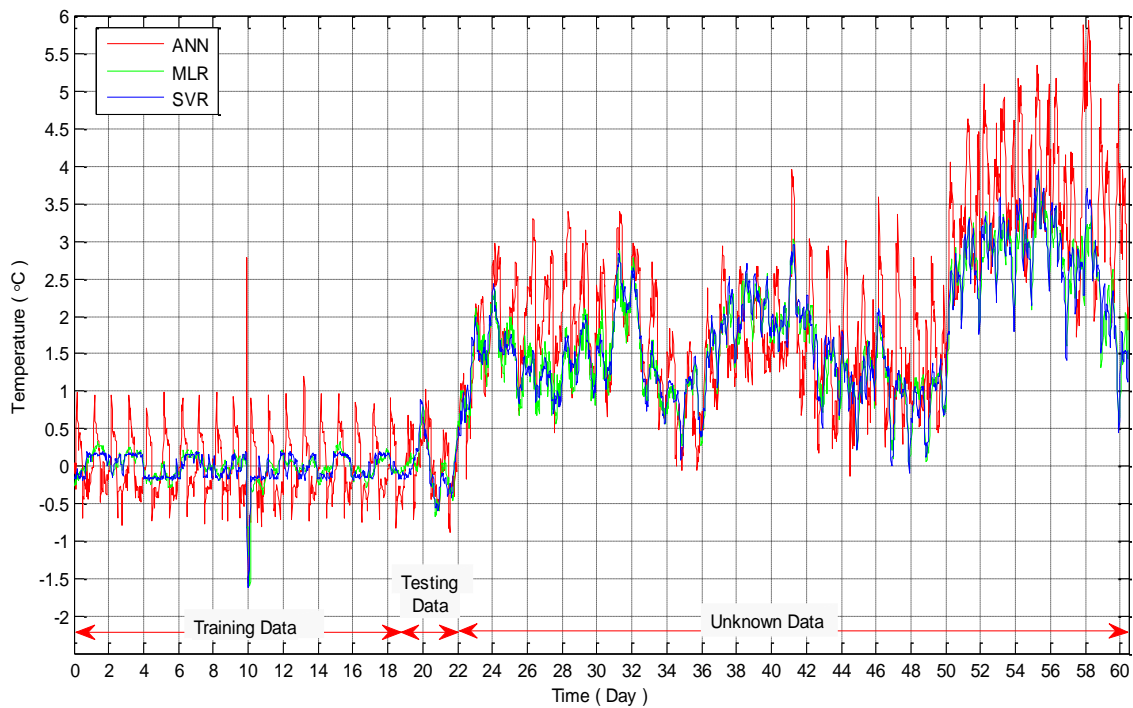

Fig. 56 Temperature prediction error for TC S11 using ANN, SVR and MLR.

78

as a hot-spot. The Mboost performed well to identify the hot-spots but had slightly underestimated the hot-spots amplitude as it can been seen from Figures 56 and 57. Mboost was able as well to identify the anomaly caused by the flooding.
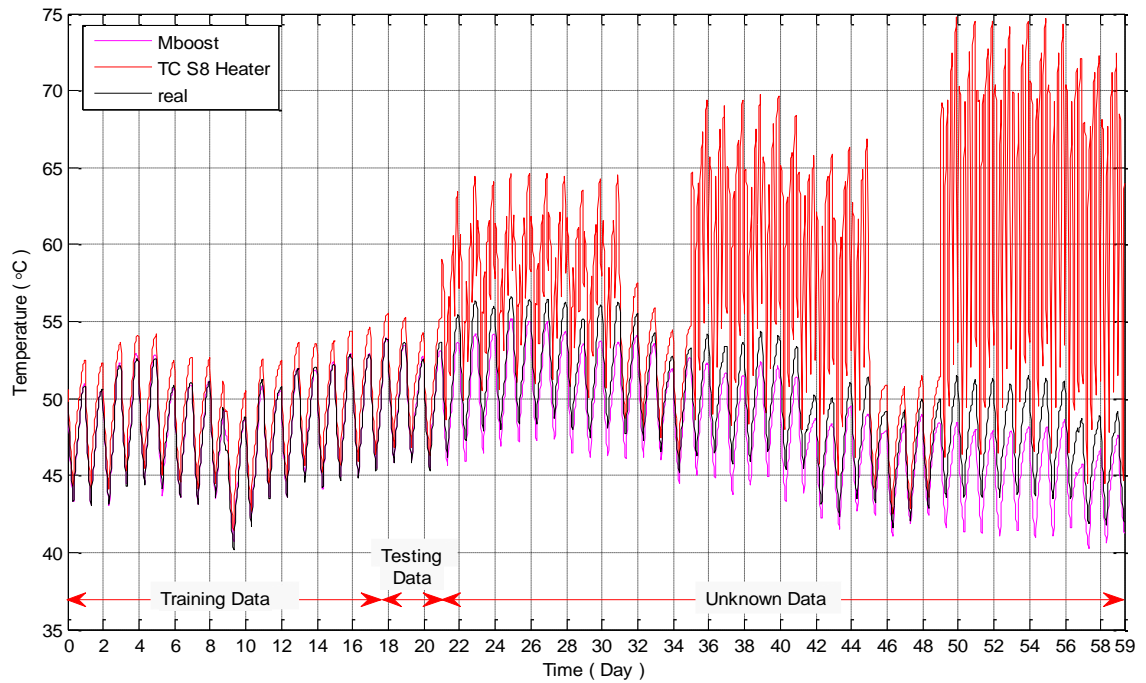

Fig. 57   Comparison between predicted temperature on Testing Data (MAPE=1.37%) and
Unknown Data (MAPE=8.12%) with the real temperature of TC S11 using Mboost.
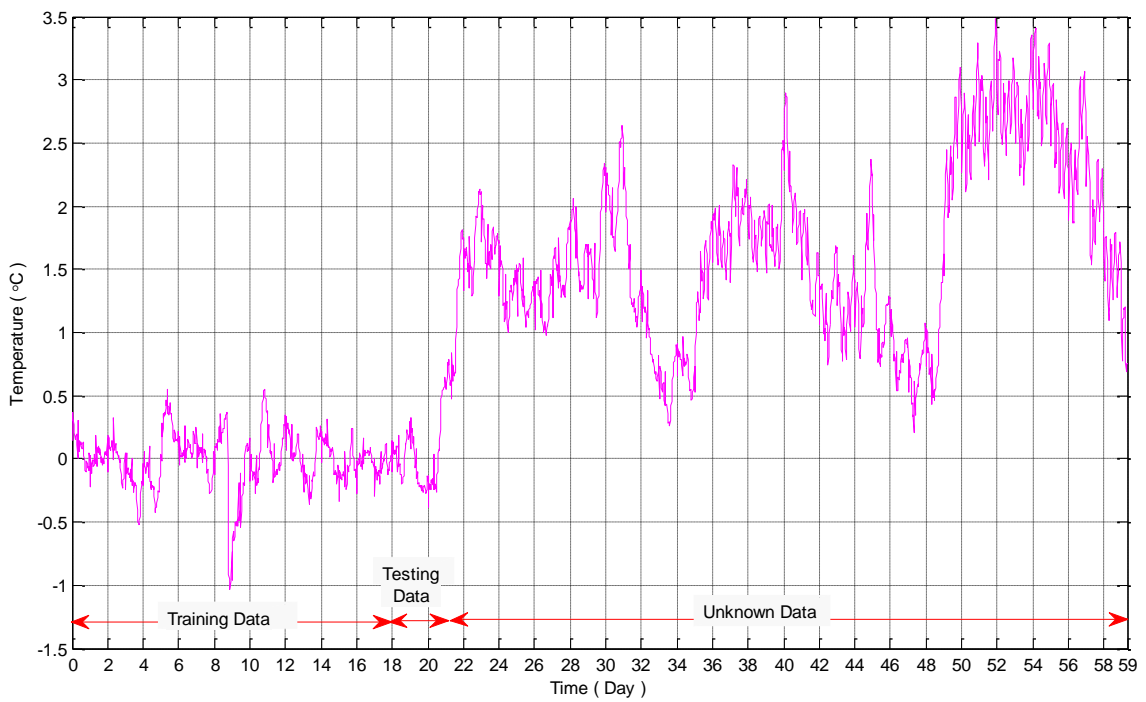

Fig. 58 Temperature prediction error for TC S11 using Mboost.

It can be seen that MLR had better performance during the cyclic load rather than the constant load experiment due to its linear method approach. The reason behind this is that during the cyclic load experiment the temperature profile on the cable depends more on the cyclic load profile rather than the air ambient temperature as happened during the constant load experiment. In the cyclic load experiment the temperature pattern is more consistent in shape because it depends more on the loading profile rather than the air ambient temperature. The amplitude of temperature pattern is dependent on the air ambient temperature but not the shape of the pattern. On the other hand during the constant load experiment the temperature pattern of the cable depends mainly on the air ambient temperature. Therefore MLR can easier develop the regression models in a more controllable environment such as the cyclic load experiment rather than in more uncontrollable environment like the constant load experiment. In order to verify the above assumption a sensitivity test was performed to identify which input feature parameters are more dominant during the two loading experiments. The input parameters were multiplied by 1.2 and 0.8 times of their values to create an uncertainty boundaries of ±20 %. The input features were varied independently one by one at the time. Afterwards the new model was produced and the new MAPE error was calculated for each of the tests. Table 11 below shows the corresponding MAPE error for each of the input features after the multiplication by 1.2 and 0.8 times.

Constant Load Experiment (MLR) Initial MAPE=1.34%			Cyclic Load Experiment (MLR) Initial MAPE=1.33%	
Parameter	x1.2	x0.8	x1.2	x0.8
Air	0.99	2.56	1.65	1.90
Solar	1.59	1.10	1.42	1.41
TC S2	2.64	1.74	3.10	4.14
Load	-	-	1.70	1.92

Table 11 Input parameters sensitivity test.

It can be seen that the air ambient temperature and TC S2 caused the biggest mean error during the constant load experiment while during the cyclic load experiment the TC S2 and the load input feature contribute to the biggest mean error. Thus it can be stated that the initial assumption that the cyclic load profile is more dominant than the air ambient temperature in the cyclic load experiment is valid.

5.2   Accuracy of Thermal Prognostic Models

It is of a great importance to have a reliable Thermal Prognostic Model which will provide confidence to users. In order to achieve that confidence, system error analysis was performed to distinguish the accuracy in temperature prediction. The model error, the input data error as well as the data logger system error were taken into the account.

Two values are experimentally consistent if the following inequality is true:

$$|A - B| \leq |\Delta A + \Delta B| \qquad (9)$$

where A and B are the values to be compared and ΔA and ΔB are the uncertainties of each of there values respectively. In this case this inequality could be used to identify possible error deviations of the real temperature measured by the thermocouple and the model predicted temperature which is greater than $|\Delta A + \Delta B|$. In this case the above equation could be written as follows:

$$|Real - Predicted| \leq |\Delta Real + \Delta Predicted| \qquad (10)$$

The ΔReal uncertainty includes the uncertainty of the thermocouple and the uncertainty from the Campbell Scientific Datalogger CR1000. The uncertainty due to the thermocouple sensor used is ±0.5ºC and the uncertainty from the CR1000 is ±0.1ºC.

The ΔPredicted uncertainty is due to the model prediction error. With a machine learning technique like SVR, there is no clear relationship between the accuracy of the inputs and the accuracy of the output. The non-linear transform due to the kernel function means that the SVR responds to specific values of inputs in different ways. Therefore, the accuracy of some values of inputs will be more or less important for the output than other values of the same inputs.

In order to investigate which parameters are the most dominant in the propagation of the model error, a sensitivity uncertainty test was performed. The model input parameters distribution was changed as shown in Figure 59 for the case of air ambient temperature. The parameters were multiplied by 1.2 and 0.8 in order to identify the error propagation boundaries of ±20% of a change on the input parameters. Solar radiation, air ambient temperature and the temperature of TC S2 are the input parameters used for the development of the constant load experiment model while for the cyclic load experiment

the load profile parameter was added. The corresponding errors were calculated and are shown in Table 12.

Constant Load Experiment (SVR) Initial MAPE=0.89%			Cyclic Load Experiment (SVR) Initial MAPE =1.32%	
Parameter	x1.2	x0.8	x1.2	x0.8
Air	1.49 (over)	2.73 (under)	1.66 (under)	2.05 (over)
Solar	0.98 (under)	0.84 (over)	1.51 (under)	1.43 (over)
TC S2	2.21 (under)	2.28 (over)	3.02 (under)	4.20 (over)
Load	-	-	1.75 (under)	1.75 (over)

over= overestimated under= underestimated

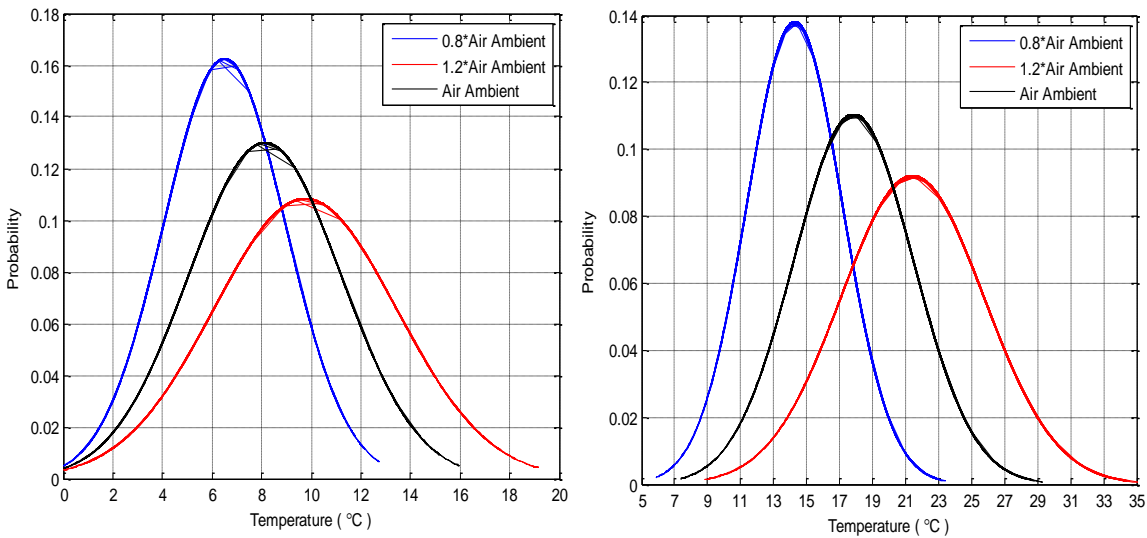Table 12 Uncertainty sensitivity test accuracies.

Fig. 59 Gaussian distribution of air ambient temperature for constant load experiment of the left and cyclic load experiment on the right.

The MAPE error prior to the change of the distribution of the input parameters was 0.89% for the constant load experiment and 1.32% for the cyclic load experiment. The air ambient temperature and the temperature of TC S2 contribute to the highest mean MAPE model prediction error during the constant loading experiment. For the cyclic load experiment the parameters that contribute to the highest mean MAPE model prediction error are the air ambient temperature, the TC S2 and the load.

In order to calculate the worst case scenario for the maximum and minimum cases the overestimated and underestimated parameters respectively where taken into account. The

maximum MAPE error for the constant load experiment was found to be 4.04 % and the minimum MAPE error 4.46%. For the cyclic load experiment the maximum MAPE error was 6.76% and the minimum MAPE error was 4.62 %. These differences can be calculated as a standard deviation of ±0.33℃ from the prediction outputs of the worst case scenarios for the constant load experiment and ±1.07℃ for the cyclic load experiment. A graphical representation of the overestimated and underestimated models during the testing period is shown in Figure 60. Therefore the total uncertainty of the system for the constant load experiment can be defined as follows:

$$|Real - Predicted| \leq |\ 0.6°C + 0.33°C|\ \ (11)$$

Hence temperature prediction errors greater than ±0.93℃ for constant load and ±1.67℃ for cyclic load have to be investigated further.

The performed model error analysis is based on the distribution of the input data of ±20%. Hence if the Gaussian distribution of the input data is smaller it will result to a smaller error propagation during the error analysis. For the constant load experiment, performed during the months of October and November, the distribution of the air ambient temperature was from 0-16℃ with standard deviation of 16℃ ± 3℃ while during the cyclic load experiment, performed from June to September, the temperature distribution of the air ambient temperature varied from 7℃ - 29℃ with a standard deviation of 22℃
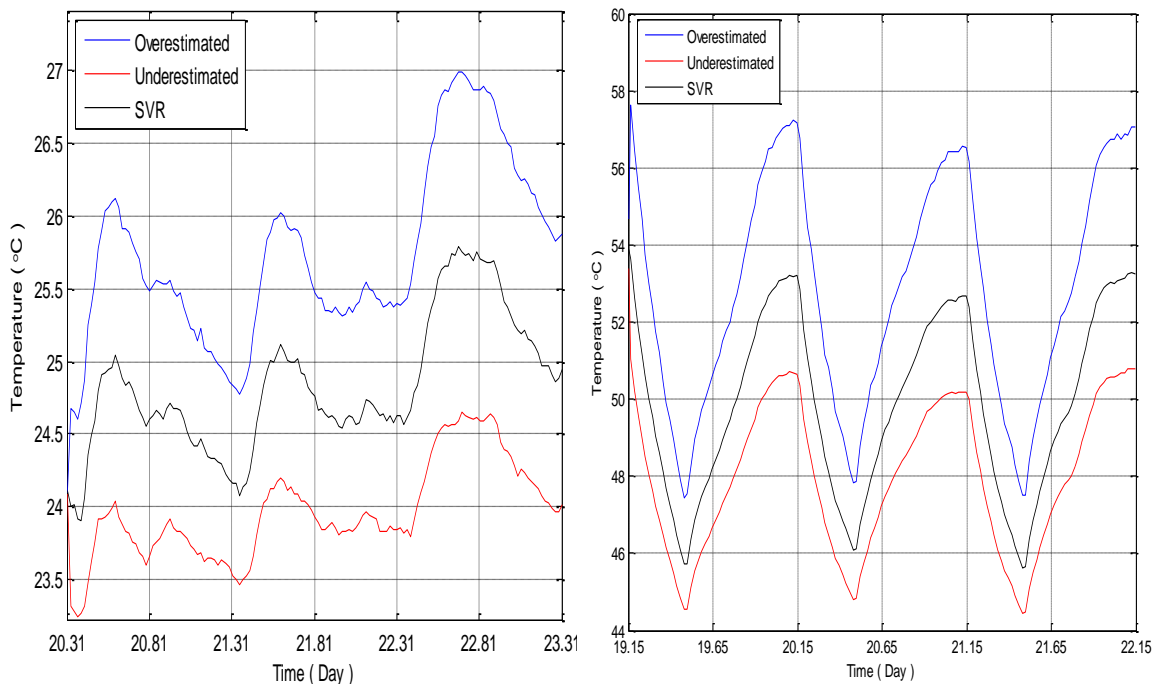

Fig. 60   Worst case scenarios (maximum and minimum) for constant load experiment of the left and
cyclic load experiment on the right.

83

± 4℃ as it can be seen in Figures 59 above. Therefore different temperature distribution results in different error propagation.

A second method to calculate the worst case scenario for the SVR model error propagation is shown below:

$$|Real - Predicted| \leq |\Delta R + 3 * \text{std}(\text{model error}) + \text{mean}(\text{model error})| \quad (12)$$

where model error is the temperature difference error calculated as the difference between the real temperature and the predicted temperature during the testing period. The 3 times standard deviation of the model error was used in order to cover 99.7% of the whole probability error that can occur during the development of the model. The model error for the case of SVR was calculated without changing the distribution of the input parameters to be ±0.32℃ for constant load experiment and ±1.09℃ for the cyclic load experiment. Hence the total uncertainty of the system for the constant load can be calculated using Equation 12. That results in an uncertainty error of ±0.92℃ for the constant load experiment and ±1.69℃ for the cyclic load experiment which is approximately 1% difference from the worst case scenarios values calculated before. Thus this method of calculating the total system error is less complex and easier to be calculated during the implementation of an online condition monitoring system. The idea is to calculate the model error during the testing time and then use that value as a measure to identify potential hot-spots in the field. A decision making algorithm which is discussed further in the Chapter 6 will provide the user with confidence and will determine if the detected abnormal activity on the cable surface is caused by a hot-spot, a power cut, a sensor failure or a model problem.

5.3 Verification of model parameters selection (Cyclic Load)

The temperature distribution of the TCs S11 and S2 was investigated in order to identify which temperature difference was the most frequent prior the introduction of the hot-spots. During the introduction of the hot-spots an increase of the temperature above the average temperature difference of TCs S11 and S2 was observed. The magnitude of that temperature increase ΔT can be calculated by:

$$\Delta T = T_{S11} - T_{S2} - T_{mean(S11,S2)} \quad (13)$$

The ΔT can be compared with the temperature difference between the real temperature of TC S11 and the predicted temperature of S11 from the model. This comparison can be used to identify if the best pair of the model parameters C and γ was selected correctly during the development of the model.

The histograms of the TC S2 and TC S11 before the introduction of the hot-spots for the constant load experiment were plotted in order to identify the most frequent temperature as is shown in Figures 61 and 62. The average temperature difference was calculated by subtracting the highest frequent temperature of TCs S2 and S11.

The average temperature difference between TC S2 and TC S11 before the introduction of the hot-spots was 3.8 ℃. The real maximum difference during the introduction of the hot-spot was 6.34 ℃ hence an increase of the temperature by 2.54 ℃ happens due to the influence of the hot-spot. The difference of the predicted temperature of the TC S11 and the real temperature of TC S11 was 2.56 ℃.

Therefore the model parameters C and γ were well chosen and the model is accurate enough, as the percentage error temperature difference of the real and the predicted values was around 1%. The above procedure was carried out to investigate if the selection of parameters C and γ for the other TCs prediction models was accurately selected.
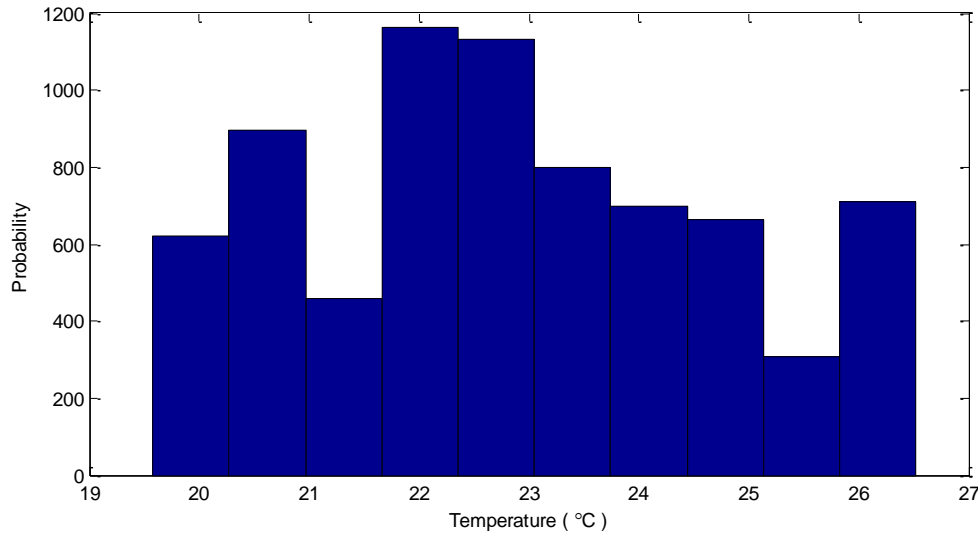

Fig. 61 Temperature distribution of TC S2 prior the influence of Hot-Spots.

For the load cycle experiment due to its more complex loading demand and temperature distribution a second approach was used. That approach did not take into account just the highest maximum temperature difference due to the introduction of the hot-spots but the

85

mean increase temperature for the different periods of the hot-spots was used. Hence the theoretical mean increase, calculated from Equation 13, for 5 W hot-spot was 1.46 ℃, for 10 W was 1.88℃ and for 15 W 2.77℃.
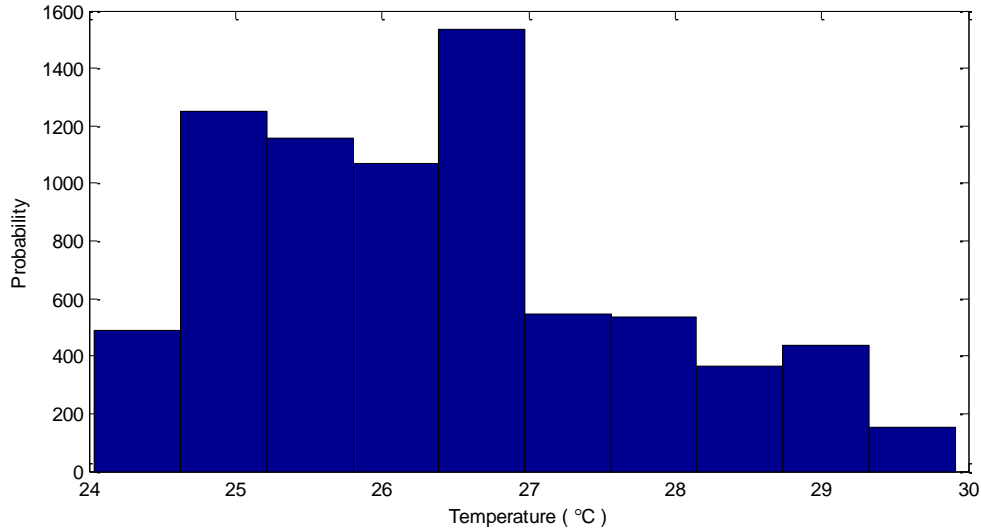

Fig. 62 Temperature distribution of TC S11 prior the influence of Hot-

The model predicted temperature difference increased for 5 W was 1.50 ℃, for 10 W 1.71 ℃ and for 15 W was 2.68℃. It can be seen in Figure 63 that the model parameters, C and γ, have been selected appropriately as they do not only give satisfactory results but as well provide a generalized solution where the output approximation waveform of it is closely matching the theoretical temperature difference.
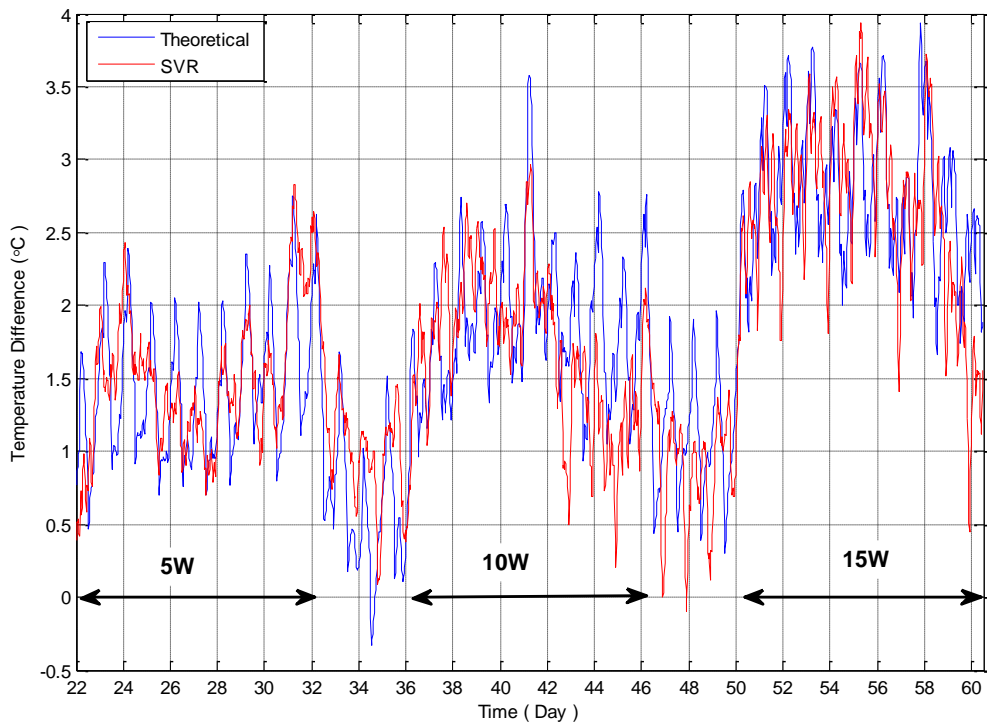

Fig. 63   Model and theoretical temperature prediction error for TC S11 during the

daily loading demand under the influence of hot-spots.

The drying out of the soil became more significant after the day 42 and can explain the reason why the theoretical temperature difference with the model temperature difference started to have a slight difference in magnitude. The theoretical temperature difference did not take into account drying out of the soil as the temperature values of the TC S11 and TC S2, which were used in Equation 13, were prior the introduction of hot-spots. While the temperature of TCs used in the model is influenced by the drying out soil process.

In comparison to the SVR the MLR, Mboost and ANN have lower generalization performance. Table 13 summarizes the performance of the other algorithms.

Method	5 W	10 W	15 W
Theory	1.46 ℃	1.88 ℃	2.77 ℃
SVR	1.50 ℃	1.71 ℃	2.68 ℃
MLR	1.50 ℃	1.68 ℃	2.66 ℃
Mboost	1.52 ℃	1.63 ℃	2.44 ℃
ANN	1.97 ℃	1.68 ℃	3.61 ℃

Table 13 Benchmarking generalization performance.

MLR showed good generalization performance as well as SVR. Mboost was the third best and ANN had the worst performance. Thus the ideal algorithm must not only be able to identify the number of the hot-spots but also accurately predict the amplitude of these hot-spots otherwise faulty decisions might be taken.

5.4   Summary

Thermal prognostic models in a soil filled trench under constant and cycling loading conditions were developed. The developed models took into account the sensitivity tests performed prior in Chapter 4. The soil filled trench is a more complex system than the air filled trench hence the suggested methodology of multiple time intervals was applied to identify the optimal number of input data required for SVR to develop a generalized model. During the loading profiles artificial hot-spots were introduced. The thermal prognostic models were able to identify the abnormal changes in the cable surface temperature due to the existence of the external heat source. Thus it was verified that the

thermal prognostic models are able to monitor specific areas of an underground cable, where hot-spots are more likely to occur such as of joints, and identify the hot-spot locations in a radius of up to 0.30 m.

From the benchmarking performed for both constant load and cyclic load experiments SVR showed the best performance in both cases. SVR was able to identify the highest number of hot-spots in both experiments as well as to produce generalized models. MLR showed satisfactory performance during the cyclic load experiment but average performance during the constant load experiment. Furthermore MLR produced models with a better generalization performance than ANN and Mboost. ANN and Mboost were not consistent and lacked the generalization feature.

An in depth investigation of system error analysis was performed. Real uncertainties due to the TCs and the data logger as well as possible prediction uncertainties were calculated in order to give a measure of confidence for the thermal prognostic models. It was found that temperature prediction errors greater than ±0.92 ℃ for the constant load experiment and ±1.69 ℃ for the cyclic load experiment have to be investigated further and will be further discussed in Chapter 6. New techniques have been introduced in order to identify if the best pair of model parameters C and γ were selected correctly during the development of the thermal prognostic models. The difference between the theoretical and model temperature difference were compared and analyzed. The results showed that the theoretical temperature difference closely matches the model temperature difference but the magnitude of their difference can be affected by the drying out process of the soil in the soil filled trench.

The implementation of suggested thermal condition monitoring prognostic system in the field experiment and analysis of the outcomes of the field experiments performed in Cyprus MV distribution substation as well as suggested Thermal Anomaly Decision Algorithm (TADA) are presented in Chapter 6.

Chapter 6 Development of a Thermal Condition Monitoring System

Collaboration with the Electricity Authority of Cyprus (EAC) and the University of Cyprus (UCY) has allowed development of an experiment in a distribution substation. Temperature condition monitoring units were installed on selected underground cable joints within an MV substation in Cyprus. Real-time current loading data, weather conditions as well as surface temperature beside the cable joints were used for the development of the thermal prognostic models. The thermal condition monitoring system installed in Cyprus is described and the results are presented as well as the suggested thermal anomaly decision algorithm which is able to identify the nature of a fault that might occur is introduced.

6.1 Cyprus Field Experiment

Cyprus represents an ideal system to study as it is an islanded network that sees heavy demand during the tourist season as well as being far smaller and less complex in design compared to UK distribution networks.

In addition, Cyprus offers environmental conditions different to UK (dry hot summers, mild winters). Hence, data collected in these conditions alongside the data collected in UK, can be a key factor to investigate a life-time of the cable in different environments and ensure the development of a universal condition monitoring thermal prognostic indicator system is effective in a variety of environments.

Collaboration with the University of Cyprus (UCY) and the Electricity Authority of Cyprus (EAC) has allowed the development of experiment in the field. Field measurements in MV substations in Cyprus have taken place. The implementation involves monitoring of weather conditions, temperature of the cable underground joints and circuit current loadings in order to gain data which will be implemented while developing the condition monitoring thermal prognostic indicator system. Joints closest to the substations are chosen as according to the literature and local experiments they are the ones where the highest percentage of failures occur as well as they have the easiest accessibility.

6.2 Cyprus Experimental Setup

The installation took place at Agios Georgios substation in Larnaca (132/11 kV), Cyprus. EAC found and exposed four cable joints. The first cable joint was a straight 3-phase PILC, the second was three XLPE straight joints and the last two cable joints were transition joints XLPE to PILC. Figure 64 shows the corresponding joints.

| PILC-PILC | XLPE-XLPE | XLPE-PILC | XLPE-PILC |
| Circuit 1 | Circuit 2 | Circuit 3 | Circuit 4 |

Fig. 64 Cable joints under investigation

First the cable joints where uncovered, then a power outage took place for each of the joints in order to install the TCs in different locations as is shown in Figures 65. As a final point cable joints were covered by inserting the appropriate backfill and placing the condition monitoring unit inside the ground. Pictures shown in Figure 66 illustrate the undertaken process.

A monitoring unit, shown in Figure 67, consists of a Campbell Scientific datalogger CR1000 which logs the temperature of the installed TCs across the cable joint and a Campbell Scientific NL120 which allows the datalogger to communicate over a dedicated Internet connection via TCP/IP connected with an ethernet cable. The four monitoring units, one for each cable joint, were assigned to a unique public IP address and connected via ethernet cable to a router. The data were collected from the dataloggers twice per day by communication over the Internet connection.
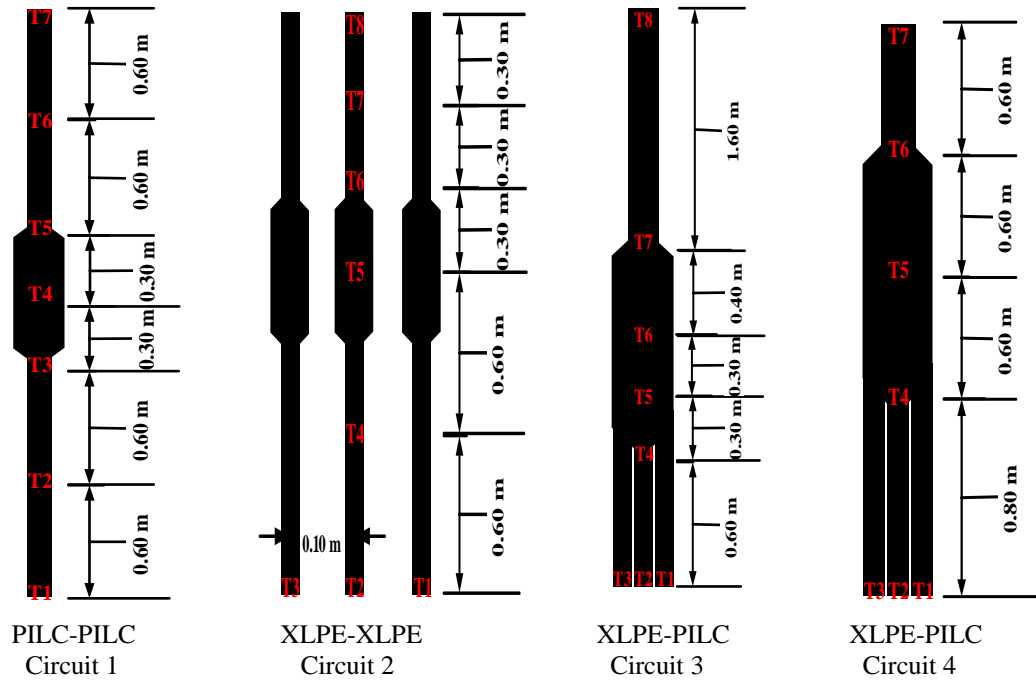
Fig. 65 Layout of TCs on the attached on the surface of the cable joint.

Fig. 66 Excavation of cable joint, installation of TCs and cover of cable joint.

In addition to the temperature logging of the cable joints, the current loading of the four cable joint circuits was monitored as well. Four RCTi-3phase Rogowski coils were used to measure the current passing through the cables for each of the circuits of the cable joints in real-time. The secondary output from the RCTi-3phase is an instantaneous DC voltage proportional to the measured primary current. A multiplexer was used to log the current measurement for each of the circuits. Figure 66 shows the installation of the Rogowski coils for one of the circuits as well as the connection of the output of the Rogowski coils to the multiplexer AM16/32.

91

A power control unit is located inside the substation. It consists of four 18 VAC transformers which are connected to four main sockets. The transformers are connected to four CH150 Campbell Scientific regulator units. The CH150 is responsible for charging the 12V battery, which powers up the data logger, as well as to supply a constant regulated 12 V output to the data logger. In case of a power interruption the batteries are enabled and back-up power is provided to the data loggers.
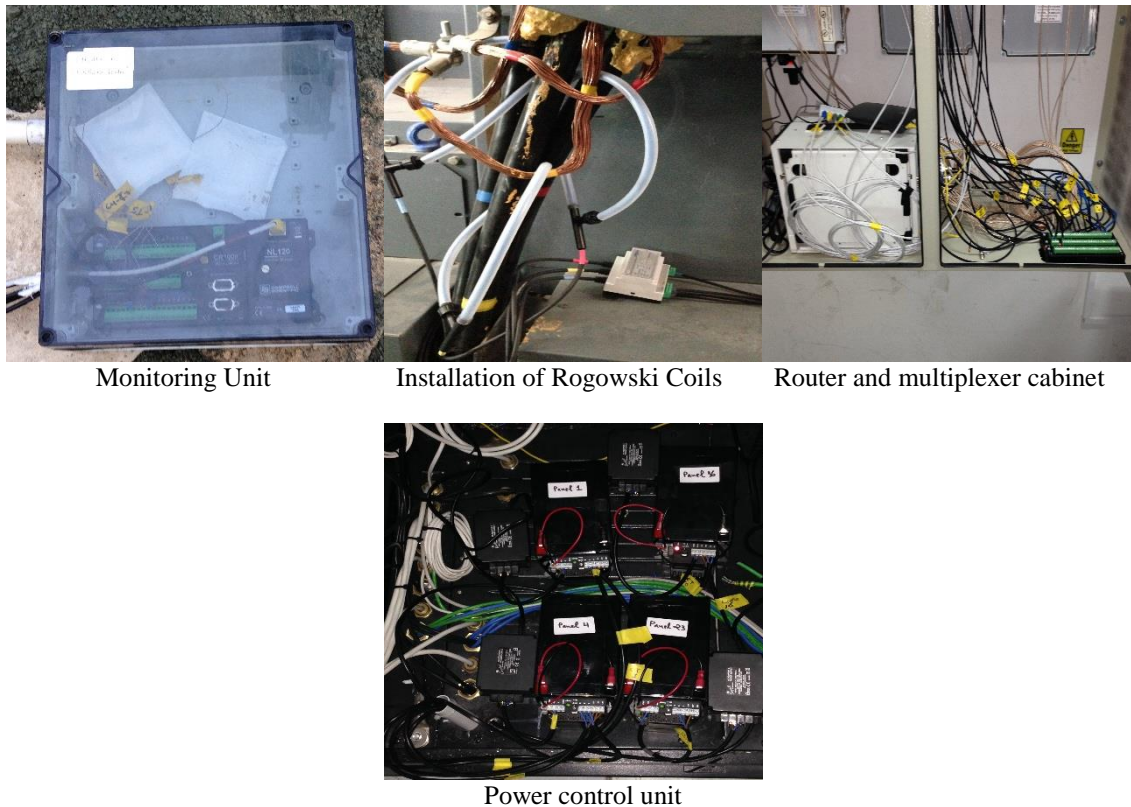

| Monitoring Unit | Installation of Rogowski Coils | Router and multiplexer cabinet |

Power control unit

Fig. 67 Monitoring Unit, installed Rogowski coils, router-multiplexer cabinet and power control unit

An underground plastic pipe duct for each data logger was installed for an ethernet cable and the power lead cable. The ethernet cable connects the data logger to the router (communication unit) and the power lead cables connect the data logger to power control unit. For the last data logger, assigned as CR1000_4, extra connection wires were required to pass through the underground pipe in order to establish the connection between the outputs of the Rogowski coils, the multiplexer AM16/32 and the data logger CR1000_4.The schematic shown in Figure 68 represents the overall connection in the substation. The factors that are required to build the thermal prognostic model for the four different cable joints are listed in the Table 14.

Factors	Unit	Measurement Interval	Averaging Interval
Air Temperature	˚C	15 minutes	30 minutes
Solar Radiation	Wm-2	15 minutes	30 minutes
Cable Temperature	˚C	5 minutes	30 minutes
Current Loading	A	5 minutes	30 minutes

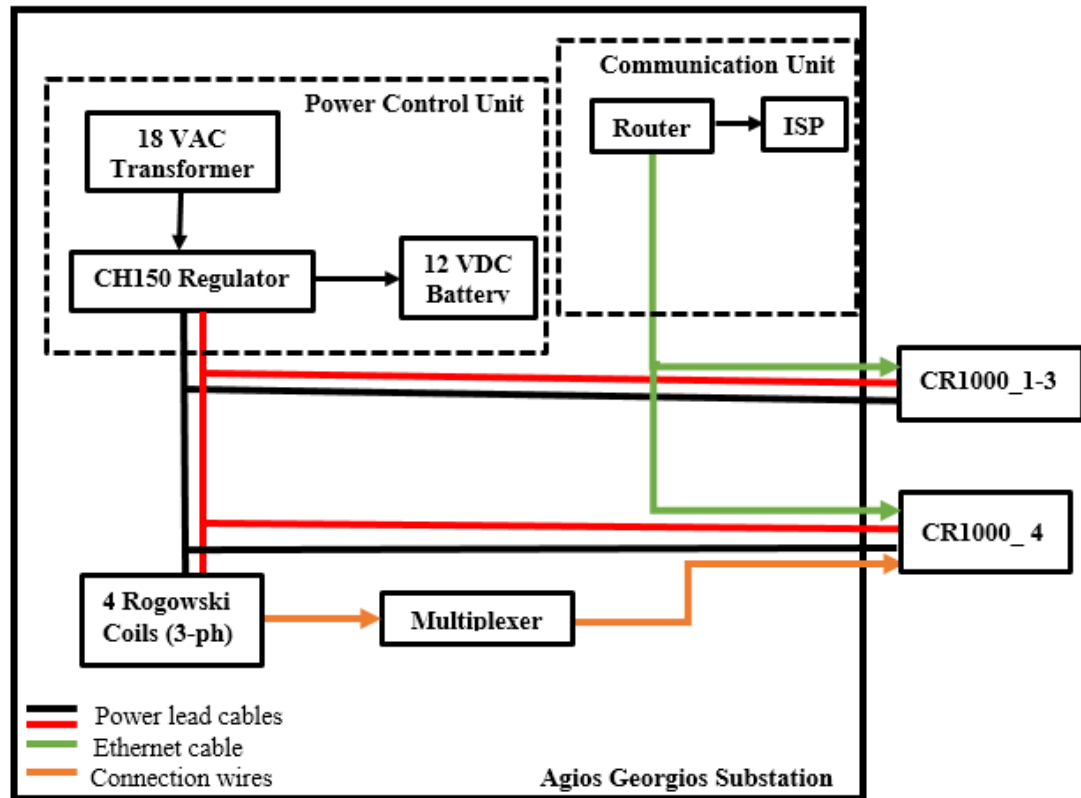Table 14 Input parameters used for the development of the thermal prognostic models

Fig. 68 Schematic diagram of the connection inside the Sub-station

6.3   Thermal Anomaly Decision Algorithm

A Thermal Anomaly Decision Algorithm (TADA) for the thermal prognostic models has been implemented. The development of the suggested algorithm will bring confidence in the reliability of the whole system as it will be able to identify and categorize potential failures to hazardous and non-hazardous.

The proposed thermal prognostic condition monitoring system is shown in Figure 69. Real time measurements update the thermal prognostic algorithm where the output of it is checked in real time by the TADA. TADA is capable of identifying whether an instantaneous difference between real temperature and predicted temperature is an actual upcoming failure alert due to the development of hot-spots or different other scenarios such as an emergency rating, power cut, heavy rain, model problem or sensor failures.
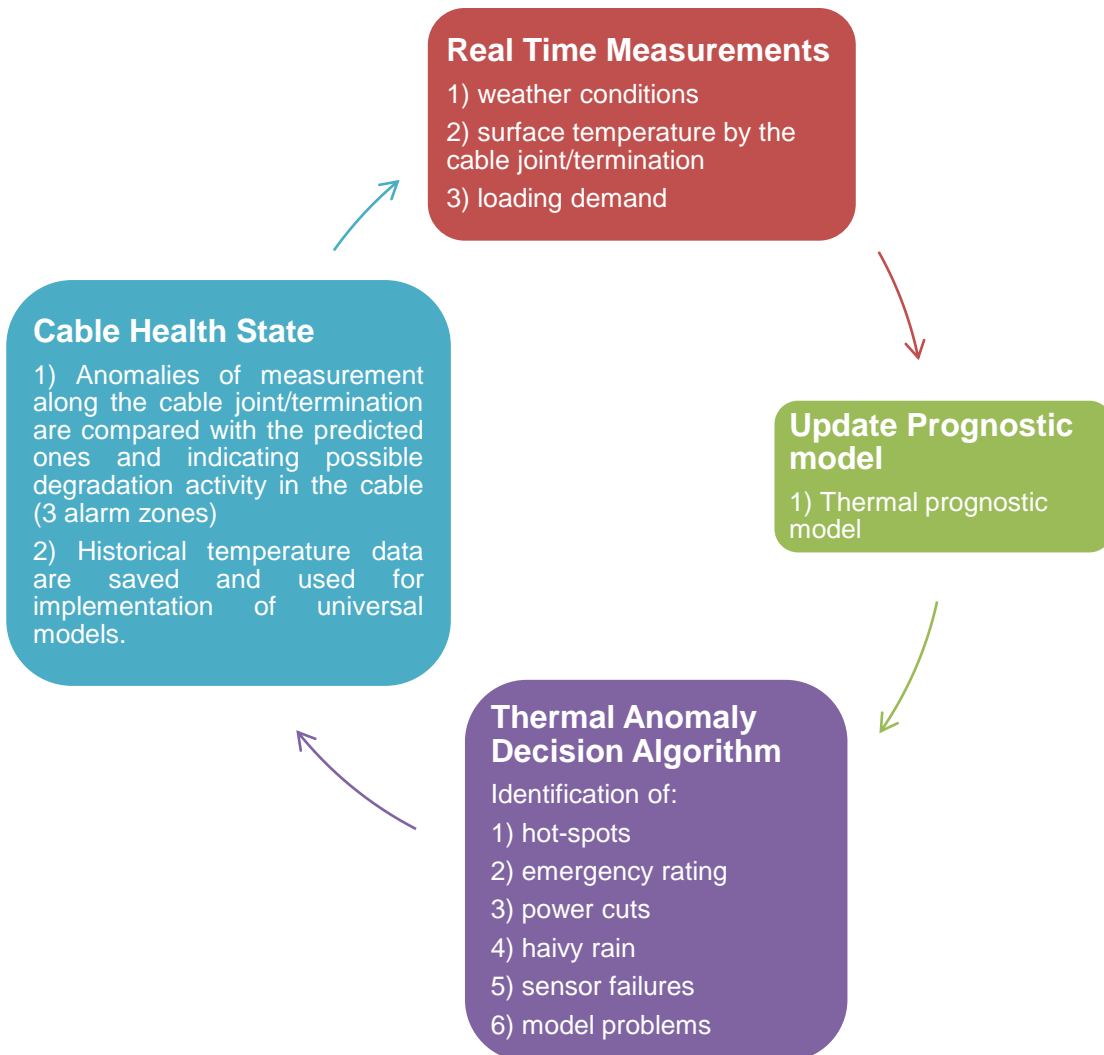
Real Time Measurements
1) weather conditions
2) surface temperature by the cable joint/termination
3) loading demand

Cable Health State
1) Anomalies of measurement along the cable joint/termination are compared with the predicted ones and indicating possible degradation activity in the cable (3 alarm zones)
2) Historical temperature data are saved and used for implementation of universal models.

Update Prognostic model
1) Thermal prognostic model

Thermal Anomaly Decision Algorithm
Identification of:
1) hot-spots
2) emergency rating
3) power cuts
4) haivy rain
5) sensor failures
6) model problems

Fig. 69 Proposed thermal condition monitoring system

94

6.3.1   TADA description

The TADA algorithm was developed taking into account the results obtained in Section 5.2, in particular Equation 12. The idea of calculating the total model error uncertainty based on the testing data standard deviation error technique is the key factor of this online decision making algorithm. Figure 70 shows the flowchart of the TADA algorithm.

With reference to Figure 70, every new output obtained by the thermal prognostic model is checked continuously by TADA. TADA automatically reads the current real temperature of the sensor under investigation R1, the predicted output temperature P1 and the current load passing through the cable L1. Then the uncertainty boundaries B1 and B2 are calculated based on the Equation 12 as shown in the flowchart detailed in Figure 70. Afterwards the temperature prediction error E1 is calculated by subtracting the P1 from R1. For any value of E1 which falls between the two boundaries no action has to be taken and the new available values of R1, P1 and L1 are read. But if the E1 is outside the two boundaries then an action is implemented. There are two possible scenarios. The first one is when E1 is greater than B2 which means that the real temperature R1 is greater than the predicted temperature P1. The second scenario is when E1 is smaller than B1 which means that P1 is greater than R1. Hence in order to investigate further the possible scenarios the previous values of load L1p and real temperatures R1p are read. Next two new variables ER_p and EL_p which represent the difference between two successive values of real temperature and load are calculated.

For the case when E1 is greater than B2, the real temperature higher than the predicted, the scenarios of emergency rating, sensor failure and hot-spot have to be identified. From the knowledge gained from the field experience and [102] a 5% unbalanced current loading is permitted. Hence for the investigated circuits in Cyprus, with current loading of 350 A, a current deviation of 17.5 A is allowed. Therefore if the difference between two successive current values, EL_p, is between ±17.5 A it can be consider to be normal. However if EL_p is out of the above range that means that we have a sudden increase of load and therefore an emergency rating in the cable which explains why the real temperature is higher than expected. No action has to be taken and the thermal model continues to work unchanged. In the case where EL_p lies within the expected boundaries we have to investigate further the difference between two successive real temperatures, ER_p. If ER_p is greater than 25℃ it means that it is the case of a sensor failure in the

system as a sudden change of temperature by an increase of 25℃ and above without sudden change of current load cannot explain why the real temperature is higher than the predicted. From the knowledge gained during the experiments in the TDHVL sudden changes of temperatures of that range happen only when thermocouples are failing. Thus if the point of installation is accessible then the thermocouple has to be replaced otherwise another nearby sensor has to be used. On the other hand if the difference of the ER_p is less than 25℃ it indicates the development of a hot-spot activity in the cable. Three alarm zones are used to identify the severity of the hot-spot activity. The temperature threshold levels for the three alarm zones were selected based on the experience gained from backfill trench experiments. The 1℃ difference between the alarm zones was selected in order to increase the sensitivity of the system. That temperature difference can be tuned accordingly after enough knowledge is gained from the field experiments. The Green zone identifies the initiation of a hot-spot activity up to 1℃ in which the operator is informed of a potential degradation activity. The second alarm is the Orange zone where the TADA identifies anomalies from 1℃ - 2℃ and suggests to the operator that an action has to be taken. The third alarm is the Red zone in which the temperature difference lies from 2℃ - 3℃ and above. The alarm informs the operator that an immediate action needs to be taken. The use of a three alarm zone strategy allows the operator to extend the lifetime of existing cables as it is possible to prevent and predict failures as well as to reduce unnecessary maintenance costs and potentially increase customer confidence.

The second scenario is where E1 is less than B1, i.e. the predicted temperature is higher than the real. This can be a case of either a possible sensor failure, a heavy rainfall, a model problem or a power cut. First the EL_p is checked if it lies within the allowed range of ±17.5 A. If not, that means that a power cut happened and resulted in the real temperature to be smaller than the predicted temperature. If yes, then the ER_p is checked if the difference between R1 and R1p is less than - 0.6℃. If that is not true it means that the model has started to over-predict the real temperature and therefore a new model is required. Otherwise if the ER_p is less than -25℃ it means that we have a sensor failure in our system. If the ER_p is less than -0.6℃ but not less than -25℃ means that the temperature drop maybe due to heavy rain because the reading of the thermocouple has been affected by wet conditions. The temperature of -0.6℃ was selected as the maximum possible uncertainty found in the field, thermocouple and datalogger, is ± 0.6℃.
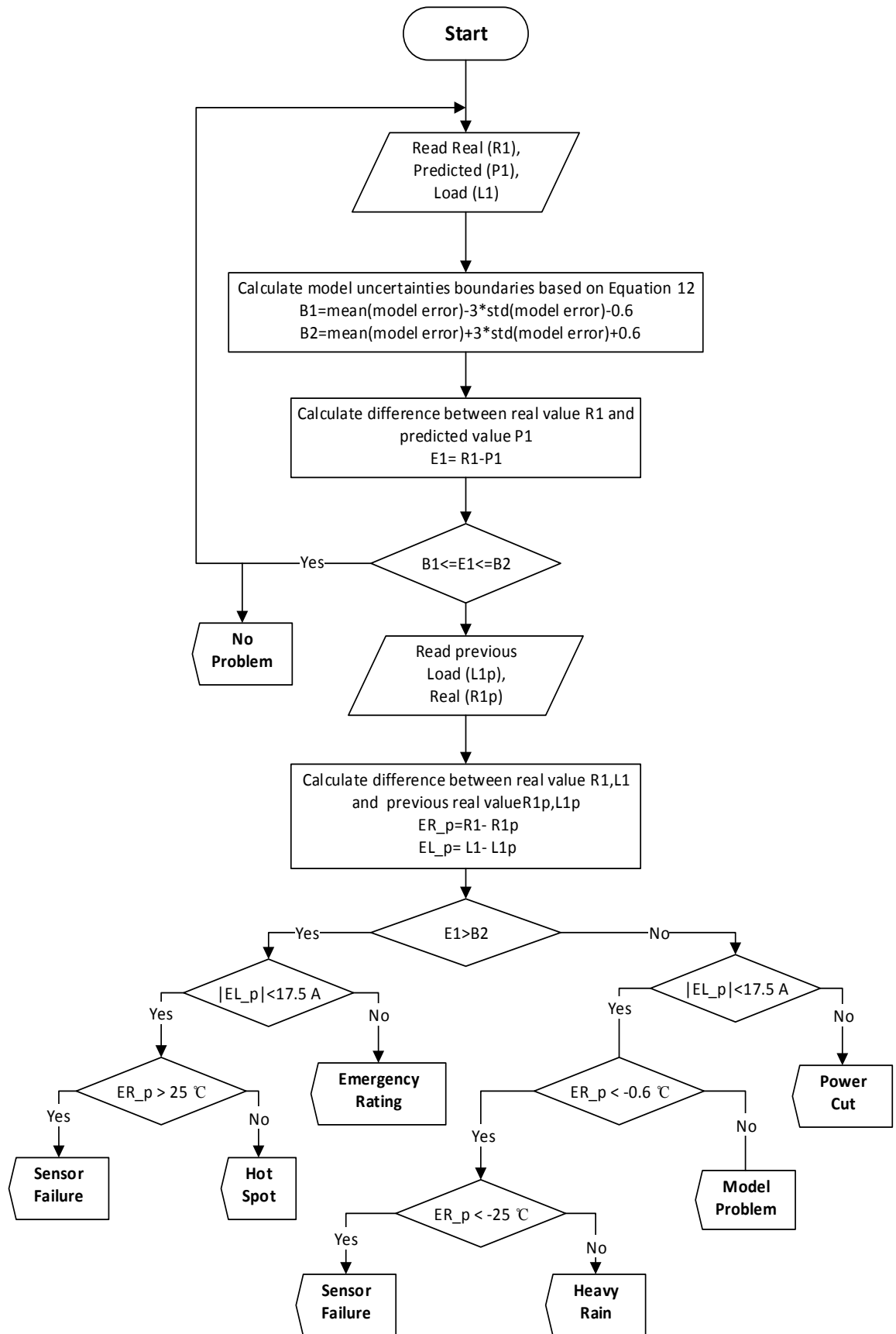
Fig. 70 TADA flowchart

The thermal anomaly decision algorithm will update the operator in real-time about the condition and the health state of the investigated circuit and will give the leverage to identify and prevent the upcoming failures. The suggested decision making algorithm takes into account the most common anomalies that can occur in the field and therefore helps to increase the confidence of the operator to take action responsibly.

6.4   Analysis of field data from Cyprus MV cable circuits

The field experiments were performed for a period of 6 months. The moving window strategy technique, described in more detail in [103], was implemented for all the investigated circuits as the amount of collected data was not enough to create general models. Data collected during the first month of the experiment was not enough to develop feasible models that would be able to work until the end of the experiment due to large changes of load and temperature profiles. Hence a moving window strategy of 56 days was performed, the first 28 days were used to train and test the model. After identifying the parameters for C and γ during the testing period of 3 days, the existing model stayed unchanged to predict the next 28 days of unknown data. After that period of 28 days that unknown data will be used as the new training and testing data for a new model while the previous training and testing data will be not taken into the account but saved as historical data in a database for a development of a universal model over time. The period of 28 days for training and testing as well as for prediction of unknown data was selected due to the satisfactory performance of SVR models developed during the backfill trench experiments. The graphical representation of the moving window strategy is shown in Figure 71.
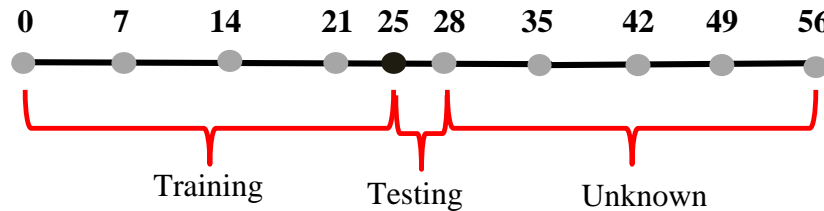
Fig. 71 Graphical representation of moving window strategy.

Implementation of the moving window strategy enables the development of small and robust models that use the latest captured data and remove the previous data to ensure that newly developed models are up-to-date with current dynamics. During the period of the unknown data the thermal anomaly decision algorithm (TADA) is activated. If TADA identifies a hot-spot, the model continues working unchanged in order not to use the hot-spot data in the development of the next model. In case of an emergency rating, power cut or a heavy rainfall the data during that period has to be excluded from the new training dataset. On the other hand if TADA identifies a model problem then the model has to be retrained again with the last 28 days of data. In this way the model works robustly without

any interference through the whole period of the experiment. Two types of activity were found in the investigated circuits during the field experiments. Hot-spots activity was identified in Circuit 3 while Circuit 2 and 4 did not show any hot-spot activity. Circuit 1 did not allow further analysis due to technical issues.

6.4.1   Circuit 3 hot-spot activity

The same analysis as previously described in Sections 5.1.1 and 5.1.5 was performed to identify the relation between the input data and the best amount of input data needed for SVR to develop robust models. The amount of input columns found for this case was 144 30 minute intervals. Hence the initial amount of training data was 22 days, 3 days of testing and therefore the first window length was 53 days. The input features used for the development of the models was the surface temperature of TCs C3_T1, C3_T2, C3_T3 as well as the current loading measured by the Rogowski coils R_C3_B, R_C3_Y and R_C3_R. Weather parameters such as solar radiation and air ambient temperature were not taken into account as were found not to affect the performance of the model as the joint is buried 1.5 meters below the ground surface.

The moving window strategy was implemented and was used to predict the temperature of TCs across the length of Circuit 3. Initially the temperature of TC C3_T6 did not show any signs of hot-spot activity as can be seen in Figures 72-75. It can be seen that the prediction error in the first moving window, Figures 72-73, started slowly to deviate but
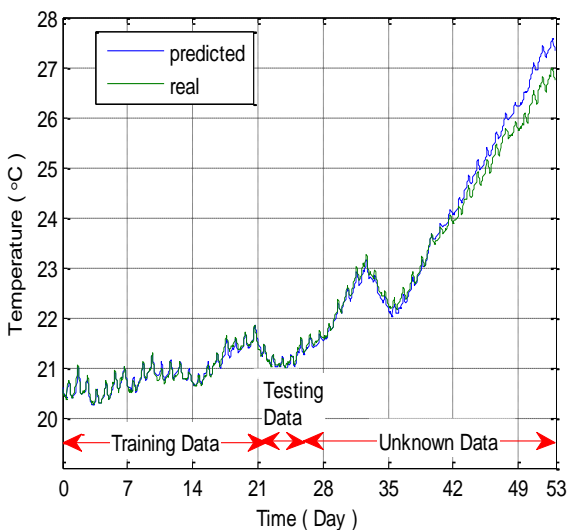

Fig. 72 Comparison between predicted temperature on Testing Data (MAPE=2.12%) and Unknown Data (MAPE=12.04%) with the real temperature of TC C3_T6.
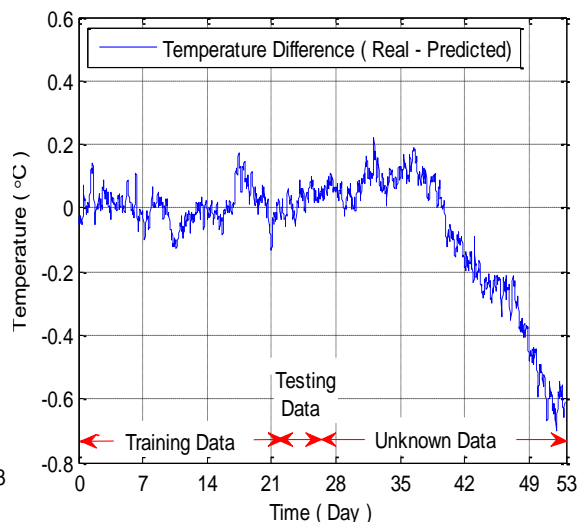
Fig. 73 Temperature prediction error for TC C3_T6.

100

still there was not a need to retrain the model as the prediction error was within the allowed error boundaries, ±0.78℃, set by TADA. The over predictive performance of the model was due to the fact that there were not enough representative patterns of data during the training period which could give the model capability to perform well during the temperature increase of the cable from day 25 and onwards. In Figures 74-75 it can be
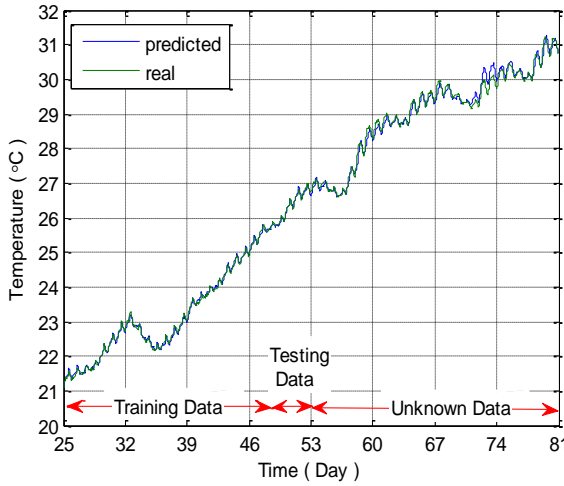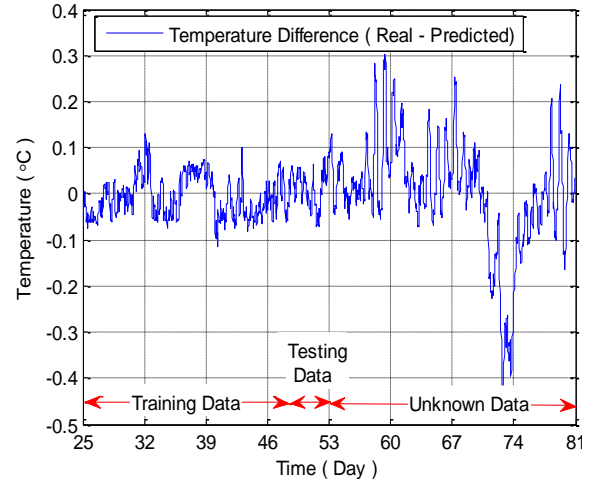

Fig. 74 Comparison between predicted temperature on Testing Data (MAPE=0.7%) and Unknown Data (MAPE=1.28%) with the real temperature of TC C3_T6.

Fig. 75 Temperature prediction error for TC C3_T6.

seen that for the second moving window the previous training data was discarded and substituted the with newer unknown data. The SVR model developed for that period performed well due to the fact that training data included temperature increase patterns similar to those found during the unknown period. Therefore the model had the capability to perform well as the temperature was increasing during the unknown data period. On day 94 of the experiment an emergency rating occurred in the Circuit 3, as can been seen in Figure 76, resulting in an increase of temperature of the cable by 1℃. Two weeks after the emergency rating the TC C3_T6 started showing the first signs of hot-spot activity.
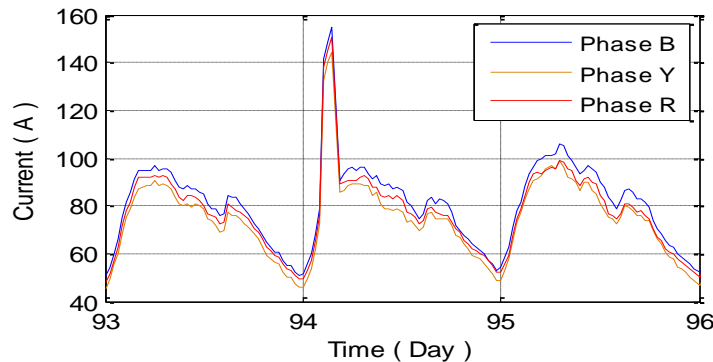

Fig. 76 Emergency rating in Circuit 3 at day 94 of the experiment.

101

As mentioned the model was left to run unchanged. The results of the model prediction are shown in Figures 77 and 79-80 below.
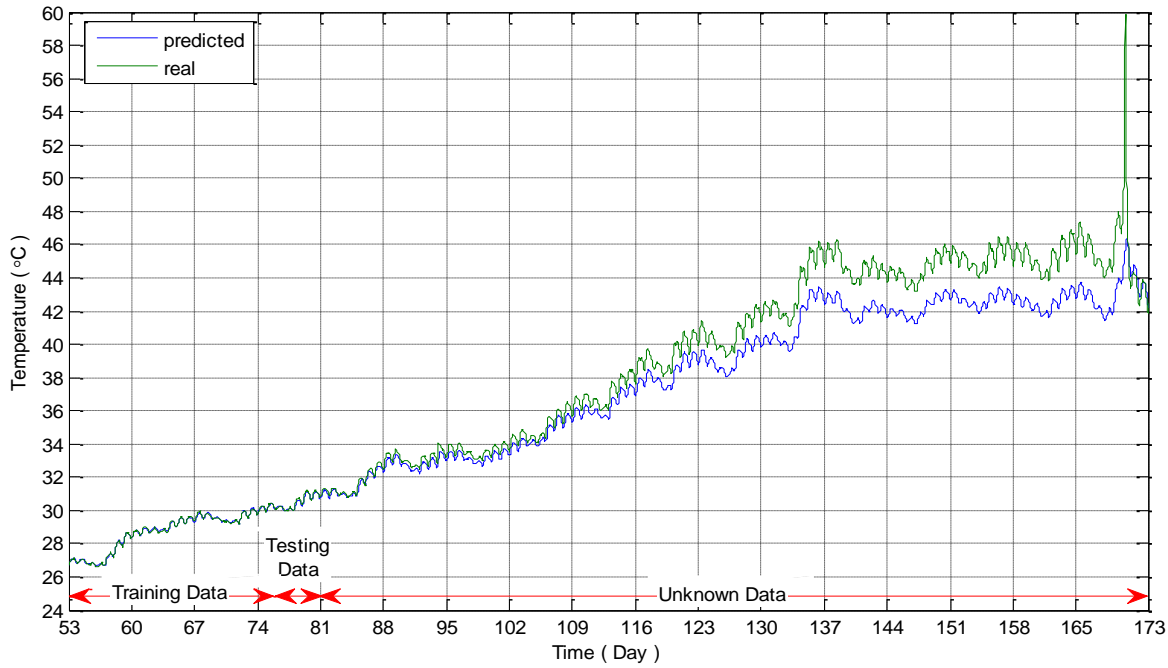

Fig. 77 Comparison between predicted temperature on Testing Data (MAPE=1.8%) and Unknown Data (MAPE=28.52%) with the real temperature of TC C3_T6.

The emergency rating, black circle 1 Figure 78, triggered and drastically accelerated the potential ongoing internal aging activity in the cable joint which resulted in the temperature build up on the cable joint around the location of the TC C3_T6 as shown in Figures 79-80. On day 170 the real temperature exceeded the expected predicted temperature by 14℃.
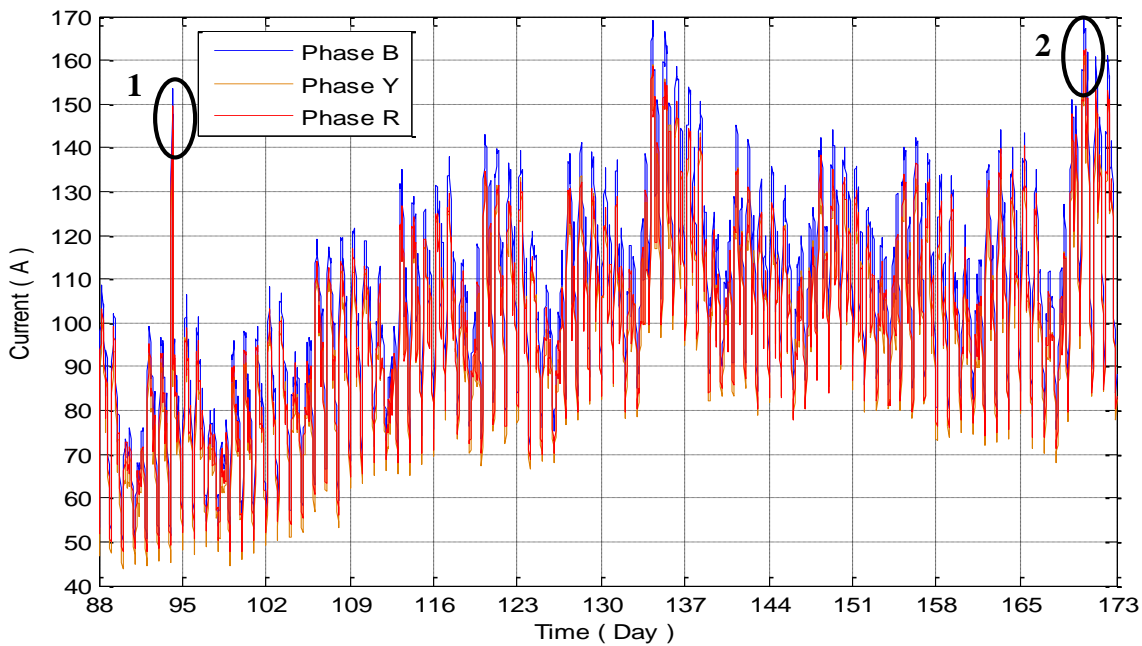
Fig. 78 Load demand for Circuit 3 from day 94 until day 173.

It can be seen from Figure 78 that on day 170, black circle 2, a high load demand rose up. The reason behind the increased load demand was a sand storm from the Sahara desert which struck Cyprus resulting in an increased usage of air conditioning by consumers. Figures 79-80 show the temperature prediction error during that period. A better understanding of the hot-spots location and magnitudes can been seen in Figure 80. Only the temperatures higher than 0.73℃ are plotted as they fall outside the allowed upper limit boundary based on Equation 12 in Section 5.2. From day 94 when the emergency
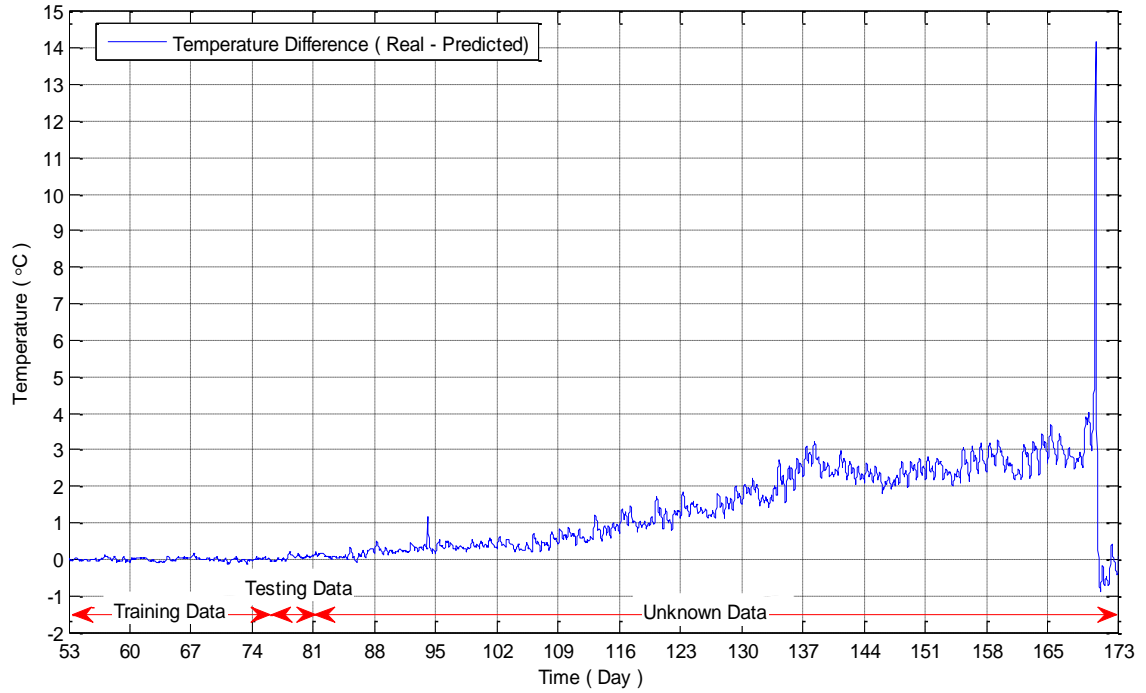
Fig. 79 Temperature prediction error for TC C3_T6.
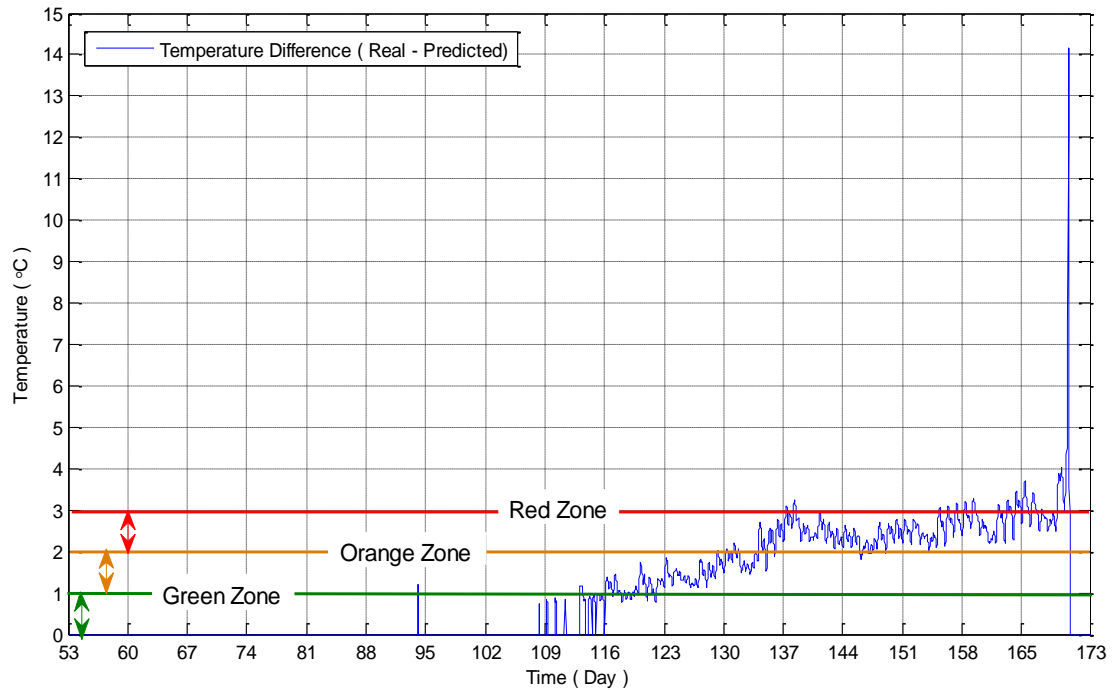

Fig. 80 Temperature prediction error and alarm zones for TC C3_T6.

103

rating happened until the day when the first hot-spots were found on day 108 a period of 2 weeks passed. From day 108 and onwards the temperature difference between real and predicted started slowly rising up every day, reaching a temperature difference increase of more than 3 ℃ 12 days prior to the huge temperature spike on day 170. The temperature difference reached its highest point of 14 ℃ within 7 hours and the total duration of the abnormal spike lasted for 12 hours. The suggested alarm zone strategy can give the system operator an insight of the current state of the cable. Already from day 134, 36 days prior to the temperature spike, the temperature difference lies within the red zone giving to the system operator enough time to take action and precautions prior to the potential failure as can be seen in Figure 80. The prediction models for TC C3_T4 and C3_T5 were also able to identify as well the abnormal temperature activity on the surface of the cable joint as shown in Figures 81-82.
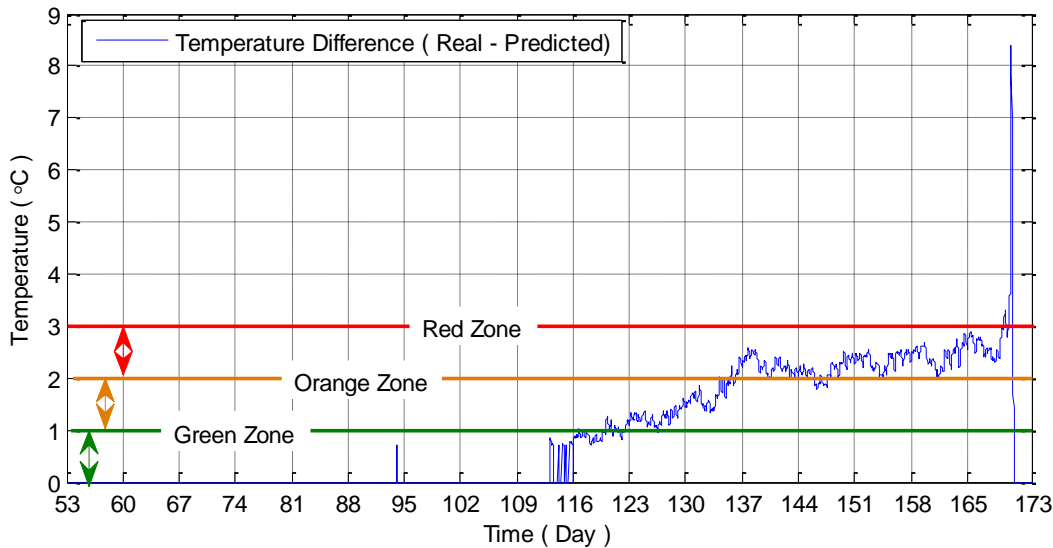

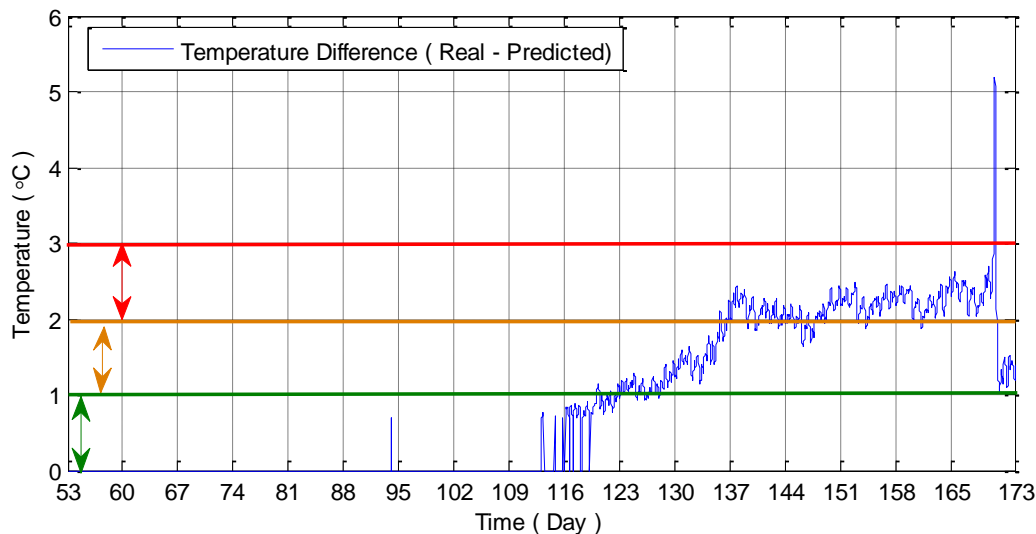Fig. 81 Temperature prediction error and alarm zones for TC C3_T5.

Fig. 82 Temperature prediction error and alarm zones for TC C3_T4.

104

The maximum temperature difference plotted against located distances of TCs is shown in Figure 83. Thus the SVR proved to produce generalized models which can be described
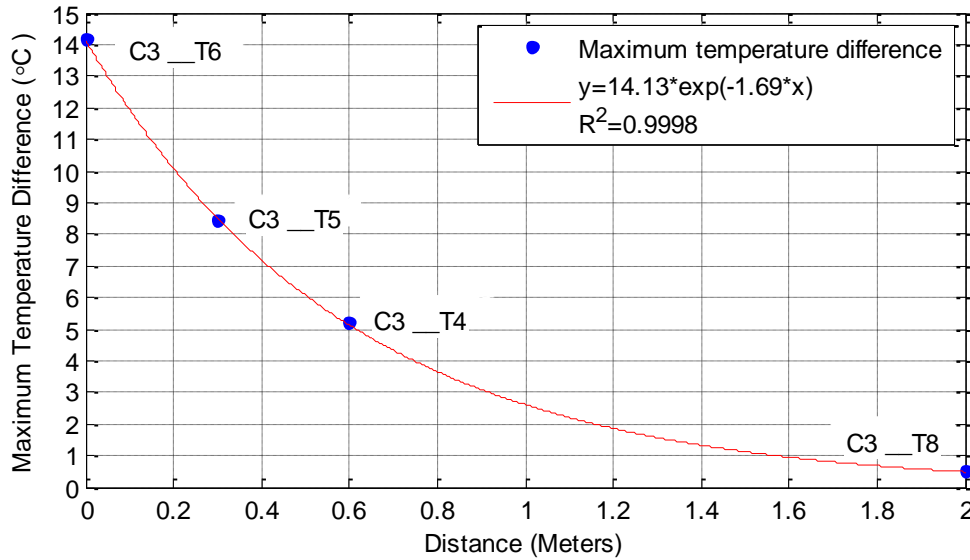

Fig. 83 Maximum temperature difference along Circuit 3.

in an exponential decay equation as expected. From the distribution of the TCs along the surface of the cable joint it was possible to identify that the location of the hot-spot was by the location of TC C3_T6. On the other hand TC C3_T8 located 2 meters away from the location of the hot-spot could not identify any temperature anomaly at all.

Despite the negative expectations the joint did not fail after the huge temperature spike on the day 170. In contrast, as can be seen from Figure 76, the real temperature dropped and matched the predicted temperature levels. One of the possible reasons for that could be explained by the self-healing behaviour of the mass impregnated cables. The TC C3_T6 is located on the surface of the PILC section of the cable joint. The self-healing properties of mass impregnated cables have been previously reported in both experimental [104] and field [105] conditions . Partial discharge activity in microvoids can initiate a degradation aging in the cable. On some occasions PD activity can stop after the electric field in the microvoids is neutralized due to the development of a carbonized path. While in some other cases as the temperature of the cable is rising, the viscosity of the mass impregnated oil inside the cable reduces and as a result it flows easier and closes the microvoids. Hence when the temperature is reduced the viscosity becomes again high and fills permanently the internal voids. After the day 170 the load reduced and possibly that was the reason for the disappearance of the spike. Further cases of self-healing phenomena in power connectors [106] due to cyclic load can result in an increase or

decrease of the resistance of the cable joint and hence create periods in time with local hot-spots in the cable joints which increase their surface temperature or decrease it respectively.

6.4.2 Circuit 2 and 4 no hot-spots

Both Circuits 2 and 4 did not show any sign of degradation activity during the period of field experiments. Circuit 2 is a shallow buried cable circuit and hence the solar radiation and air ambient temperature parameters were taken into account in addition to the surface temperature of TCs C2_T1, C2_T2, C2_T3 as well as the average current loading measured by the Rogowski coils R_C2_B, R_C2_Y and R_C2_R. For Circuit 4 the surface temperature of TCs C4_T1, C4_T2, C4_T3 as well as the average current loading measured by the Rogowski coils R_C4_B, R_C4_Y and R_C4_R. The solar radiation and air ambient temperature were not used as the Circuit 4 is a deeper buried cable. The amount of input columns, based on the above mentioned analysis in Section 5.1.1 and 5.1.5, were 48 30 minutes intervals for both Circuit 2 and 4.

After the installation, Circuit 2 started experiencing a technical issue. Due to the limited space around the location of Circuit 2 it was decided to mount the condition monitoring unit on the wall as is shown in Figure 84. During the collection of the data a strange noise started to appear on the data every day at around 08:00 in the morning as is shown in Figure 85. Plotting the captured raw data of the datalogger revealed that this effect was due to sunlight on the surface of the datalogger enclosure and causing the temperature of

Fig. 84 Circuit 2 monitoring unit during interference period.

the on board thermistor of the datalogger to rapidly change. The datalogger uses the temperature of the on board thermistor as a reference point to calculate the temperature of the thermocouples connected to it. As the temperature of the thermistor was not appropriate, it caused the noise effect on the raw data. The problem was solved by simply adding a wooden screen in front of the enclosure as it can be seen in Figure 86. For that reason the data analysed for Circuit 2 was reduced by 42 days than that for Circuit 4.
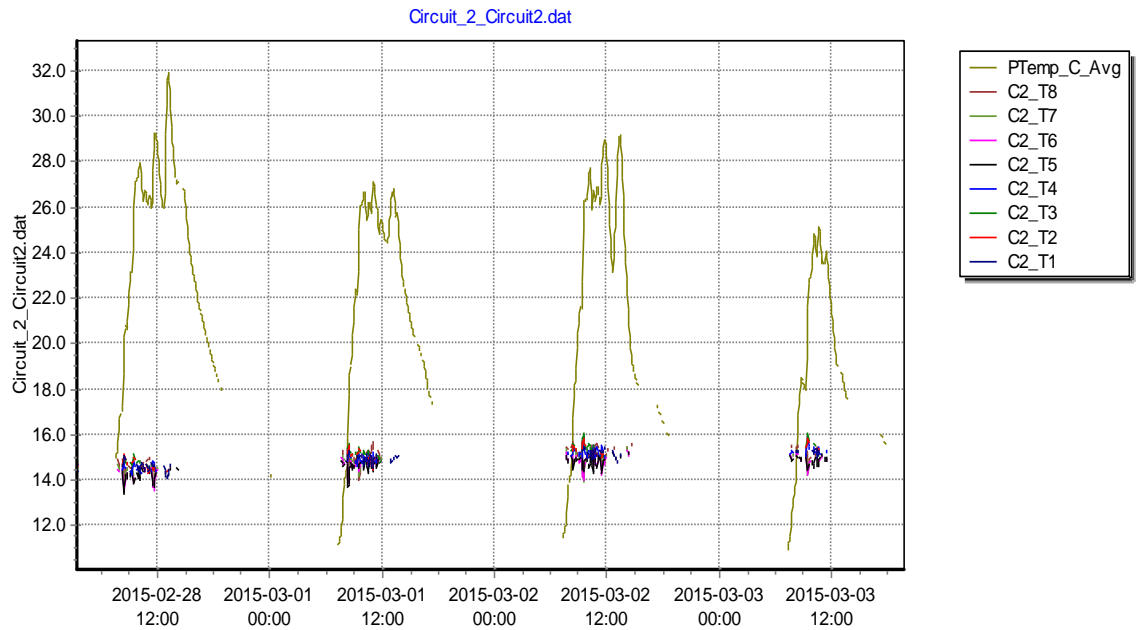

Fig. 85 Circuit 2 raw data interference period.

Fig. 86 Circuit 2 monitoring unit solution.

107

The TCs C2_T5 and C4_T5 of Circuits 2 and 4 respectively were chosen to show prediction results presented in Figures 87-106. The initial amount of training data was 24 days, 3 days for testing and initial moving window length of 55 days. Afterwards the moving window was kept to a size of 56 days.
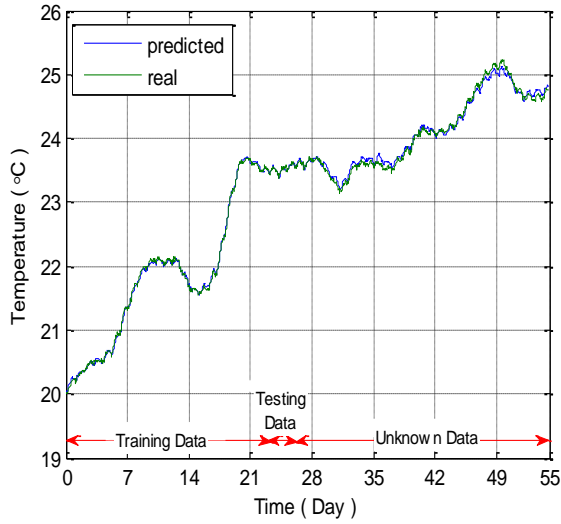

Fig. 87 Comparison between predicted temperature on Testing Data (MAPE=0.69%) and Unknown Data (MAPE=1.31%) with the real temperature of TC C2_T5.
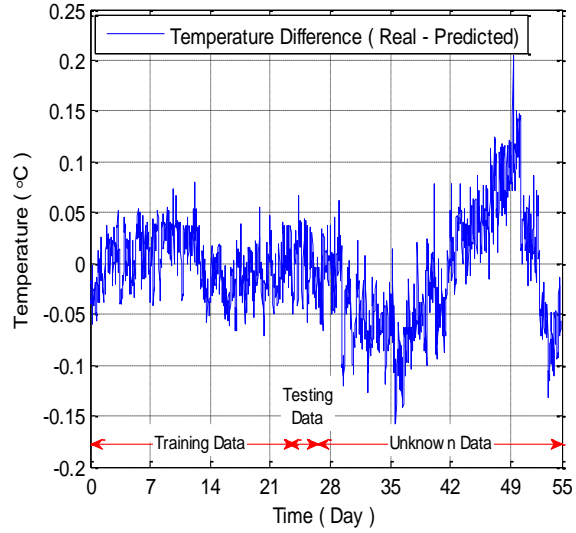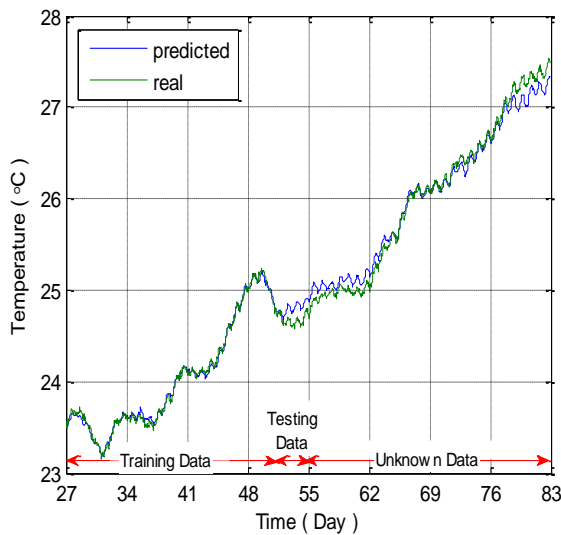

Fig. 88 Temperature prediction error for TC C2_T5.

Fig. 89 Comparison between predicted temperature on Testing Data (MAPE=1.34%) and Unknown Data (MAPE=3.34%) with the real temperature of TC C2_T5.

Fig. 90 Temperature prediction error for TC C2_T5.

108

Fig. 91 Comparison between predicted temperature on Testing Data (MAPE=0.92%) and Unknown Data (MAPE=1.68%) with the real temperature of TC C2_T5.
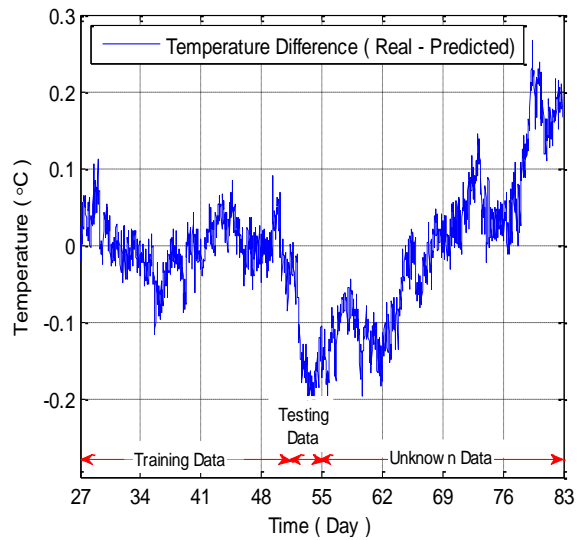
Fig. 92 Temperature prediction error for TC C2_T5.

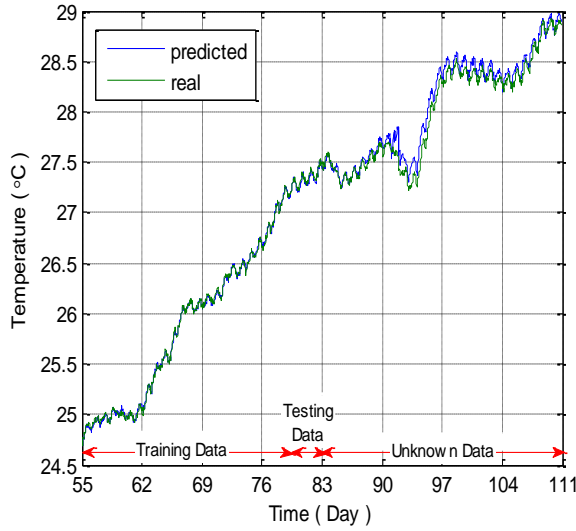

Fig. 93 Comparison between predicted temperature on Testing Data (MAPE=0.84%) and Unknown Data (MAPE=1.55%) with the real temperature of TC C2_T5.

Fig. 94 Temperature prediction error for TC C2_T5.

The models produced by the moving window technique were well tuned with appropriate parameters and produced robust and generalized models throughout the whole period of the experiment. There were not any signs of degradation activity detected during the period of 133 days that the experiment lasted. Figures 95-106 show the prediction results for TC C4_T5.

Fig. 95 Comparison between predicted temperature on Testing Data (MAPE=1.06%) and Unknown Data (MAPE=1.23%) with the real temperature of TC C4_T5.
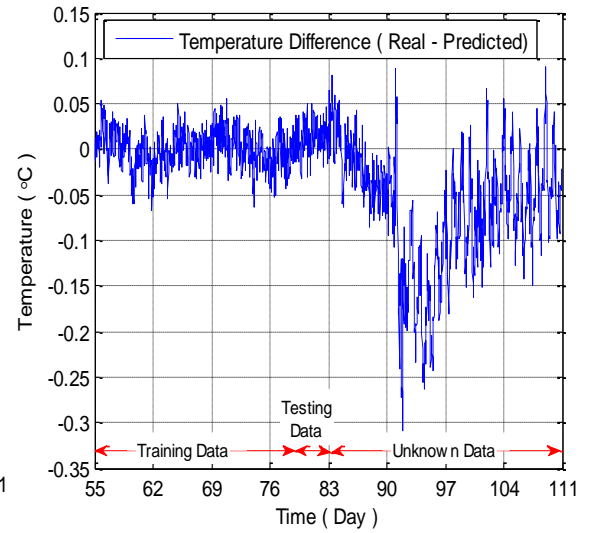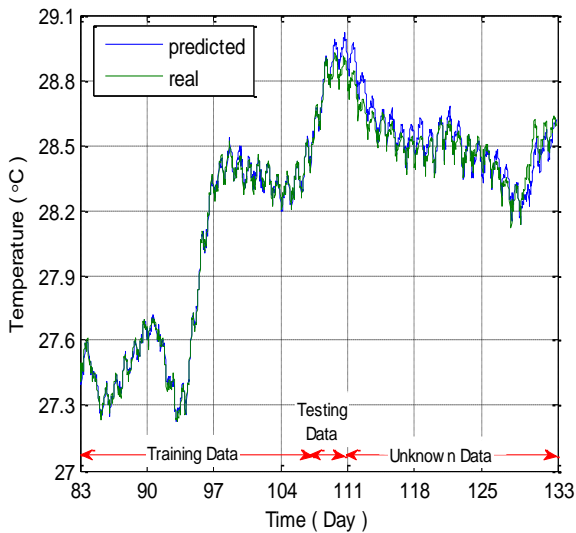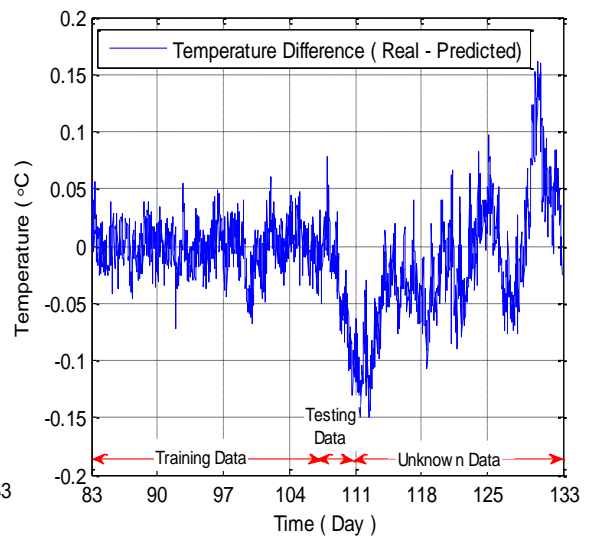
Fig. 96 Temperature prediction error for TC C4_T5.
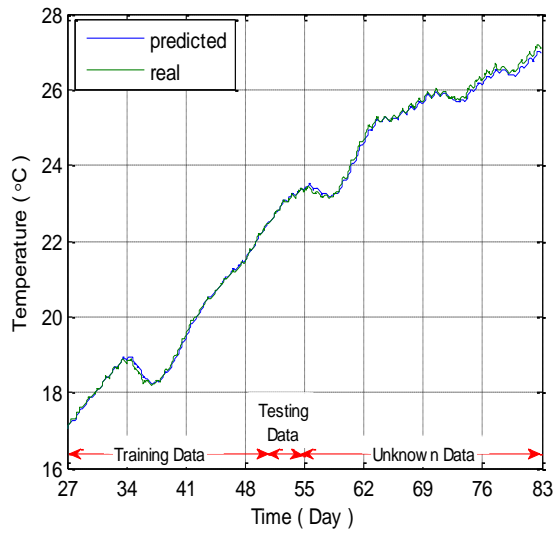
Fig. 97 Comparison between predicted temperature on Testing Data (MAPE=0.55%) and Unknown Data (MAPE=0.99%) with the real temperature of TC C4_T5.
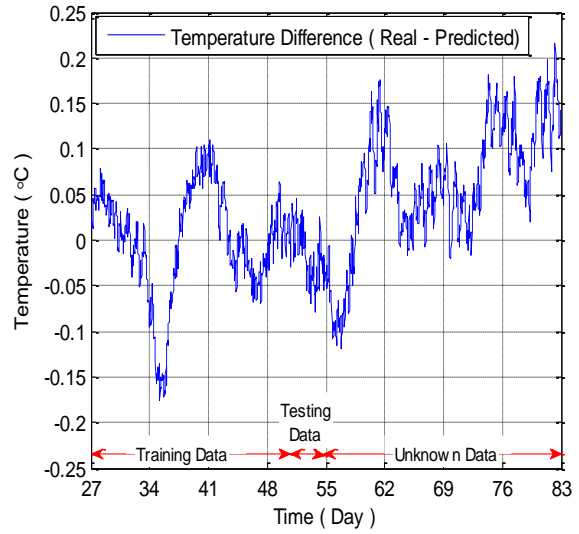
Fig. 98 Temperature prediction error for TC C4_T5.

It can be observed that the performance of the prognostic models was satisfactory and there were not any signs of possible hot-spots in the investigated underground cable joint. The predicted temperature with the real measured temperature were very close to each

other. The results for the further four moving windows are also satisfactory and are presented in Figures 99-106.
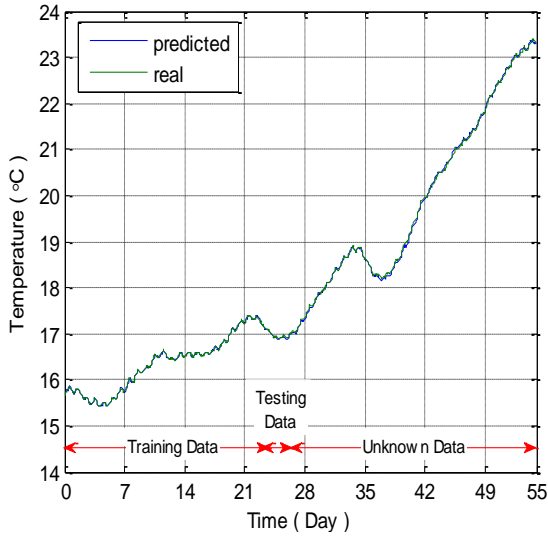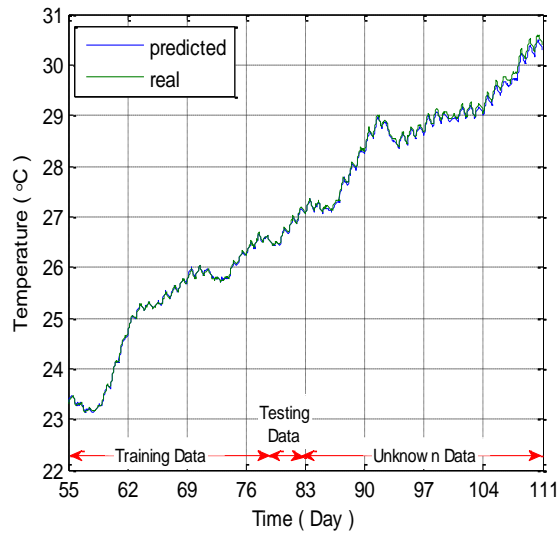

Fig. 99 Comparison between predicted temperature on Testing Data (MAPE=0.45%) and Unknown Data (MAPE=0.77%) with the real temperature of TC C4_T5.
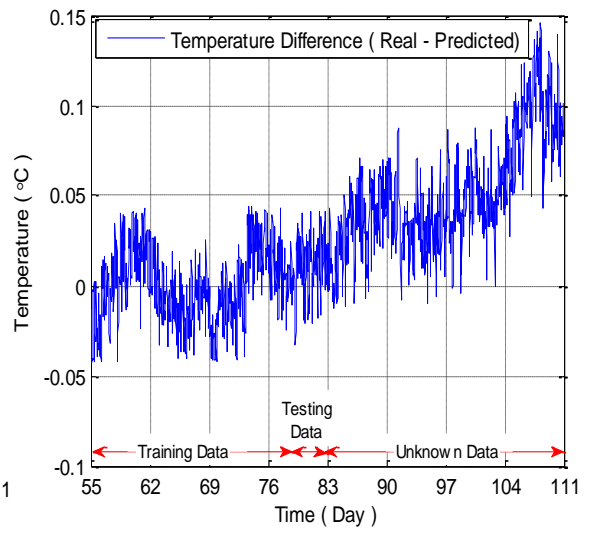
Fig. 100 Temperature prediction error for TC C4_T5.
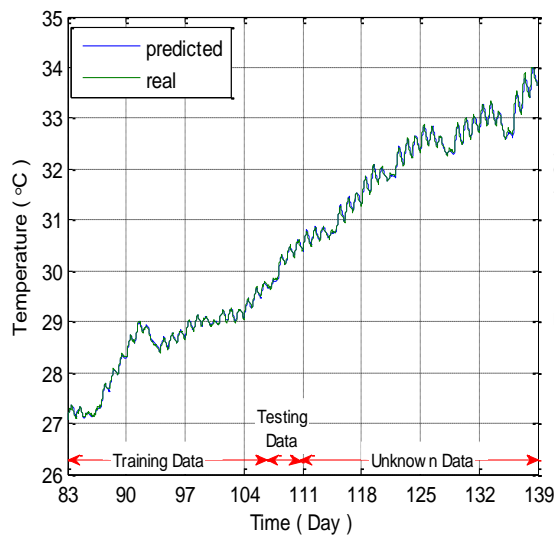
Fig. 101 Comparison between predicted temperature on Testing Data (MAPE=0.42%) and Unknown Data (MAPE=0.70%) with the real temperature of TC C4_T5.
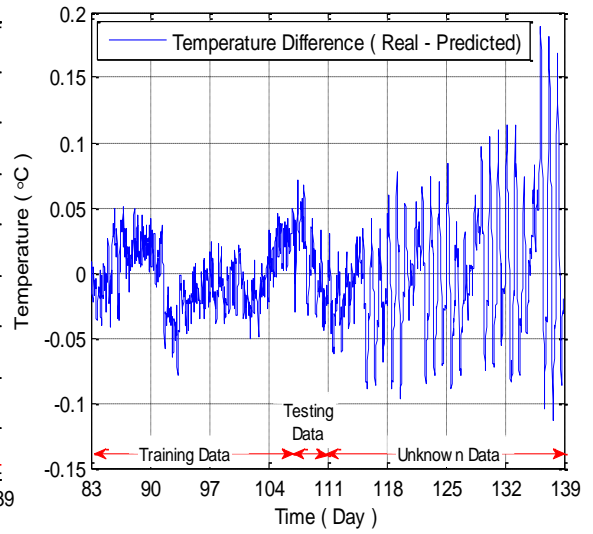
Fig. 102 Temperature prediction error for TC C4_T5.

111
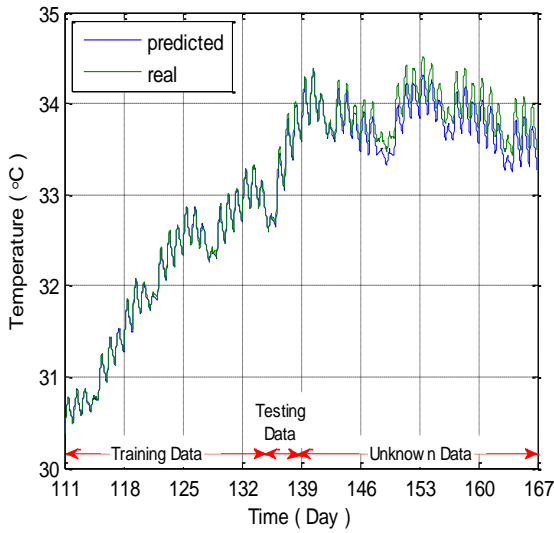
Fig. 103 Comparison between predicted temperature on Testing Data (MAPE=1.46%) and Unknown Data (MAPE=1.82%) with the real temperature of TC C4_T5.
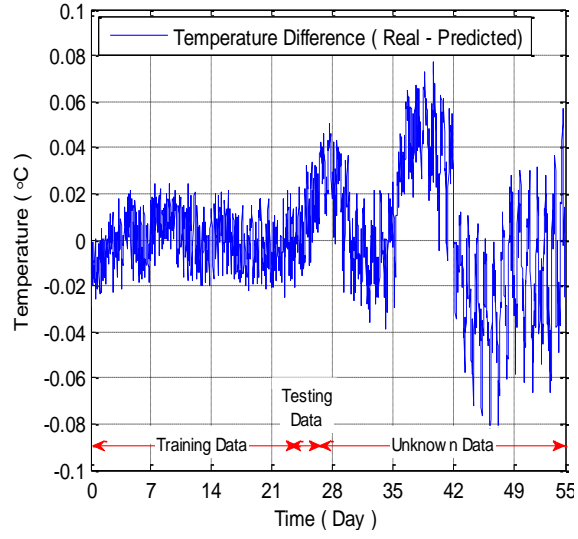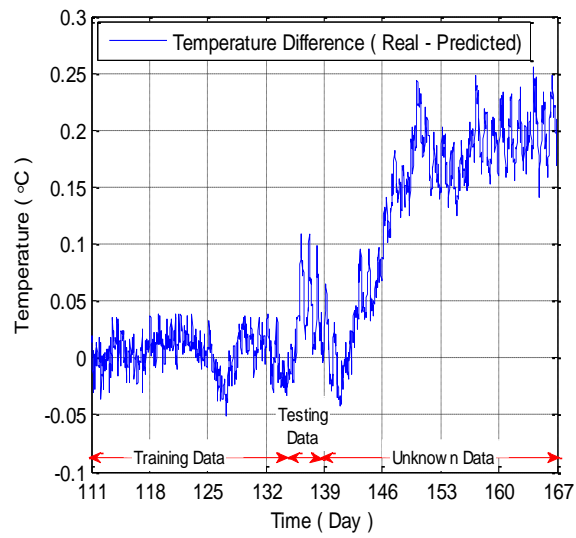

Fig. 104 Temperature prediction error for TC C4_T5.
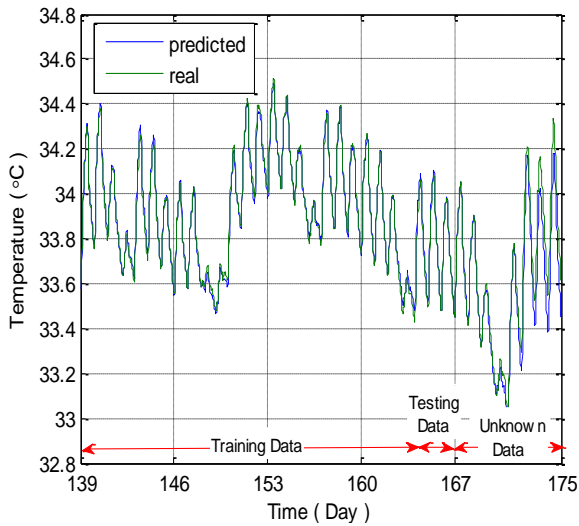
Fig. 105 Comparison between predicted temperature on Testing Data (MAPE=1.25%) and Unknown Data (MAPE=1.80%) with the real temperature of TC C4_T5.
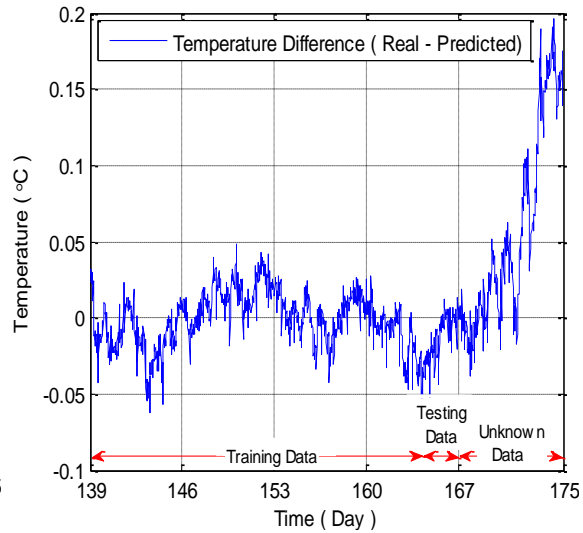
Fig. 106 Temperature prediction error for TC C4_T5.

Circuit 4 was monitored for a period of almost 6 months and did not show any signs of degradation activity. The temperature of TC C4_T5 was predicted accurately taking into account the parameters mentioned previously which verified once again that they were chosen appropriately.

112

6.5   Summary

After the satisfactory results obtained from the soil trench experiments, a field experiment was setup up in Cyprus. Four temperature condition monitoring units were installed on 3 different types of underground cable joints, commonly found in Cyprus. The collected data were used for the development of real-time condition monitoring prognostic health systems.

A thermal anomaly decision algorithm (TADA) was implemented in order to give real-time needed confidence to the network operators about the condition of their circuits. TADA was able to identify that Circuit 3 had severe issues with hot-spot activity and therefore required immediate actions to be taken. The thermal prognostic model was able to predict accurately the first signs of a severe degradation activity in the cable joint of Circuit 3 two months prior its occurrence which led to an abnormal temperature spike of 14 °C. The catastrophic failure of the cable joint was avoided due the self-healing behaviour of the mass impregnated cables inside the cable joint. As it can be seen from the last three days of the field experiment the above phenomenon removed completely the hot-spot activity. Hence the strategy to leave the model unchanged during the first signs of hot-spots activity has proven to be reasonable. Circuit 2 and 4 showed no signs of degradation activity and verified the efficiency and the robustness of the SVR algorithm.

It has been reported from previous studies from IREQ [12] that the locations of hot-spots in cable joints matched locations of the failures and were always combined with PD activity. On the other hand, PD activity never leads by itself to a failure while a hot-spot is a clear indicator of a progressing problem. From the experimental results obtained for Circuit 3 it can be verified that an abnormal temperature led to degradation activity. Thus for cable joints the predictive thermal condition monitoring technique can be more effective and appropriate rather than PD monitoring alone.

The use of such systems within power networks will provide a smarter way of prognostic condition monitoring which is based on improved models and reduced reliance on measurements in real-time. The use of suggested thermal models will enable the power network operators to maximize asset utilization and minimize constraint costs in the system.

Chapter 7 Conclusions and Future Work

This research aimed to develop a reliable and robust online condition monitoring thermal prognostic indicator system which will reduce the risk of failures in a power distribution network. A condition monitoring thermal prognostic system was developed taking into the account real-time weather conditions, surface temperature of the cable joints or terminations and loading demand which updates a thermal prognostic model giving a more accurate prognosis and pre-failure indication.

It has been established that aging of the underground cables happens due to the electrical, mechanical and environmental factors or a combination of them. The most dominant factor influencing the aging of the underground cable and hence the lifetime of the cable was found to be thermomechanical aging. Thermomechanical aging happens due to the daily loading cycles which cause cyclical heating and cooling of the cable which results in cable movement and bending. The above mentioned movement and bending mostly causes damage to the cable sheath near the joints. That might lead to the formation of microvoids which can cause under the wet or dry environmental conditions water or electric trees. Mechanical damage to the cable can be also caused due to the high ambient temperatures which result in drying out of the soil. A combination of high ambient temperatures and high loading cable demands can cause overheating of the cable which will result in a cable and cable joint failure due to the breakdown of the cable insulation.

It was found that cable joints and terminations are one of the weakest points in underground cable systems and the state of the joints and terminations health directly reflects in a more reliable power network. Hence monitoring the operational condition and health of the joints and terminations can increase the reliability of power networks, reduce costly repairs and increase customer confidence.

Over the past decade various diagnostic and condition monitoring techniques for cable joints and terminations have been developed. Some of them are based on optical gas sensors, temperature sensing with GPRS data transmission, partial discharge diagnostic and condition monitoring units and finally temperature monitoring units for cable joints and terminations.

A review of published literature revealed the great need of reliable predictive capabilities that continuously predict and monitor real-time the health state of the underground cable joints and terminations and are able to identify degradation activity at an early stage. It was found that abnormal temperature changes on the surface of the investigated accessories are closely related to health condition and are caused by thermomechanical, environmental, electrical factors or a combination of them. Hence it was decided to develop an online condition monitoring thermal prognostic indicator system which can be used to indicate and prevent possible upcoming failures prior to their occurrence.

It was established through the thermal simulation models in COMSOL that internal faults inside the cables will generate heat and depending on the size of the internal fault will increase the surface temperature of the cable several meters away from the location of the fault. A thirty minutes prediction horizon was chosen as it took that amount of time to detect the temperature increase by 1°C at 0.25 m away from the location of the smallest fault of 2.5 W used during modelling. In order to develop a suggested thermal prognostic capability the SVR algorithm has been used for the implementation of thermal prognostic simulation models for air filled and soil filled trenches rather than ANN, MLR and Mboost due to its better generalization ability as evidenced by the results of benchmarking tests of the four investigated algorithms.

The implementation of the thermal prognostic model in the air filled trench and the 33kV thermal cycle experiment based on the SVR showed very satisfying results. The thermal prognostic models that have been developed were able to identify the increase of the surface cable temperature produced by the introduction of the hot-spots. A new methodology has been introduced through a series of various sensitivity tests which enabled easier and more effective development of thermal prognostic models. It was concluded that the best data averaging time is every 30 minutes, that the most dominant weather parameters are solar radiation and air ambient temperature, that the time gap between peak of solar radiation and peak of cable temperature provides vital information about the amount of input data needed and finally that the model is able to give satisfactory prediction results up to 2 hours ahead.It was found that the TCs can be used to detect temperature anomalies within the radius of 0.35 m from the location of the heat source. Therefore if the TCs are placed within close proximity to the investigated monitoring areas, such as cable joints and terminations in air, they can be effectively used

to implement prognostic models that are able to detect and predict a possible cable accessories degradation activity at an early stage.

The SVR was used to develop and implement the thermal prognostic model in the soil filled trench for both constant and cycling load experiments. The performed benchmarking for both constant and cyclic load experiments justified the choice of SVR as it showed best overall performance for both cases. The developed models are able to identify anomalies of cable temperature 30 minutes into the future. The prediction output can be used to identify a possible sign of upcoming degradation activity in the cable. It has been proven that it is possible to monitor specific areas of an underground cable, where hot-spots are more likely to occur, such as joints buried in the soil. It was found that the most effective distance for the thermal prognostic model to identify the location of the hot-spots in the soil, is in a radius of up to 0.30 m. A methodology for calculating the total system error for an online condition monitoring thermal prognostic indicator system has been developed. In addition to above a verification technique for the selected, during the initial development of the model, parameters C and γ was developed.

The field experiment in an MV substation in Cyprus was used to test the performance and robustness of the thermal prognostic models on real underground cable joints. Four different underground cable joints were monitored by the thermal prognostic models. Real-time measurements such as solar radiation, air ambient temperature, cable circuits loading as well as surface temperature by the cable joints were used to update the thermal prognostic models.

The suggested thermal anomaly decision algorithm (TADA) proved to give a real-time insight into the level of current degradation activity within the cable joint based on the developed 3 zones alarm system strategy. The thermal prognostic models for Circuit 3 combined with the 3 zones alarm system strategy of TADA were able to identify the initial stages of a degradation activity in the investigated cable joint which was initiated by the emergency rating on the 94th day of the experiment. It detected severe hot-spot activity in Circuit 3 two months prior to the abnormal temperature increase of 14 °C on the surface of the cable joint. Due to the self-healing abilities of mass impregnated cables a potential failure was avoided. On the other hand there were not any signs of degradation activity in Circuits 2 and 4 which once again confirmed the efficiency and the robustness of the SVR algorithm.

Thus if the knowledge of the Circuit 3 health state was available prior to the performed emergency rating then the abnormal hot-spot activity within the joint could be avoided. In most of the cases it was not possible to observe the current health state of the accessories and therefore lack of that knowledge can lead to taking wrong decisions which cause catastrophic failures in the power network. In the near future where smart grids will expand even more in the distribution systems, it will be necessary to know real-time the exact health state of the assets. The suggested thermal prognostic condition monitoring techniques and alarm zones strategy can be effectively implemented by DNOs to predict real-time the condition of the assets in order to successfully perform and schedule necessary maintenance.

7.1   Future work

The power industry needs to move towards online prognostic condition based maintenance. It will give the power operators the ability to predict and prevent failures by monitoring online health state of their assets. Any deviations from the predicted health state of the investigated assets should be considered as an indication of a possible instability in the health condition of the assets. This thesis has proved that predictive maintenance approach is feasible and applicable as it was able to indicate a developing fault in a cable joint. The initial installation cost of the developed technique is much lower comparing to the cost of the majority diagnostic techniques currently available on the market. Furthermore the cost of the suggested system can be further reduced with the use of dedicated lower cost condition monitoring units which have the capability to connect to the internet through GSM network, ethernet connection or over Wi-Fi. Nowadays with the vast amount of data collected from the power networks and with the development of cheaper and more reliable sensors as well as with already available cloud storage an online prognostic systems should not be difficult to build and install within the power networks.

Further research is needed to improve understanding of the assets within the current power networks that may be affected significantly after the introduction of the smart grids. Smart grids will make the existing power networks more complex, will generate new power flow loads and add the new stresses to the existing power network systems. For the case of underground cable joints it would be beneficial to further investigate the stress/strain factor by the end of the cable joints. Development of prognostic stress/strain

models together with thermal prognostic models could give even better prediction results as it will enable to fully monitor the thermomechanical aging effect on the underground cable joints. Hence it is of a great importance to further investigate the most vital factors which need to be monitored and will directly translate into the health condition of the different assets. Identification of these monitoring factors and development of predictive models will bring us a step closer to the implementation of predictive based maintenance.

In the future the suggested online condition monitoring thermal prognostic indicator system can be installed in the distribution networks for such institutions and facilities of urban infrastructure as hospitals, airports, ports and other facilities which require reliable and an uninterrupted power supply.

Appendix

Appendix 1 Cable model in COMSOL

The properties of an 11kV XLPE cable are shown in Table 15. Thermal properties of the materials are from [107].

Component	Outer Diameter (mm)	Material	Thermal Conductivity (W/m·K)	Volumetric Heat Capacity (MJ/m³K)
Conductor	13.1	Copper	400	3.45
Dielectric	19.9	XLPE	0.286	2.4
Bedding	24.2	Semicon	0.286	2.4
Armour	26.9	Aluminum	205	2.42
Outer Sheath	31	PE	0.286	2.4

Table 15 Cable properties

The soil has the same thermal parameters and is treated as a uniform medium with thermal resistivity of 1.2 KmW^{-1} and volumetric heat capacity of 1 $MJm^{-3}K^{-1}$. The cable initializes
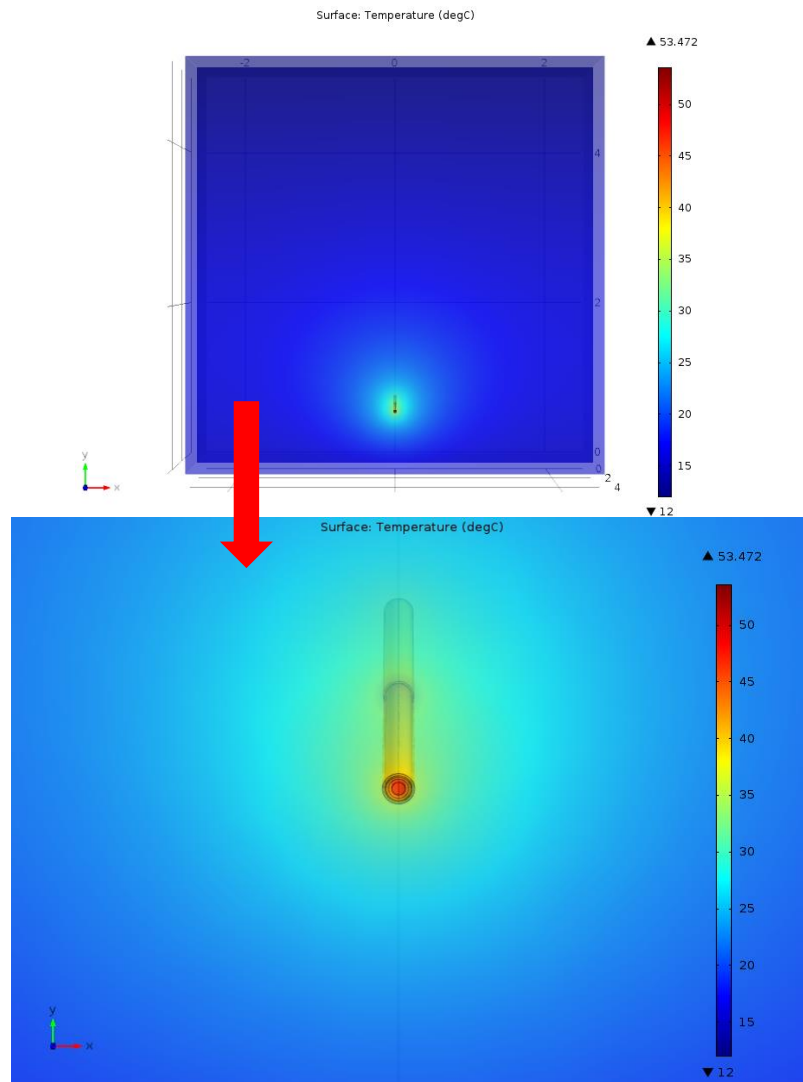
Fig. 107 Cable temperature under transient conditions.

119

first by solving a steady state solution without the introduction of the hot-spot with a current loading of 100 A and then a transient solution including the hot-spot as can be seen in Figure 107. The hot-spot was located in the middle of the cable and just above the conductor covering ¼ of the circumference of the conductor with a width of 2mm and total area of 68 cm^2. In terms of model boundaries conditions the cable is enclosed in a surrounding backfill box which represents the ambient environment. The backfill box height is 5 m and it is big enough to assume no heat flux crosses the side boundaries as can be seen from Figure 107. The meshing was selected carefully to give the best compromises between solution speed and accuracy. The difference between an extremely fine meshing and meshing used was of the order of 0.01 ℃. Therefore the extremely fine mesh was not necessary. The meshing used is shown in Figure 108.
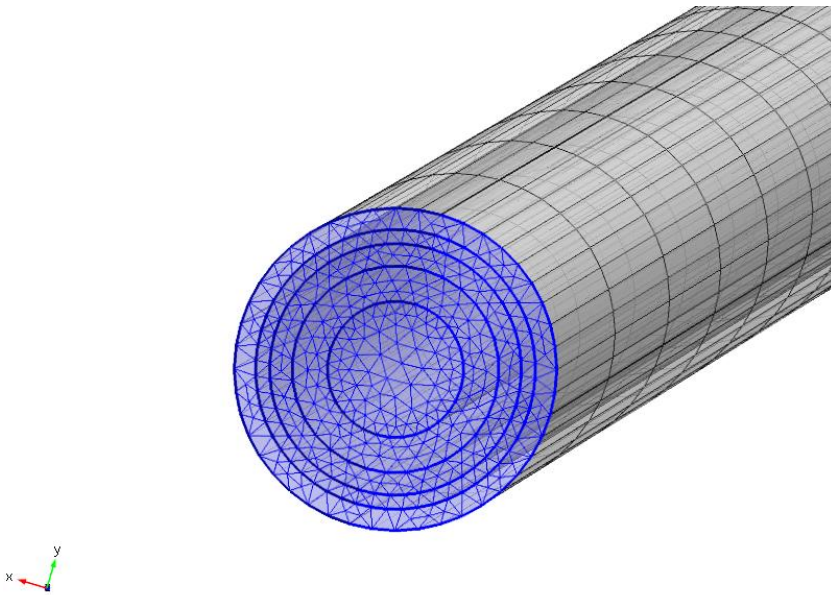
Fig. 108 Cable meshing.

Appendix 2 Implementation of Machine Learning Algorithms

The implementation stages for the development of a thermal prognostic model is shown in Figure 109. The real time measurements data such as weather conditions, surface temperature and loading demand are averaged every 30 minutes. Then input features are scaled from 0 to1 and are input to the different machine learning algorithms for training and testing. The different Machine learning algorithms might require tuneable parameters which can be found through experimental testing. Finally, the machine learning algorithm obtains the prediction results which are compared for benchmarking. An example of the system architecture used for neural network is given in Figure 110.
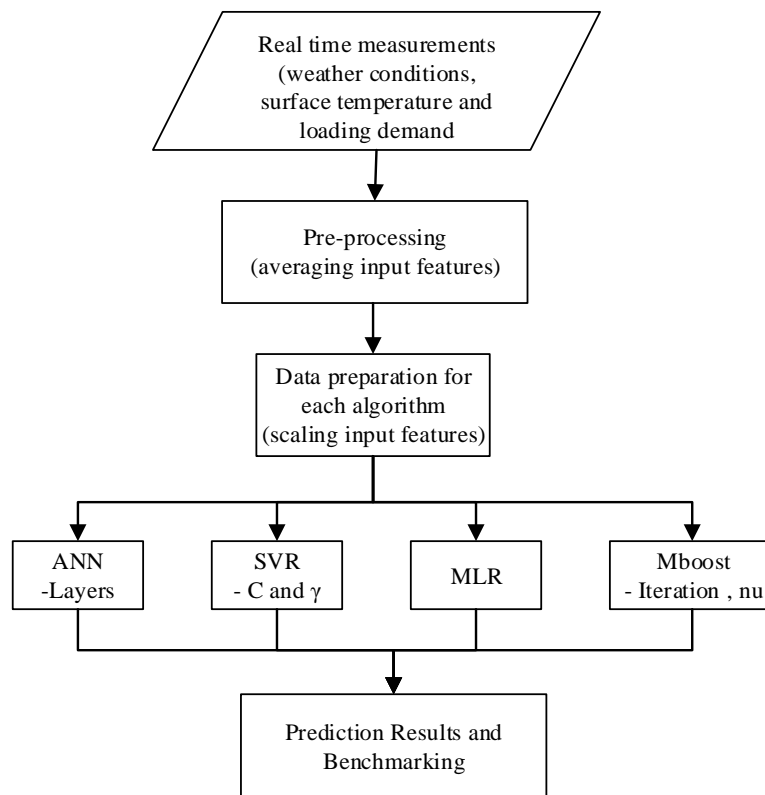
Fig. 109 Machine learning implementation flowchart
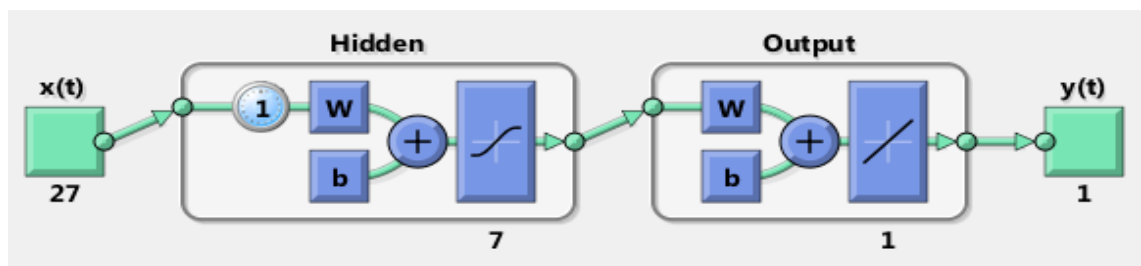
Fig. 110 Architecture of neural network with 27 input features and 7 hidden

Appendix 3 Variac Control Unit Schematic, Pictures and Instrumentation

Below is the schematic of the Variac control unit and the pictures associate with the variac control unit.
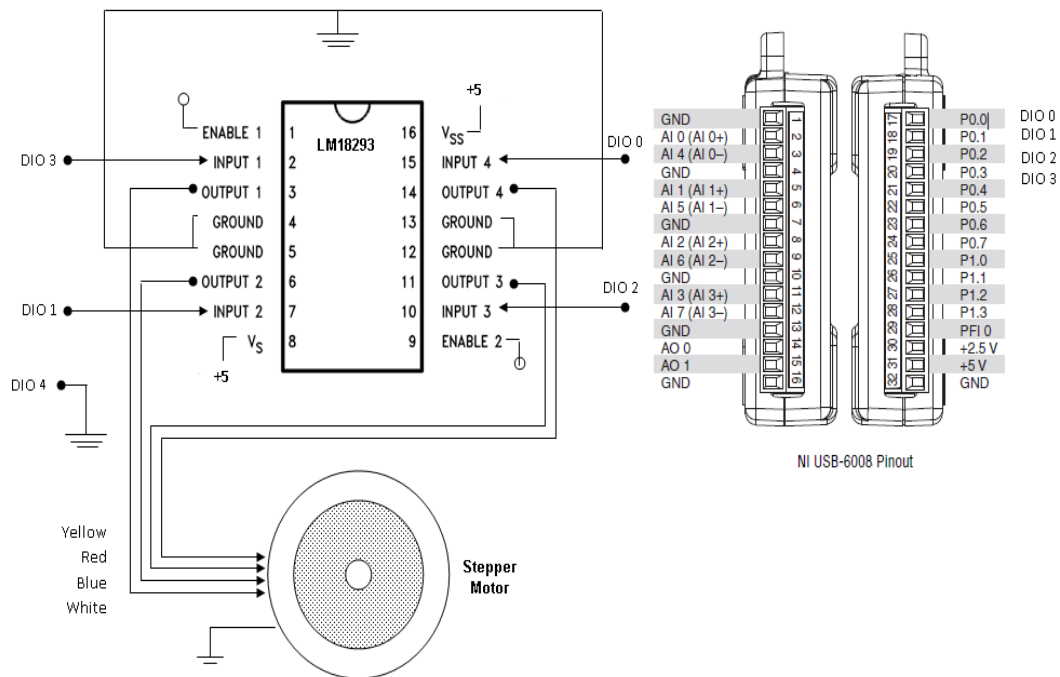
Fig. 111 Schematic diagram of the connection between Stepper motor and NI USB-6008
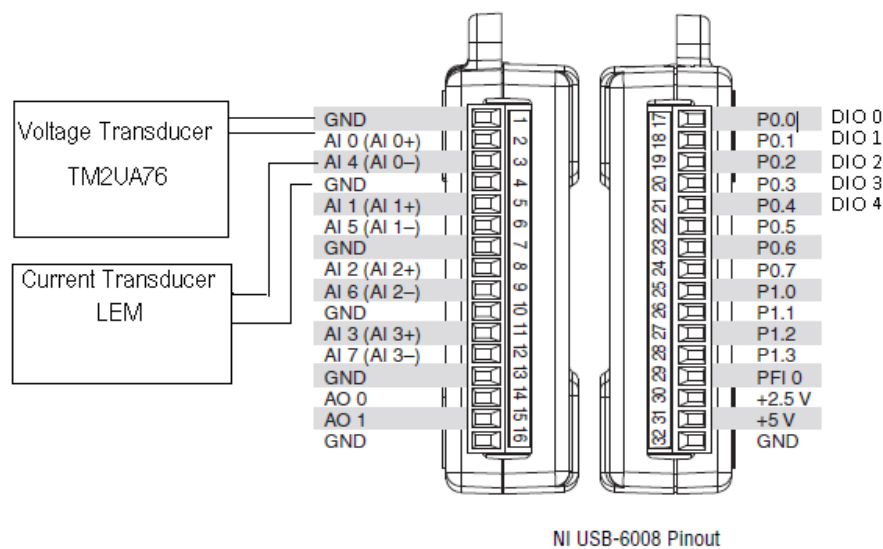
Fig. 112 Schematic diagram of the connection between Voltage and Current transducers with NI USB-6008

Fig. 113 Front side of variac unit
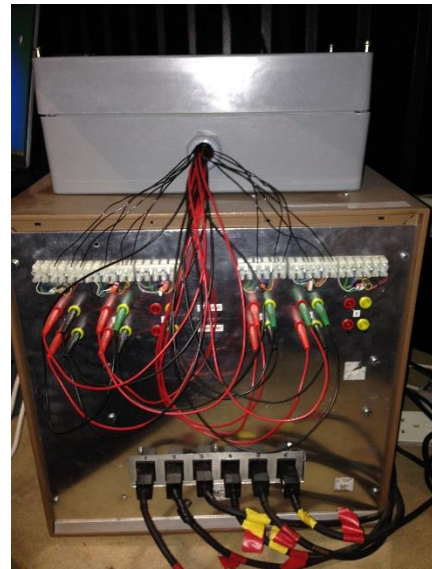
Fig. 114 Back side of variac unit
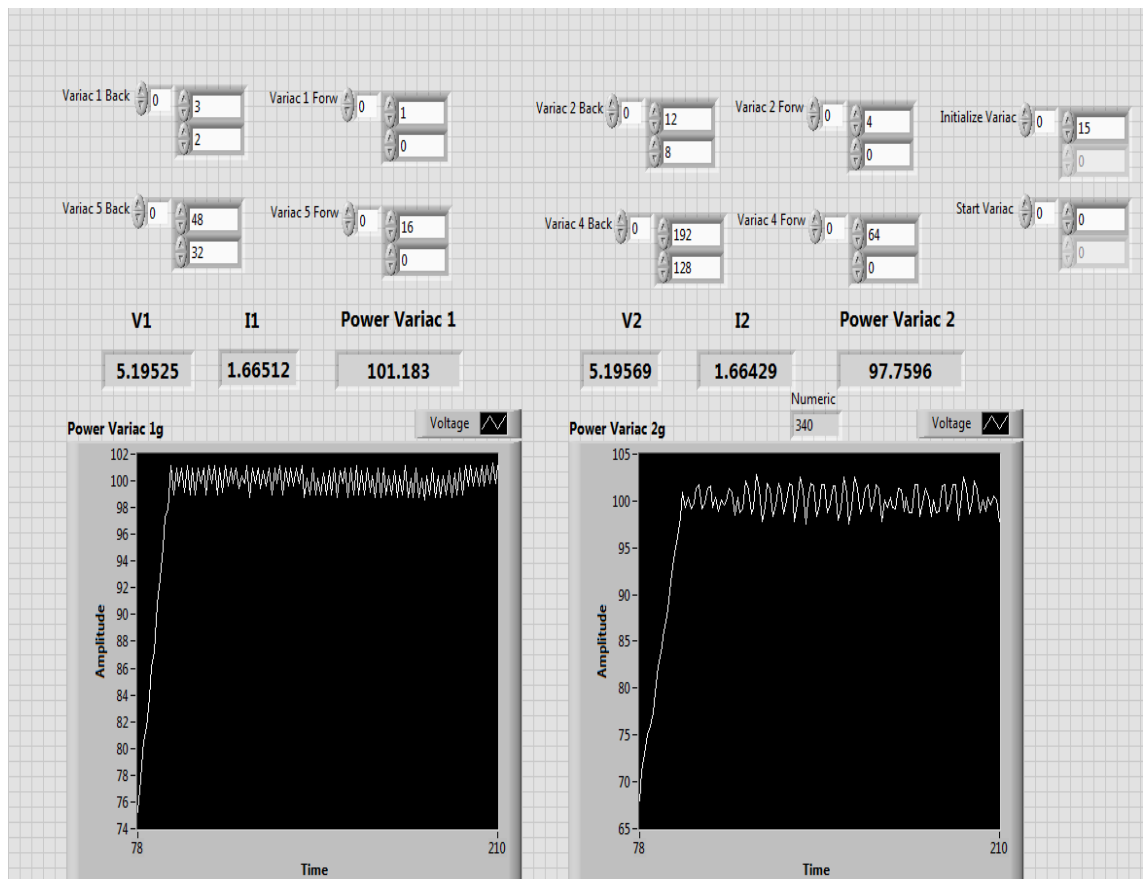
Fig. 115 Experimental Framework for load/ time power demand profiles

123

The implementation of the data monitoring system for the temperatures of the surface through as well as the weather conditions can be seen in Figure 116.
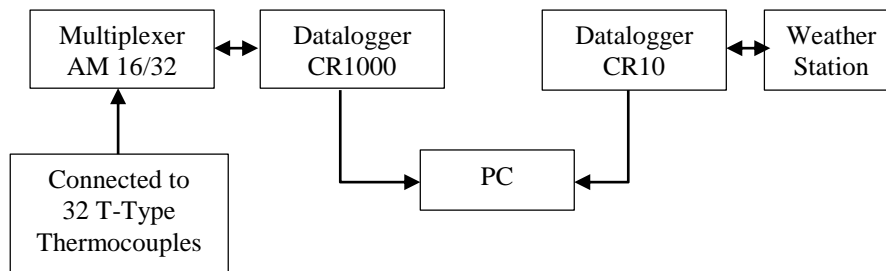
Fig. 116 Data monitoring system for surface through and weather station.

Appendix 4 Datasheets

CR1000 Specifications

Electrical specifications are valid over a -25° to +50°C, non-condensing environment, unless otherwise specified. Recalibration recommended every three years. Critical specifications and system configuration should be confirmed with Campbell Scientific before purchase.

PROGRAM EXECUTION RATE
10 ms to one day @ 10 ms increments

ANALOG INPUTS (SE1-SE16 or DIFF1-DIFF8)
8 differential (DF) or 16 single-ended (SE) individually configured input channels. Channel expansion provided by optional analog multiplexers.

RANGES and RESOLUTION: Basic resolution (Basic Res) is the A/D resolution of a single A/D conversion. A DIFF measurement with input reversal has better (finer) resolution by twice than Basic Res.

Range (mV)[1]	DF Res (µV)[2]	Basic Res (µV)
±5000	667	1333
±2500	333	667
±250	33.3	66.7
±25	3.33	6.7
±7.5	1.0	2.0
±2.5	0.33	0.67

[1] Range overhead of ~9% on all ranges guarantees that full-scale values will not cause over range.
[2] Resolution of DF measurements with input reversal.

ACCURACY[3]:
±(0.06% of reading + offset), 0° to 40°C
±(0.12% of reading + offset), -25° to 50°C
±(0.18% of reading + offset), -55° to 85°C (-XT only)

[3] Accuracy does not include the sensor and measurement noise. Offsets are defined as:
Offset for DF w/input reversal = 1.5·Basic Res + 1.0 µV
Offset for DF w/o input reversal = 3·Basic Res + 2.0 µV
Offset for SE = 3·Basic Res + 3.0 µV

ANALOG MEASUREMENT SPEED:

Integration Type/Code	Integration Time	Settling Time	Total Time[4] SE w/ No Rev	Total Time[4] DF w/ Input Rev
250	250 µs	450 µs	~1 ms	~12 ms
60 Hz[5]	16.67 ms	3 ms	~20 ms	~40 ms
50 Hz[5]	20.00 ms	3 ms	~25 ms	~50 ms

[4] Includes 250 µs for conversion to engineering units.
[5] AC line noise filter.

INPUT NOISE VOLTAGE: For DF measurements with input reversal on ±2.5 mV input range (digital resolution dominates for higher ranges).
250 µs Integration: 0.34 µV RMS
50/60 Hz Integration: 0.19 µV RMS

INPUT LIMITS: ±5 Vdc

DC COMMON MODE REJECTION: >100 dB

NORMAL MODE REJECTION: 70 dB @ 60 Hz when using 60 Hz rejection

INPUT VOLTAGE RANGE W/O MEASUREMENT CORRUPTION: ±8.6 Vdc max.

SUSTAINED INPUT VOLTAGE W/O DAMAGE: ±16 Vdc max.

INPUT CURRENT: ±1 nA typical, ±6 nA max. @ 50°C; ±90 nA @ 85°C

INPUT RESISTANCE: 20 GΩ typical

ACCURACY OF BUILT-IN REFERENCE JUNCTION THERMISTOR (for thermocouple measurements):
±0.3°C, -25° to 50°C
±0.8°C, -55° to 85°C (-XT only)

ANALOG OUTPUTS (VX1-VX3)
3 switched voltage, sequentially active only during measurement.
RANGE AND RESOLUTION:

Channel	Range	Resolution	Current Source/Sink
(VX 1–3)	±2.5 Vdc	0.67 mV	±25 mA

ANALOG OUTPUT ACCURACY (VX):
±(0.06% of setting + 0.8 mV), 0° to 40°C
±(0.12% of setting + 0.8 mV), -25° to 50°C
±(0.18% of setting + 0.8 mV), -55° to 85°C (-XT only)

VX FREQUENCY SWEEP FUNCTION: Switched outputs provide a programmable swept frequency, 0 to 2500 mv square waves for exciting vibrating wire transducers.

PERIOD AVERAGE
Any of the 16 SE analog inputs can be used for period averaging. Accuracy is ±(0.01% of reading + resolution), where resolution is 136 ns divided by the specified number of cycles to be measured.
INPUT AMPLITUDE AND FREQUENCY:

Voltage Gain	Input Range (±mV)	Signal (peak to peak) Min. (mV)[6]	Signal (peak to peak) Max (V)[7]	Min Pulse Width (µV)	Max[8] Freq (kHz)
1	250	500	10	2.5	200
10	25	10	2	10	50
33	7.5	5	2	62	8
100	2.5	2	2	100	5

[6] Signal centered around Threshold (see PeriodAvg() Instruction).
[7] With signal centered at the datalogger ground.
[8] The maximum frequency = 1/(twice minimum pulse width) for 50% of duty cycle signals.

RATIOMETRIC MEASUREMENTS
MEASUREMENT TYPES: Provides ratiometric resistance measurements using voltage excitation. 3 switched voltage excitation outputs are available for measurement of 4- and 6-wire full bridges, and 2-, 3-, and 4-wire half bridges. Optional excitation polarity reversal minimizes dc errors.

RATIOMETRIC MEASUREMENT ACCURACY:[9],[10],[11]
±(0.04% of Voltage Measurement + Offset)

[9] Accuracy specification assumes excitation reversal for excitation voltages < 1000 mV. Assumption does not include bridge resistor errors and sensor and measurement noise.
[10] Estimated accuracy, ΔX (where X is value returned from the measurement with Multiplier = 1, Offset = 0):
BrHalf() Instruction : $\Delta X = \Delta V_1/V_x$
BrFull() Instruction $\Delta X = 1000·\Delta V_f/V_x$, expressed as mV·V⁻¹.
ΔV^{-f} is calculated from the ratiometric measurement accuracy. See Resistance Measurements Section in the manual for more information.
[11] Offsets are defined as:
Offset for DIFF w/input reversal = 1.5·Basic Res + 1.0 µV
Offset for DIFF w/o input reversal = 3·Basic Res + 2.0 µV
Offset for SE = 3·Basic Res + 3.0 µV
Excitation reversal reduces offsets by a factor of two.

PULSE COUNTERS (P1-P2)
2 inputs individually selectable for switch closure, high frequency pulse, or low-level ac. Independent 24-bit counters for each input.

MAXIMUM COUNTS PER SCAN: 16.7x10⁶

SWITCH CLOSURE MODE:
Minimum Switch Closed Time: 5 ms
Minimum Switch Open Time: 6 ms
Max. Bounce Time: 1 ms open w/o being counted

HIGH-FREQUENCY PULSE MODE:
Maximum Input Frequency: 250 kHz
Maximum Input Voltage: ±20 V
Voltage Thresholds: Count upon transition from below 0.9 V to above 2.2 V after input filter with 1.2 µs time constant.

LOW-LEVEL AC MODE: Internal ac coupling removes ac offsets up to ±0.5 Vdc.
Input Hysteresis: 12 mV RMS @ 1 Hz
Maximum ac Input Voltage: ±20 V
Minimum ac Input Voltage:

Sine Wave (mV RMS)	Range(Hz)
20	1.0 to 20
200	0.5 to 200
2000	0.3 to 10,000
5000	0.3 to 20,000

DIGITAL I/O PORTS (C1-C8)
8 ports software selectable, as binary inputs or control outputs. Provide on/off, pulse width modulation, edge timing, subroutine interrupts / wake up, switch closure pulse counting, high frequency pulse counting, asynchronous communications (UARTs), and SDI-12 communications. SDM communications are also supported.

LOW FREQUENCY MODE MAX: <1 kHz

HIGH-FREQUENCY MODE MAX: 400 kHz

SWITCH-CLOSURE FREQUENCY MAX: 150 Hz

EDGE TIMING RESOLUTION: 540 ns

OUTPUT VOLTAGES (no load): high 5.0 V ±0.1 V; low <0.1

OUTPUT RESISTANCE: 330 Ω

INPUT STATE: high 3.8 to 16 V; low -8.0 to 1.2 V

INPUT HYSTERESIS: 1.4 V

INPUT RESISTANCE: 100 kΩ with inputs <6.2 Vdc
220 Ω with inputs ≥6.2 Vdc

SERIAL DEVICE/RS-232 SUPPORT: 0 TO 5 Vdc UART

SWITCHED 12 VDC (SW-12)
1 independent 12 Vdc unregulated source is switched on and off under program control. Thermal fuse hold current = 900 mA at 20°C, 650 mA at 50°C, 360 mA at 85°C.

EU DECLARATION OF COMPLIANCE
https://s.campbellsci.com/documents/us/compliance/eudoc_cr1000-series.pdf
https://s.campbellsci.com/documents/us/compliance/eudoc_cr1000kd.pdf

COMMUNICATIONS
RS-232 PORTS:
DCE 9-pin: (not electrically isolated) for computer connection or connection of modems not manufactured by Campbell Scientific.
COM1 to COM4: 4 independent Tx/Rx pairs on control ports (non-isolated); 0 to 5 Vdc UART
Baud Rates: selectable from 300 bps to 115.2 kbps.
Default Format: 8 data bits; 1 stop bits; no parity
Optional Formats: 7 data bits; 2 stop bits; odd, even parity

CS I/O PORT: Interface with telecommunications peripherals manufactured by Campbell Scientific.

SDI-12: Digital control ports C1, C3, C5, and C7 are individually configured and meet SDI-12 Standard v 1.3 for datalogger mode. Up to 10 SDI-12 sensors are supported per port.

PERIPHERAL PORT: 40-pin interface for attaching CompactFlash or Ethernet peripherals

PROTOCOLS SUPPORTED: PakBus, AES-128 Encrypted PakBus, Modbus, DNP3, FTP, HTTP, XML, HTML, POP3, SMTP, Telnet, NTCIP, NTP, Web API, SDI-12, SDM.

SYSTEM
PROCESSOR: Renesas H8S 2322 (16-bit CPU with 32-bit internal core running at 7.3 MHz)

MEMORY: 2 MB of flash for operating system; 4 MB of battery-backed SRAM for CPU usage and final data storage; 512 kB flash disk (CPU) for program files.

REAL-TIME CLOCK ACCURACY: ±3 min. per year. Correction via GPS optional.

REAL-TIME CLOCK RESOLUTION: 10 ms

SYSTEM POWER REQUIREMENTS
VOLTAGE: 9.6 to 16 Vdc

INTERNAL BATTERIES: 1200 mAh lithium battery for clock and SRAM backup that typically provides three years of backup

EXTERNAL BATTERIES: Optional 12 Vdc nominal alkaline and rechargeable available. Power connection is reverse polarity protected.

TYPICAL CURRENT DRAIN at 12 Vdc:
Sleep Mode: < 1 mA
1 Hz Sample Rate (1 fast SE meas.): 1 mA
100 Hz Sample Rate (1 fast SE meas.): 6 mA
100 Hz Sample Rate (1 fast SE meas. w/RS-232 communication): 20 mA
Active external keyboard display adds 7 mA (100 mA with backlight on).

PHYSICAL
DIMENSIONS: 23.9 x 10.2 x 6.1 cm (9.4 x 4 x 2.4 in); additional clearance required for cables and leads.

MASS/WEIGHT: 1 kg / 2.1 lb

WARRANTY
3 years against defects in materials and workmanship.

SPECIFICATIONS

The following electrical specifications are valid for an ambient temperature range of -25 to +50°C unless otherwise specified.

ANALOG INPUTS

NUMBER OF CHANNELS: 6 differential or up to 12 single-ended. Each differential channel can be configured as two single-ended channels.

CHANNEL EXPANSION: The Model AM416 Relay Multiplexer allows an additional 64 single-ended channels to multiplex into four CR10 single-ended channels. Up to three AM416's can be connected to one CR10.

ACCURACY OF VOLTAGE MEASUREMENTS AND ANALOG OUTPUT VOLTAGES:
0.2% of FSR, 0.1% of FSR (0 to 40°C)

RANGE AND RESOLUTION: Ranges are software selectable for any channel. Resolution for a single-ended measurement is twice the value shown.

Full Scale Range	Resolution
± 2500 millivolts	333 microvolts
± 250 millivolts	33.3 microvolts
± 25 millivolts	3.33 microvolts
± 7.5 millivolts	1.00 microvolts
± 2.5 millivolts	0.33 microvolts

INPUT SAMPLE RATES: The fast A/D conversion uses a 0.25 ms signal integration time and the slow conversion uses a 2.72 ms signal integration. Two integrations, separated in time by 1/2 of an AC line cycle, are used with the 60 Hz or 50 Hz noise rejection option. Differential measurements include a second sampling with reversed input polarity to reduce thermal offset and common mode errors. Input sample rates are the time required to measure and convert the result to engineering units.

Fast single-ended voltage:	2.6 ms
Fast differential voltage:	4.2 ms
Slow single-ended voltage:	5.1 ms
Slow differential voltage:	9.2 ms
Differential with 60 Hz rejection:	25.9 ms
Fast differential thermocouple:	8.6 ms

INPUT NOISE VOLTAGE:

Fast differential	---	0.82 microvolts RMS
Slow differential	---	0.25 microvolts RMS
Differential with 60 Hz rejection	---	0.18 microvolts RMS

COMMON MODE RANGE: ± 2.5 volts.

DC COMMON MODE REJECTION: > 140 dB.

NORMAL MODE REJECTION: 70 dB (60 Hz with slow differential measurement).

INPUT CURRENT: 3 nanoamps maximum.

INPUT RESISTANCE: 200 gigohms.

EXCITATION OUTPUTS

DESCRIPTION: The CR10 has 3 switched excitations, active only during measurement, with only one output active at any time. The off state is high impedance.

RANGE: ± 2.5 volts.

RESOLUTION: 0.67 millivolts.

ACCURACY: Same as voltage input.

OUTPUT CURRENT: 20 mA @ ± 2.5 V; 35 mA @ ± 2.0 V; 50 mA @ ± 1.5 V.

FREQUENCY SWEEP FUNCTION: A swept frequency, square wave output between 0 and 2.5 volts is provided for vibrating wire transducers. Timing and frequency range are specified by the instruction.

RESISTANCE AND CONDUCTIVITY MEASUREMENTS

ACCURACY: 0.015% of full scale bridge output, limited by the matching bridge resistors. The excitation voltage should be programmed so the bridge output matches the full scale input voltage range.

MEASUREMENT TYPES: 6-wire and 4-wire full bridge, 4-wire, 3-wire, and 2-wire half bridge. Bridge measurements are ratiometric and dual polarity to eliminate thermal emf's. AC resistance measurements use a dual polarity 0.75 ms excitation pulse for ionic depolarization, with the signal integration occurring over the last 0.25 ms.

PERIOD AVERAGING MEASUREMENTS

DEFINITION: The time period for a specified number of cycles of an input frequency is measured, then divided by the number of cycles to obtain the average period of a single cycle.

INPUTS: Any single-ended analog channel; signal dividing or AC coupling is normally required.

INPUT FREQUENCY RANGE:

Range Code	Preamp Gain	Input Hysteresis	Maximum Frequency
4	1	10 mV	200 kHz
3	10	1.0 mV	50 kHz
2	33	0.3 mV	20 kHz
1	100	0.1 mV	8 kHz

REFERENCE ACCURACY: ± 40 ppm.

RESOLUTION: ± 100 nanoseconds divided by the number of cycles measured. Resolution is reduced by signal noise and for signals with a slow transition through the zero voltage threshold.

TIME REQUIRED FOR MEASUREMENT: Signal period times the number of cycles measured plus 1.5 cycles.

PULSE COUNTERS

NUMBER OF PULSE COUNTER CHANNELS: 2 eight bit or 1 sixteen bit; software selectable.

MAXIMUM COUNT RATE: 2000 Hz, eight bit counter; 250 kHz, sixteen bit counter. Pulse counter channels are scanned at 8 Hz.

MODES: Switch closure, high frequency pulse, and low level AC.

SWITCH CLOSURE MODE
Minimum Switch Closed Time: 5 milliseconds.
Minimum Switch Open Time: 6 milliseconds.
Maximum Bounce Time: 1 millisecond open without being counted.

HIGH FREQUENCY PULSE MODE
Minimum Pulse Width: 0.002 milliseconds.
Maximum Input Frequency: 250 kHz.
Voltage Thresholds: Count upon transition from below 1.5 V to above 3.5 V.
Maximum Input Voltage: ± 20 V.

LOW LEVEL AC MODE
(Typical of magnetic pulse flow transducers or other low voltage, sine wave outputs).
Minimum AC Input Voltage: 6 mV RMS.
Input Hysteresis: 11 mV.
Maximum AC Input Voltage: 20 V RMS.
Frequency ranges on next column.

Frequency Range:

AC Input (RMS)	Range
20 mV	1 Hz to 100 Hz
50 mV	0.5 Hz to 400 Hz
150 mV to 20 V	0.3 Hz to 1000 Hz

(Consult factory if higher frequencies are desired.)

DIGITAL I/O PORTS

8 ports, software selectable as binary inputs or control outputs.

OUTPUT VOLTAGES (no load): high 5.0 V ± 0.1V; low < 0.1 V.

OUTPUT RESISTANCE: 500 Ω.

INPUT STATE: high 3.0 V to 5.5 V; low -0.5 V to 0.8 V.

INPUT RESISTANCE: 100 kΩ.

TRANSIENT PROTECTION

All input and output connections to the CR10 module are protected using RC filters or transzorbs connected to a heavy copper bar between the circuit card and the case. The CR10WP Wiring Panel includes additional spark gap and transzorb protection.

CPU AND INTERFACE

PROCESSOR: Hitachi 6303.

MEMORY: 32K ROM, 64K RAM.

DISPLAY: 8 digit LCD (0.5" digits).

PERIPHERAL INTERFACE: 9 pin D-type connector for keyboard display, storage module, modem, printer, cassette, and RS-232 adapter. Baud rates selectable at 300, 1200, 9600 and 76,800.

CLOCK ACCURACY: ± 1 minute per month.

MAXIMUM PROGRAM EXECUTION RATE: System tasks initiated in sync with real-time up to 64 Hz. One measurement with data transfer is possible at this rate without interruption.

SYSTEM POWER REQUIREMENTS

VOLTAGE: 9.6 to 16 volts.

TYPICAL CURRENT DRAIN: 0.5 mA quiescent, 13 mA during processing, and 35 mA during analog measurement.

BATTERIES: Any 12 volt battery can be connected as a primary power source. Enclosures with power supply options are available.

PHYSICAL SPECIFICATIONS

SIZE: 7.8" x 3.5" x 1.5" - Measurement & Control Module; 9" x 3.5" x 2.9" - with CR10WP Wiring Panel. Additional room required for connectors.

WEIGHT: 2 lbs.

WARRANTY

Two years against defects in materials and workmanship.

Specifications

- Power:[a] 9.6 to 16 Vdc (under load)
- Scan Advance: Occurs on the leading edge of the clock pulse transition (from below 1.5 V to above 3.3 V)
- Minimum Clock Pulse Width: 1 ms
- Maximum Actuation Time for Relay: 20 ms
- Relay Operation: break before make
- Initial Relay Resistance, Closed: 0.1 Ω
- Maximum Switching Current:[b] 500 mA
- Maximum Switching Voltage:[c] 50 Vdc
- Minimum Contact Life: 10^7 closures
- CE Compliance: EN 61326: 1998 EN 55022: 1998 Class B
- Surge: Complies with IEC61000-4-5, test level 3 (±2 kV, 2 Ω coupling impedance)
- Weight: 680 g (1.5 lb)
- Dimensions: 22.0 x 10.1 x 6.6 cm (8.7 x 4.0 x 2.6 in)

Clock Levels

- Scan Advance: Occurs on the leading edge of the clock pulse transition (from below 1.5 V to above 3.3 V)
- Maximum Voltage: 8 Vdc

ESD

- Air Discharge: Complies with IEC61000-4-2, test level 4 (±15 kV)
- Contact Discharge: Complies with IEC61000-4-2, test level 4 (±8 kV)

Current Drain (typical)

- Quiescent: < 210 µA
- Active: 6 mA

Reset Levels

- Inactive: < 0.9 V
- Active: 3.3 to 8 V
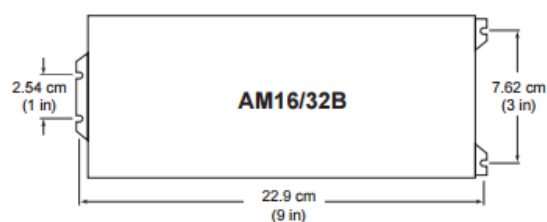
Mounting bracket dimensions

---

[a] The power requirements for AM16/32B multiplexers with serial numbers less than 5056 were 11.3 to 16 Vdc (under load; -25° to +50°C) and 11.8 to 16 Vdc (under load; -55° to +85°C).

[b] Switching currents greater than 30 mA (occasional 50 mA acceptable) degrade the suitability of that channel for switching low-voltage signals.

[c] A voltage divider such as the VDIV10:1 may be needed between the AM16/32B and the datalogger to stay within the input limits of the datalogger channel.

T-type thermocouple Tolerance IEC 584 Class 1 was used.

temperature and process technology

LABFACILITY
TEMPERATURE & PROCESS TECHNOLOGY

PTFE Exposed Welded Tip Thermocouples

Available in type K & T

- ♦ Thermocouple types K & T
- ♦ Fast response, welded exposed junction
- ♦ 1, 2 , 3 & 5 metre long PTFE twin twisted cable
- ♦ 1/0.2mm conductors
- ♦ Temperature range −75°C to +250°C

- ♦ Tolerance to IEC 584 Class 1
- ♦ Colour code to IEC 584-3
- ♦ Good mechanical strength and flexibility, resistant to oils, acids and other adverse fluids
- ♦ Ideal for test & development applications

T/C Type	Length	Manufacturing Part Number	+Positive tail wire	-Negative tail wire	Farnell Order Code
'K'	1 metres	Z2-K-PTFE-TT-1/0.2-1.0-T	Green	White	707-6150
'K'	2 metres	Z2-K-PTFE-TT-1/0.2-2.0-T	Green	White	707-6162
'K'	3 metres	Z2-K-PTFE-TT-1/0.2-3.0-T	Green	White	163-3481
'K'	5 metres	Z2-K-PTFE-TT-1/0.2-5.0-T	Green	White	163-3482
'T'	1 metres	Z2-T-PTFE-TT-1/0.2-1.0-T	Brown	White	707-6174
'T'	2 metres	Z2-T-PTFE-TT-1/0.2-2.0-T	Brown	White	707-6186
'T'	3 metres	Z2-T-PTFE-TT-1/0.2-3.0-T	Brown	White	163-3483
'T'	5 metres	Z2-T-PTFE-TT-1/0.2-5.0-T	Brown	White	163-3484
'K'	1 metres	Z2-K-PTFE-TT-1/0.2-1.0-Tx5	Green	White	859-8223 (pack of 5)
'K'	2 metres	Z2-K-PTFE-TT-1/0.2-2.0-Tx5	Green	White	859-8150 (pack of 5)
'T'	1 metres	Z2-T-PTFE-TT-1/0.2-1.0-Tx5	Brown	White	859-8231 (pack of 5)
'T'	2 metres	Z2-T-PTFE-TT-1/0.2-2.0-Tx5	Brown	White	859-8169 (pack of 5)

Tolerance classes for thermocouples according to the IEC 60 584-2:1995

Thermocouple	Class 1 (°C)	Class 2 (°C)	Class 3 (°C)
Type T			
Temperature	- 40 ≤ t ≤ 125	-40 ≤ t ≤ 133	-67 ≤ t ≤ 40
Tolerance	±0,5	±1	±1
Temperature	125 ≤ t ≤ 350	133 ≤ t ≤ 350	-200 ≤ t ≤ -67
Tolerance	±0,004·|t|	±0,0075·|t|	±0,015·|t|
Type E			
Temperature	-40 < t ≤ 375	-40 ≤ t ≤ 333	-167 ≤ t ≤ 40
Tolerance	±1,5	±2,5	±2,5
Temperature	375 ≤ t ≤ 800	333 ≤ t ≤ 900	-200 ≤ t ≤ -167
Tolerance	±0,004·|t|	±0,0075·|t|	±0,015·|t|
Type J			
Temperature	-40 < t ≤ 375	-40 ≤ t ≤ 333	-
Tolerance	±1,5	±2,5	-
Temperature	375 ≤ t ≤ 750	333 ≤ t ≤ 750	-
Tolerance	±0,004·|t|	±0,0075·|t|	-
Type K and N	*Also see the diagramme below*		
Temperature	-40 < t ≤ 375	-40 ≤ t ≤ 333	-167 ≤ t ≤ 40
Tolerance	±1,5	±2,5	±2,5
Temperature	375 ≤ t ≤ 1000	333 ≤ t ≤ 1200	-200 ≤ t ≤ -167
Tolerance	±0,004·|t|	±0,0075·|t|	±0,015·|t|
Type S and R			
Temperature	0 < t ≤ 1100	0 ≤ t ≤ 600	-
Tolerance	±1	±1,5	-
Temperature	1100 ≤ t ≤ 1600	600 ≤ t ≤ 1600	-
Tolerance	±[1+0,003(t-1100)]	±0,0025·|t|	-
Type B			
Temperature	-	-	600 ≤ t ≤ 800
Tolerance	-	-	±4
Temperature	-	600 ≤ t ≤ 1700	800 ≤ t ≤ 1700
Tolerance	-	±0,0025·|t|	±0,005·|t|

Temperature referency
Reference point is 0 °C

Explanation
|t| = is the positive value of the temperature t.

Tolerances
The tolerances of the table should be taken as guideline values. They are valid only for unused thermocouples.

Sources of error
Many factors such as high temperature combined with time of exposure, vacuum, or drawn wire can quickly lead to deviations that override the tolerances given in the table.

NB
The coloured markings used here have nothing to do with any colour coding of thermocouples.
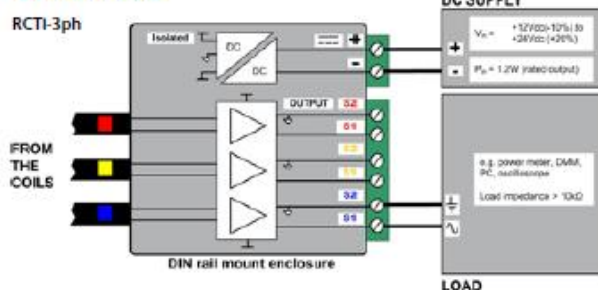
Rogowski coil

# RCT*i-3ph* Specifications

Rated current (rms)	250A	2500A	16000A
	500A	3000A	20000A
	800A	4000A	25000A
	1000A	5000A	30000A
	1600A	8000A	40000A
	2000A	10000A	50000A

Rated output (Full scale FS)	5.0Vrms (±7.07V peak)
Output limit	150% FS (±10.6V peak)
Supply voltage (Wide input)	12Vdc (-10%) to 24Vdc (+20%)
Max. Input power	1.2W
Operating temperature range	−5°C to +65°C *(Integrator electronics)* −20°C to +80°C *(Coil and cable)*
Bandwidth (-3dB) (<2000A) (≥2000A)	0.6Hz to 1MHz (300mm) 600kHz (700mm) 0.2Hz to 1MHz (300mm) 600kHz (700mm)
Phase shift @50Hz (<2000A) (≥2000A)	0.9±0.1 degrees 0.4±0.1 degrees
Accuracy (typ.)	±1.0% of reading (5% to 150% FS, 25°C)
Output load	> 10.0kΩ
Coil Length	300mm, 500mm or 700mm *Custom lengths available*
Cable Length (coil to electronics)	1m or 2.5m *Custom lengths available*

Connections

RCTI-3ph

DIN rail mount enclosure

Dimensions

All dimensions mm

Diameter (mm) = Coil Length (mm) / 3.2
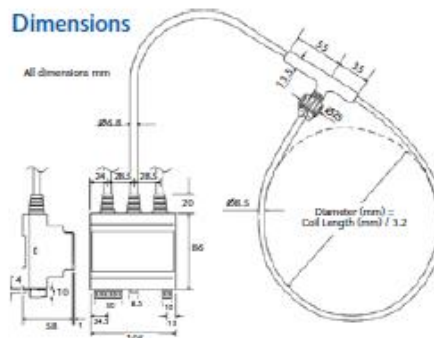
Features

- **Traceable calibration**
  - Every unit is supplied with a traceable calibration certificate
  - No magnetic materials means excellent linearity <0.1% reading
- **Fully isolated measurement**
  - Isolated power supply 2kVdc
  - Coil rated at 2kVpeak (withstand test is 4kVrms / 50Hz/ 60 sec)
- **Small DIN rail (or panel mount) enclosure – UL94 V-0 rated**

Options

- **Isolated BNC-BNC cable split option**
  - Between coil and electronics to enable ease of installation e.g. threading through existing conduit. Standard cable permanently fixed.

Standards and Approvals

- **CE marked**
- **Complies with EMC EN 61326-1 2006**
- **PEM Ltd is an ISO9001:2008 registered company**
- **Complies with IEC61010-1:2001**

Order code RCTI-3ph

The RCTI-3ph order code can be generated as follows:

Rated current (A)	Cable Length (m)	Coil Length (mm)	Options
250A	1m	300mm	BC-BNC
500A	2.5m	500mm	Split in Cable
...	...	700mm	
50000A	Custom lengths	... Custom lengths	

For example: RCTI-3ph/500 /1/700 /BC has a rated primary current 500A, 1m cable, 700mm coil and a BNC - BNC split in the cable

Further information

The RCTI-3ph can be configured to suit a great many applications. If your requirement is outside that listed in this datasheet please contact us to discuss your application.

More detailed technical advice is available at www.pemuk.com

Power Electronic Measurements

Gloucester House, Wellington Street, Long Eaton, Nottingham. NG10 4HT. United Kingdom.
T +44 (0) 115 946 9657.
F +44 (0) 115 946 8515.
E info@pemuk.com
W www.pemuk.com

List of References

[1]   B. Leyland, "Auckland central business district power failure," *Power Eng. J.*, vol. 12, no. 3, pp. 109–114, Jun. 1998.

[2]   J. Densley, "Ageing mechanisms and diagnostics for power cables - an overview," *IEEE Electr. Insul. Mag.*, vol. 17, no. 1, pp. 14–22, Jan. 2001.

[3]   R. Hartkein *et al.*, "Diagnostic Testing of Underground Cable Systems (Cable Diagnostic Focused Initiative)," NEETRAC, Atlanta, GA, DOE Award No. DE-FC02-04CH11237 (NEETRAC Project Numbers: 04-211/04-212/09-166, Georgia Tech Research Corporation, Dec. 2010.

[4]   N. Hampton, "Historical Overview of Medium & High Voltage Cables," presented at *Doble Conference*, July 2012.

[5]   B. Van Maanen *et al.*, "Failures in underground power cables – return of experience," in *JICABLE'15, 9th Int. Conf. on Insulated Power Cables*, Versailles, France, June 21 - 25, 2015, pp. 1 - 5.

[6]   R.-N. Wu and C.-K. Chang, "The Use of Partial Discharges as an Online Monitoring System for Underground Cable Joints," *IEEE Trans. Power Deliv.*, vol. 26, no. 3, pp. 1585–1591, Jul. 2011.

[7]   P. C. J. M. van der Wielen and E. F. Steennis, "Experiences with Continuous Condition Monitoring of In-Service MV Cable Connections," in *Power Systems Conf. and Expo.*, Seattle, WA, Mar. 15 - 18, 2009, pp. 1–8.

[8]   D. Fournier *et al.*, "Detection , Localization and Interpretation of Partial Discharge in the Underground Distribution Network At Hydro-Québec," in *CIRED 2005, 18th Int. Conf. and Exhibition on Electricity Distribution*, Turin, Italy, June 6-9, 2005,pp. 1–4.

[9]   D. Fournier and N. Amyot, "Diagnostic of overheating underground distribution cable joints," in *CIRED 2001, 16th Int. Conf. and Exhibition on Electricity Distribution*, Amsterdam, Netherlands, June 18 - 21, 2005, pp. 1–4..

[10]   C. Y. Choo and F. A. Auditore, "Strategic Replacement of 220 kV Cable at Taranaki Combined Cycle Station," in *Electricity Engineers Association Conf.*, Christchurch, New Zealand, June 17-18, 2010, pp. 1- 6.

[11]   P. Zayicek and H. Kaplan, "Infrared thermography field application guide," EPRI, Palo Alto, CA, Tech. Rep. TR-107142, Jan. 1999.

[12]   L. Lamarre, D. Fournier, and R. Morin, "Early detection of faults in underground distribution cable joints by partial discharge measurements," in *Proc. of 4th Int. Conf. on Properties and Applications of Dielectric Materials*, Brisbane, Australia, July 3 -8, 1994, vol. 2, pp. 864–867.

[13]   C. T. Maney, "Benefits of urban underground power delivery," *IEEE Technol. Soc. Mag.*, vol. 15, no. 1, pp. 12–22, 1996.

[14]   V. K. Mehta and R. Mehta, *Principles of Power System: Including Generation, Transmission, Distribution, Switchgear and Protection*. S. Chand, 2005.

[15]   C. a. Bauer and R. J. Nease, "Evaluation of Cable Movement due to Cyclic Loading," *Trans. Am. Inst. Electr. Eng. Part III Power Appar. Syst.*, vol. 73, no. 1, p. 62, 1954.

[16] C. S. Schifreen, "Cyclic movement of cable — Its causes and effects on cable-sheath life," *Electr. Eng.*, vol. 63, no. 12, pp. 1121–1129, Dec. 1944.

[17] G. Luoni, G. Maschio, and W. G. Lawson, "Study of mechanical behaviour of cables in integral-pipe water-cooled systems," *Proc. Inst. Electr. Eng.*, vol. 124, no. 3, p. 295, 1977.

[18] M. Iordanescu, "Analysis of thermomechanical bending of self-contained oil-filled cables in ducts," *IEEE Trans. Power Syst.*, vol. 3, no. 1, pp. 343–350, 1988.

[19] C. E. Betzer, "Determination of the Life to Fracture by Bending of Lead Sheaths on under-Ground Power Cable," *Trans. Am. Inst. Electr. Eng. Part III Power Appar. Syst.*, vol. 81, no. 3, pp. 907–911, Apr. 1962.

[20] C. T. Nicholson and T. J. Brosnan, "An investigation of the relationship between temperature and movement of cables in ducts," *Electr. Eng.*, vol. 63, no. 10, pp. 723–728, Oct. 1944.

[21] E. Ildstad, K. A. G. Plassen and H. Faremo, "Remnant Static Mechanical Stresses and Water Tree Ageing of XLPE Power Cables," in *JICABLE'15, 9th Int. Conf. on Insulated Power Cables*, Versailles, France, June 21 - 25, 2015, pp. 1-5.

[22] E. Ildstad and S. T. Hagen, "Electrical treeing and breakdown of mechanically strained XLPE cable insulation," in *Conference Record of the 1992 IEEE International Symposium on Electrical Insulation*, 1992, pp. 135–139.

[23] V. Yaroslavskiy, C. Katz, and M. Olearczyk, "Condition Assessment of Belted PILC Cables After 7 to 68 Years of Service," *IEEE Trans. Power Deliv.*, vol. 26, no. 3, pp. 2018–2025, Jul. 2011.

[24] J. Tarnowski, M. Iordanescu and R. Awad, "Restraining devices to counter the migration of HV cables in duct," in *9th Int. Conf. on Transmission and Distribution Construction, Operation and Live-Line Maintenance Proc.*, Montreal, Canada, Oct. 8-12, 2000, pp. 78–82.

[25] Department of Environment Food and Rural Affairs, "Adapting to Climate Change: helping key sectors to adapt to climate change," Mar. 2012.

[26] J. Lyall, "Deciding Soil Thermal Resistivity Values: The Problem, Risk and a Solution," in *Australasian Universities Power Engineering Conference*, Sept. 25-28, Hobart, Australia, 2005, pp. 1-4.

[27] B. Leyland, "Auckland central business district supply failure: the ministerial inquiry," *Power Eng. J.*, vol. 12, no. 6, pp. 269–273, Dec. 1998.

[28] A. Sturchio, G. Fioriti, M. Pompili and B. Cauzillo, "Failure rates reduction in SmartGrid MV underground distribution cables: Influence of temperature," in *2014 AEIT Annual Conference - From Research to Industry: The Need for a More Effective Technology Transfer (AEIT)*, Trieste, Italy, Sept. 18-19, 2014, pp. 1–6.

[29] E. J. Brooks, C. H. Gosling and W. Holdup,"Moisture control of cable environment with particular reference to surface troughs," *Proc. Inst. Electr. Eng.*, vol. 120, no. 1, pp. 51-60, Jan. 1973.

[30] Minghua Li, Bingyin Xu and Zhang Yan, "A novel sheath fault location method for high voltage power cable," in *Proc. of the 7th Int. Conf. on Properties and Applications of Dielectric Materials*, Nagoya, Japan, 2003, pp. 195–198.

[31] E. Da Silva *et al.*, "Diagnosis of XLPE insulated cables aged under conditions of multiple stresses: thermoelectric and humidity," in *Conf. Record of the 1998 IEEE*

Int. Symp. on Electrical Insulation, Arlington, USA, June 7-10, 1998, pp. 117–121.

[32]   N. Klairuang, T. Khatsaengand, and J. Hokierti, "Lightning electric field in the soil and its effect to buried cables," in *Int. Power Engineering Conf.*, Singapore, Nov. 29-Dec.2 , 2005, pp. 782–787.

[33]   BICC Cables, *Electric Cables Handbook*. Wiley, 1997.

[34]   *IEEE Standard for Test Procedures and Requirements for Alternating-Current Cable Terminations Used on Shielded Cables Having Laminated Insulation Rated 2.5 kV through 765 kV or Extruded Insulation Rated 2.5 kV through 500 kV,* IEEE Std 48-2009 (Revision of IEEE Std 48-1996) , pp.1-41, Aug. 2009.

[35]   P. Leemans *et al.*, "Thermal behavior of connectors in joints," in *CIRED 2013, 22th Int. Conf. and Exhibition on Electricity Distribution*, Stockholm, Sweeden, June 10-13, 2013, pp. 1–4.

[36]   H. Liu *et al.*, "Research of state monitoring and pre-warning system of cable joint in distribution power grids," *Int. Conf. on Power Systems Technology*, Chongqing, China, Oct. 22-26, 2007, pp. 1–5.

[37]   R. A. Jongen, P. H. F. Morshuis, J. J. Smit, and A. L. J. Janssen, "Influence of ambient temperature on the failure behavior of cable joints," in *CEIDP 2007, Conference on Electrical Insulation and Dielectric Phenomena*, Vancouver, Canada, Oct. 14-17, 2007, pp. 643–646.

[38]   R. Jongen, E. Gulski and J. Smit, "Failures of medium voltage cable joints in relation to the ambient temperature." in *CIRED 2009, 20th Int. Conf. and Exhibition on Electricity Distribution*, Prague, Czech Republic, June 8-11, 2009, pp. 1–4.

[39]   E. F. Steennis *et al.*, "The effect of high current loads on joints in MV cable systems," in *CIRED 2011, 21th Int. Conf. and Exhibition on Electricity Distribution*, Frankfurt, Germany, June 6-9, 2011, pp. 1–4.

[40]   B. Hennuy, F. Steennis, B. Van Maanen, E. De Ridder, S. Stul, and P. Colin, "New qualification tests for high loaded joints," in *JICABLE'15, 9th Int. Conf. on Insulated Power Cables*, Versailles, France, June 21-25, 2015, pp. 1–6.

[41]   T. Parker and N. Hampton, "Impact of filled-strand conductor on connector temperatures for Medium Voltage joints," in *JICABLE'11, 8th Int. Conf. on Insulated Power Cables*, Versailles, France, June 20- 23, 2011, pp. 1-6.

[42]   B. Hennuy *et al.*, "Measurement of the force induced by thermal expansion of conductor of MV cables and impact on MV joints," in *CIRED 2013, 22th Int. Conf. and Exhibition on Electricity Distribution*, Stockholm, Sweeden, June 10-13, 2013, pp. 1–4

[43]   K. P. Meena *et al.*, "Failure analysis of Medium Voltage Cable accessories during qualification tests," in *IEEE 10th Int. Conf. on the Properties and Applications of Dielectric Materials*, Bangalore, India, July 24-28, 2012, pp. 1–4..

[44]   F. W. Heinrichs, "The Impact of Fault-Detection Methods and Analysis on the Transformer Operating Decision," *IEEE Trans. Power Deliv.*, vol. 2, no. 3, pp. 836–842, 1987.

[45]   T. Sasaki, M. Kurihara, M. Uchida, T. Nakamura, and H. Kawakami, "Oil-filled cable surveillance system using newly developed optical fiber gas sensor," *IEEE Trans. Power Deliv.*, vol. 11, no. 2, pp. 656–662, Apr. 1996.

[46] M. Xianbo and H. Xiaoguang, "Design of on-line temperature monitoring system for power cable joints based on supercapacitor," in *IEEE 10th International Conference on Industrial Informatics*, 2012, pp. 837–840.

[47] C. Wenzhi *et al.*, "The design of temperature monitoring system for power cable joint," in *2012 IEEE Int. Conf. on Condition Monitoring and Diagnosis*, Bali, Indonessia, Sept. 23-27, 2012, pp. 671–676.

[48] S. Nakamura, S. Morooka and K. Kawasaki, "Conductor temperature monitoring system in underground power transmission XLPE cable joints," *IEEE Trans. Power Deliv.*, vol. 7, no. 4, pp. 1688–1697, 1992.

[49] U. Patel *et al.*, "MV cable termination failure assessment in the context of increased use of power electronics," in *EIC 2011, Electrical Insulation Conf.*, Annapolis, USA, June 5-8, 2011, pp. 418–422.

[50] L. Ming, F. Sahlen, S. Halen, G. Brosig, and L. Palmqvist, "Impacts of high-frequency voltage on cable-terminations with resistive stressgrading," *Proc. 2004 IEEE Int. Conf. Solid Dielectr.*, vol. 1, no. 1, 2004.

[51] U. Patel and S. H. Jayaram, "Impact of poor power quality on stress grading system of cable termination," in *CEIDP 2012, Conference on Electrical Insulation and Dielectric Phenomena*, Montreal, Canada, Oct. 14-17, 2012, pp. 463–466.

[52] H. G. Sedding *et al.*, "Assessment of station cable condition using wireless telemetry and diagnostic tests," in *Electrical Insulation Conf. and Electrical Manufacturing and Coil Winding Conf.*, Cincinnati, USA, Oct. 16-18, 2001, pp. 353–357.

[53] J. Côté and A. Bellemare, "Hydro-Québec Experience With Infrared Imaging for the Maintenance of the Undergrouns Medium-Voltage Cable System," in *JICABLE'11, 8th Int. Conf. on Insulated Power Cables*, Versailles, France, June 20- 23, 2011, pp. 1-4.

[54] D. Fournier, S. Poirier and J. Frate, "Field case study of Medium-Voltage Cable Accessories with Partial Discharges in the Hydro-Quebec Underground Distribution Network," in in *CIRED 2007, 19th Int. Conf. and Exhibition on Electricity Distribution*, Vienna, Austria, May 21-24, 2007, pp. 1–3.

[55] M. Villaran and Robert Lofaro, *Condition Monitoring of Cables*. Brookhaven National Laboratory, 2009.

[56] G. Vachtsevanos, F. L. Lewis, M. Roemer, A. Hess, and B. Wu, *Intelligent Fault Diagnosis and Prognosis for Engineering Systems*. Wiley, 2006.

[57] A. K. S. Jardine, D. Lin, and D. Banjevic, "A review on machinery diagnostics and prognostics implementing condition-based maintenance," *Mech. Syst. Signal Process.*, vol. 20, no. 7, pp. 1483–1510, Oct. 2006.

[58] V. M. Catterson, J. Melone, and M. S. Garcia, "Prognostics of transformer paper insulation using statistical particle filtering of on-line data," *IEEE Electr. Insul. Mag.*, vol. 32, no. 1, pp. 28–33, Jan. 2016.

[59] E. Gulski *et al.*, "Knowledge Rules Support for CBM of Power Cable Circuits," in *Cigre Session* 2002, Paris, France, Aug. 25-30, 2002, pp. 1–12.

[60] P. Lewin, "High Voltage Insulation System Condition Monitoring : Ensuring Future Smart Grids are Resilient and Reliable," in *ICPADM 2015, 11th Int. Conf. on the Properties and Applications of Dielectric Materials*, Sydney, Australia, July

19-22, 2015, pp. 1–6.

[61]   J. I. Aizpurua and V. M. Catterson, "Towards a Methodology for Design of Prognostic Systems," *Int. J. Progn. Heal. Manag.*, pp. 1–13, 2015.

[62]   S. Liu, Y. Wang, and F. Tian, "Prognosis of Underground Cable via Online Data-Driven Method With Field Data," *IEEE Trans. Ind. Electron.*, vol. 62, no. 12, pp. 7786–7794, 2015.

[63]   B. Sachan *et al.*, "Prediction of Power Cable Failure Rate Based on Failure History and Operational Conditions," in *JICABLE'15, 9th Int. Conf. on Insulated Power Cables*, Versailles, France, June 21 - 25, 2015, pp. 1–6.

[64]   S. H. Nam *et al.*, "Appication Results of Real-Time Ampacity Estimation System and Intelligent Power Cable System," in *JICABLE'07, 7th Int. Conf. on Insulated Power Cables*, Versailles, France, June 24 - 28, 2007, pp. 1–6.

[65]   J. Cho *et al.*, "Development and Improvement of an Intelligent Cable Monitoring System for Underground Distribution Networks Using Distributed Temperature Sensing," *Energies*, vol. 7, no. 2, pp. 1076–1094, Feb. 2014..

[66]   M. H. Luton *et al.*, "Real Time Monitoring of Power Cables by Fibre Optic Technologies Tests , Applications and Outlook," in *JICABLE '03, 6th Int. Conf. on Insulated Power Cables*, Versailles, France, June 22 - 24, 2003, pp. 1–6.

[67]   D. Freedman, *Statistical Models: Theory and Practice*. Cambridge University Press, 2009.

[68]   X. Yan, *Linear Regression Analysis: Theory and Computing*. World Scientific, 2009.

[69]   I. M. Herrig, S. I. Böer, N. Brennholt, and W. Manz, "Development of multiple linear regression models as predictive tools for fecal indicator concentrations in a stretch of the lower Lahn River, Germany.," *Water Res.*, vol. 85, pp. 148–157, Aug. 2015.

[70]   S. Azadi and A. Karimi-Jashni, "Verifying the performance of artificial neural network and multiple linear regression in predicting the mean seasonal municipal solid waste generation rate: A case study of Fars province, Iran.," *Waste Manag.*, Oct. 2015.

[71]   L. Hu, Z. G. Zhang, A. Mouraux, and G. D. Iannetti, "Multiple linear regression to estimate time-frequency electrophysiological responses in single trials," *Neuroimage*, vol. 111, pp. 442–53, May 2015.

[72]   I. Yilmaz and O. Kaynar, "Multiple regression, ANN (RBF, MLP) and ANFIS models for prediction of swell potential of clayey soils," *Expert Syst. Appl.*, vol. 38, no. 5, pp. 5958–5966, May 2011.

[73]   H.T. Pao, "A comparison of neural network and multiple regression analysis in modeling capital structure," *Expert Syst. Appl.*, vol. 35, no. 3, pp. 720–727, Oct. 2008.

[74]   L. Guo and X. Deng, "Application of Improved Multiple Linear Regression Method in Oilfield Output Forecasting," in *2009 International Conference on Information Management, Innovation Management and Industrial Engineering*, 2009, vol. 1, pp. 133–136.

[75]   Y. Freund and R. Schapire, "A desicion-theoretic generalization of on-line learning and an application to boosting," *J. Comput. Syst. Sci.*, vol. 55, no. 1, pp. 119–139,

1997.

[76] J. Friedman, T. Hastie, and R. Tibshirani;, "Additive logistic regression: A statistical view of boosting," *Ann. Stat.*, vol. 28, no. 2, pp. 337 – 407, 2000.

[77] J. H. Friedman, "Greedy Function Approximation: A Gradient Boosting Machine," *Ann. Stat. 29, 1189–1232*, vol. 29, pp. 1189–1232, 2001.

[78] J. Hastie, Trevor Tibshirani, Robert Friedman, *The Elements of Statistical Learning: Data Mining, Inference, and Prediction*. Springer New York, 2003.

[79] J. R. Lloyd, "GEFCom2012 hierarchical load forecasting: Gradient boosting machines and Gaussian processes," *Int. J. Forecast.*, vol. 30, no. 2, pp. 369–374, Apr. 2014.

[80] S. Ben Taieb and R. J. Hyndman, "A gradient boosting approach to the Kaggle load forecasting competition," *Int. J. Forecast.*, vol. 30, no. 2, pp. 382–394, Apr. 2014.

[81] T. Abdunabi and O. Basir, "Predicting a biological response of molecules from their chemical properties using diverse and optimized ensembles of stochastic gradient boosting machine," in *2014 IEEE Int. Conf. on Big Data (Big Data)*, Washington, USA, Oct. 27-30, 2014, pp. 10–17

[82] Y. Zhang and A. Haghani, "A gradient boosting method to improve travel time prediction," *Transp. Res. Part C Emerg. Technol.*, vol. 58, pp. 308–324, Sep. 2015.

[83] L. Guelman, "Gradient boosting trees for auto insurance loss cost modeling and prediction," *Expert Syst. Appl.*, vol. 39, no. 3, pp. 3659–3667, Feb. 2012.

[84] A. Natekin and A. Knoll, "Gradient boosting machines, a tutorial.," *Front. Neurorobot.*, vol. 7, p. 21, Jan. 2013.

[85] A. P. Engelbrecht, *Computational Intelligence: An Introduction*. John Wiley & Sons, 2007.

[86] R. F. Chevalier *et al.*, "Support vector regression with reduced training sets for air temperature prediction: a comparison with artificial neural networks," *Neural Comput. Appl.*, vol. 20, no. 1, pp. 151–159, Apr. 2010.

[87] A. J. Smola and B. Schölkopf, "A tutorial on support vector regression," *Stat. Comput.*, vol. 14, no. 3, pp. 199–222, Aug. 2004.

[88] V. N. Vapnik, *The Nature of Statistical Learning Theory*. New York, NY: Springer New York, 1995.

[89] E. G. Ortiz-García *et al.*, "Accurate local very short-term temperature prediction based on synoptic situation Support Vector Regression banks," *Atmos. Res.*, vol. 107, pp. 1–8, Apr. 2012.

[90] A. Paniagua-Tineo *et al.*, "Prediction of daily maximum temperature using a support vector regression algorithm," *Renew. Energy*, vol. 36, no. 11, pp. 3054–3060, Nov. 2011.

[91] M. H. Zangooei and S. Jalili, "Protein secondary structure prediction using DWKF based on SVR-NSGAII," *Neurocomputing*, vol. 94, pp. 87–101, Oct. 2012.

[92] C. J. Lu, T. S. Lee and C. C. Chiu, "Financial time series forecasting using independent component analysis and support vector regression," *Decis. Support Syst.*, vol. 47, no. 2, pp. 115–125, May 2009.

[93] R. Kromanis and P. Kripakaran, "Support vector regression for anomaly detection

from measurement histories," *Adv. Eng. Informatics*, vol. 27, no. 4, pp. 486–495, Oct. 2013.

[94]   R. Kohavi, "A Study of Cross-Validation and Bootstrap for Accuracy Estimation and Model Selection," *IJCAI'95 Proc. 14th Int. Jt. Conf. Artif.* , vol. 2, pp. 1137–1143 , 1995.

[95]   M. Castro-Neto *et al.*, "Online-SVR for short-term traffic flow prediction under typical and atypical traffic conditions," *Expert Syst. Appl.*, vol. 36, no. 3 PART 2, pp. 6164–6173, 2009.

[96]   V. N. Vapnik, *Statistical learning theory*. Wiley, 1998.

[97]   C. J. C. Burges, "A Tutorial on Support Vector Machines for Pattern Recognition," *Data Min. Knowl. Discov.*, vol. 2, pp. 121–167, 1998.

[98]   B. Schölkopf, P. Simard, a. Smola, and V. Vapnik, "Prior knowledge in support vector kernels," *Adv. Neural Inf. Process. Syst.*, vol. 10, pp. 640–646, 1998.

[99]   B. Schölkopf and A. J. Smola, *Learning with Kernels: Support Vector Machines, Regularization, Optimization, and Beyond*. MIT Press, 2002.

[100] C. C. Chang and C. J. Lin, "LIBSVM: A Library for Support Vector Machines," *ACM Trans. Intell. Syst. Technol.*, vol. 2, no. 3, pp. 1–27, Apr. 2011

[101] J. E. Theed, "Environmental parameters for cable ratings," Ph.D dissertation, Dept. Elect. and Comp. Sci., Uni. of Sotouthampton, Southampton, 1998.

[102] H. K. Wong *et al.*, "Detection of open-circuit fault in 11kV ring circuits by unbalanced current measurement," *PESC '06, Power Systems Conf. Expo.*, Atlanta, USA, Oct. 29-Nov. 1, 2006, pp. 1240–1243.

[103] H. Jin *et al.,*"Multi-model adaptive soft sensor modeling method using local learning and online support vector regression for nonlinear time-variant batch processes," *Chem. Eng. Sci.*, vol. 131, pp. 282–303, 2015.

[104] J. A. Hunter,"*An investigation into partial discharge activity within three-phase belted cables,*" Ph.D dissertation, Dept. Elect. and Comp. Sci., Uni. of Sotouthampton, Southampton, Jan. 2013..

[105] P. C. J. M. van der Wielen,"*On-Line Detection and Location of Partial Discharges In Medium Voltage Cables,*" Ph.D dissertation, Dept. Elect. Eng., Eindhoven Uni., Eindhoven, Apr. 2005.

[106] D. Fournier, "Aging of defective electrical joints in underground power distribution systems," *Electrical Contacts, 1998. Proceedings of the Forty-Fourth IEEE Holm Conference on*, Arlington, VA, USA, 1998, pp. 179-192.

[107] *IEC 60853. Electric cables. Calculation of the cyclic and emergency current rating of cables. part 2: Cyclic rating of cables greater than 18/30 (36)kV and emergency ratings for cables of all voltages,* 1989